RADC–TR –78–38
Interim Technical Report
February 1978
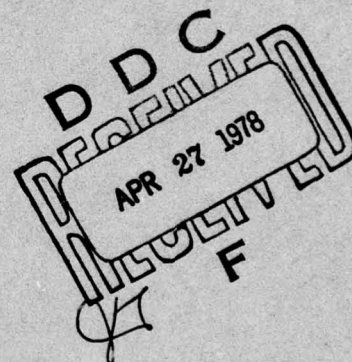
LASER WINDOW MATERIALS AND OPTICAL COATING SCIENCE

Hughes Research Laboratories

DDC
APR 27 1978
F

Sponsored By

DEFENSE ADVANCED RESEARCH PROJECTS AGENCY (DOD)

ARPA Order No. 2415

Monitored By

ROME AIR DEVELOPMENT CENTER

Air Force Systems Command

Griffiss Air Force Base, NY 13441

ARPA Order No. 2415

Contract No. F19628-76-C-0309

Program Code No. 1E50

Principal Investigator: M. Braunstein
Phone No. (213) 456-6411

Contractor:
  Hughes Research Laboratories

AFSC Project Scientist: H. Posen
Phone No. (617) 861-3532

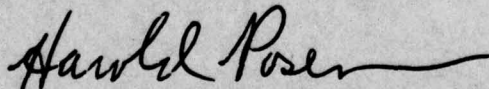Effective Date of Contract:
  19 September 1976

Contract Expiration Date:
  19 December 1977

The views and conclusions contained in this document are those of the authors and should not be interpreted as necessarily representing the official policies, either expressed or implied, of the Defense Advanced Research Projects Agency or the U.S. Government.

This report has been reviewed and is approved for publication.

This technical report has been reviewed and approved for publication by RADC (OI).

APPROVED: *Harold Posen*

HAROLD POSEN
Contract Monitor

APPROVED: *Robert M. Barrett*

ROBERT M. BARRETT
Director
Solid State Sciences Division

SECURITY CLASSIFICATION OF THIS PAGE (When Data Entered)

REPORT DOCUMENTATION PAGE		READ INSTRUCTIONS BEFORE COMPLETING FORM
1. REPORT NUMBER RADC-TR-78-38	2. GOVT ACCESSION NO.	3. RECIPIENT'S CATALOG NUMBER
4. TITLE (and Subtitle) LASER WINDOW MATERIALS AND OPTICAL COATING SCIENCE		5. TYPE OF REPORT & PERIOD COVERED Interim Technical Report 19 Mar 1977 – 19 Sept 1977
		6. PERFORMING ORG. REPORT NUMBER Semiannual Tech. No. 2
7. AUTHOR(s) M. Braunstein, S.D. Allen, J.A. Harrington, M.E. Pedinoff, J.E. Rudisill, R.R. Turk, R.C. Pastor, D.E. Zuccaro		8. CONTRACT OR GRANT NUMBER(s) F19628-76-C-0309 ARPA Order-2415
9. PERFORMING ORGANIZATION NAME AND ADDRESS Hughes Research Laboratories 3011 Malibu Canyon Road Malibu, California 90265		10. PROGRAM ELEMENT, PROJECT, TASK AREA & WORK UNIT NUMBERS ARPA Order No. 2415 Program Code No. 1E50
11. CONTROLLING OFFICE NAME AND ADDRESS Defense Advanced Projects Agency 1400 Wilson Blvd. Arlington, VA 22209		12. REPORT DATE February 1978
		13. NUMBER OF PAGES 129
14. MONITORING AGENCY NAME & ADDRESS(if different from Controlling Office) Deputy for Electronic Technology (RADC/ESM) Hanscom AFB, MA 01731 Contract Monitor: Harold Posen		15. SECURITY CLASS. (of this report) Unclassified
		15a. DECLASSIFICATION DOWNGRADING SCHEDULE

16. DISTRIBUTION STATEMENT (of this Report)

Semiannual Technical rept. no. 2, 19 Mar - 19 Sep 77

Approved for public release; distribution unlimited.

17. DISTRIBUTION STATEMENT (of the abstract entered in Block 20, if different from Report)

18. SUPPLEMENTARY NOTES

19. KEY WORDS (Continue on reverse side if necessary and identify by block number)

Infrared laser windows, surface finishing, thin films, antireflection-coatings, surface characterization, optical evaluations and laser calorimetry at 10.6 μm, 5.3 μm, 3.8 μm, and 2.8 μm, infrared ellipsometry, modulated light ellipsometer, potassium chloride, calcium fluoride.

20. ABSTRACT (Continue on reverse side if necessary and identify by block number)

We report on the objectives and the progress achieved in a program to establish a definitive correlation between preparation procedures and optical performance of antireflective coated windows for high-power infrared lasers: HF (2.7 μm), DF (3.8 μm), CO (5.3 μm), and CO_2 (9.27 and 10.6 μm). The window materials that are under investigation include selected alkali halides and alkaline earth fluorides, in both single and polycrystalline form and of alloyed and unalloyed composition.

DD FORM 1473 EDITION OF 1 NOV 65 IS OBSOLETE

The enclosed papers discuss the results of our work reported at the topical meeting on High Power Laser Optical Components and Component Materials and the Materials for High Power Lasers Symposium at the National Bureau of Standards facility in Boulder, Colorado, October 3-6, 1977. The papers are relevant to the major task subdivisions of our program; surface finishing, reactive atmosphere processing, window coatings, optical evaluation and infrared ellipsometry measurements. In addition to the papers which are an accomplishment of the contract supported effort, a paper on "Optical Absorption in UV Laser Window Materials" resulting from research supported by Hughes Aircraft Company's internal research and development funds is also included because of its relevance to the technology of highly transparent solids.

TABLE OF CONTENTS

3

INTRODUCTION

This is the second semiannual technical report of the "Laser Window Materials and Optical Coating Science" program (Contract F19628-76-C-0309), which is being conducted by the Hughes Research Laboratories (HRL) under the technical monitorship of Rome Air Development Center (RADC/ESM). The ultimate objective of this program is to establish a correlation between preparation procedures and the optical performance of anti-reflective (AR) coated windows for high-power infrared lasers: HF (2.7 μm), DF (3.8 μm), CO (5.3 μm), and CO_2 (9.27 and 10.6 μm). The window materials to be investigated include selected alkali halides and alkaline earth fluorides. These window materials are both single and polycrystalline and of alloyed and unalloyed composition.

Under preparation procedures, we have included specification of window substrate growth (RAP or conventional) and treatment (forging, polishing) parameters and, in addition, the vacuum (uv or conventional) conditions under which a variety of AR coatings (film materials and coating designs) have been applied. The optical performance parameters are the resultant transmission and absorption of the AR-coated high-power infrared laser windows.

The tasks under this program are organized into seven broad categories. First, the application of reactive atmosphere processing (RAP) chemistry techniques to the growth, polishing, grain growth stabilization, and AR coating passivation of poly- and single-crystal KCl and of alkaline earth fluorides. Second, the application of press forging to RAP materials to enhance yield strength, and a study of the grain growth kinetics in such press forged materials. Third, a study of chemical-mechanical surface finishing techniques for the preparation of laser window materials. Fourth, a characterization of substrate and coating surface finishing using (1) scanning electron microscopy and X-ray diffraction, and (2) structural and chemical analysis using low-energy electron diffraction (LEED), Auger electron spectroscopy (AES), and microprobe techniques. Fifth, a comparison of AR coatings prepared under ultrahigh vacuum ($<10^{-9}$ Torr) and conventional (10^{-6} to 10^{-9} Torr)

5

conditions and by ion beam sputtering techniques. Sixth, an optical
evaluation of the AR-coated windows using infrared spectrophotometry,
absorption calorimetry, ellipsometry, and scattering measurements. And
seventh, a selection of substrate materials and AR-coated window speci-
ments for study of laser damage mechanisms (this is performed by
Dr. M. Bass and his group at the USC Center for Laser Studies).

Coordination is being maintained between this research program and
(1) the programs conducted by Dr. M. Bass at the University of Southern
California on laser damage to windows, (2) Dr. M. Shen's program at the
University of California on organic polymer coatings, and (3) Dr. H.
Bennett's program at the Naval Weapons Center, China Lake, California.

During this report period, Laser damage threshold measurements at
9.27 and 10.6 μm on antireflection-coated KCl samples were performed in
cooperation with J. Detrio of the University of Dayton Research Institute
to complement the laser damage effort by Dr. M. Bass and his group. In
addition, optical evaluation work was performed in cooperation with
Dr. M. Hass and his associates at the Naval Research Laboratory during
this report period.

In addition to the papers which report on DARPA-supported research,
we have included a paper (Low Loss 9.27 μm AR Coatings for KCl) which
reports on work supported by the Air Force Materials Laboratory, Wright-
Patterson Air Force Base. A number of samples produced under DARPA
contract were tested for laser damage threshold under this program and
are included in the paper.

SURFACE FINISHING OF POLYCRYSTALLINE CaF_2 and SrF_2 FOR USE AS HF/DF LASER WINDOWS

R.R. Turk, J.A. Harrington, J. Johnston, C. Haeussler, and R.L. Joyce

Hughes Research Laboratories
Malibu, California 90265

ABSTRACT

Laser windows of CaF_2 and SrF_2 for HF and DF wavelengths require unique solutions to problems in both surface finishing and cleaning. Polycrystalline blanks, substituted for single crystal to reduce sensitivity to drastic cleavage, present some grains in orientations which suffer microcleavage during grinding. These microcleavages are revealed as pits in the polished surface. We present a formula for isotropic, cleavage-free grinding on soft laps followed by chemical-mechanical polishing to remove final scratches. Absorption at both HF and DF wavelengths is given as a function of polishing method and final surface cleaning technique.

INTRODUCTION AND BACKGROUND

Infrared laser windows for HF (2.8 μm) and DF (3.8 μm) wavelengths must be finished flat and parallel to pass an undistorted laser beam. Windows of CaF_2 and SrF_2 are favored for 2.8 μm and 3.8 μm because of their low absorption and high strength. However, a marked tendency toward catastrophic cleavage on the (111) plane suggests that, for increased reliability, the structure should be polycrystalline with a fine grain size.

Optical finishing requires that material be removed from the window surfaces by successive grinding and polishing steps. These leave damaged layers that exhibit high absorption. A combination of chemical and mechanical surface removal offers the best chance of obtaining flat

surfaces that are reasonably free from damage. But a problem is posed by the use of polycrystalline materials.

While strength of a polycrystalline window blank is higher and catastrophic cleavage is minimized, microcleavage on the (111) planes can cause extensive damage to grains oriented in cleavage-sensitive directions. This damage occurs during grinding, but only becomes visible as deep pits in the course of fine polishing (Figure 1). This was recognized for single-crystal windows,[1] and orientations have been specified that are insensitive to cleavage. Grinding of a polycrystalline surface, however, reveals many poorly oriented grains that can damage deeply. These cleavage-oriented grains, coupled with the use of a coarse, hard abrasive on a nonyielding lap surface, results in surface pitting. These conditions provide the high local stresses conducive to local cleavage.

EXPERIMENTAL POLISHING PROCEDURE

Polycrystalline material for this investigation had a grain size of 1 to 3 mm. This was prepared by press-forging boules of reactive atmosphere processed (RAP) CaF_2 and SrF_2 at $900^{\circ}C$. These were single-crystal boules, oriented along the <111> direction, and reduced in height from 85 to 90%.[2]

Our general approach to finishing included use of an abrasive of reduced hardness for most stages of coarse grinding coupled with resilient laps to prevent high impressed stresses.

Two grinding steps and four polishing steps are used. Initial flattening is obtained by grinding with 18 μm garnet (a friable form of $Fe_3Al_2(S_1O_4)_3$) on a glass lap in a water vehicle. The friability of this form of garnet compensates for its hardness of 8 to 9 on the Moh scale. A second grinding step with 8 μm garnet uses a soft pitch (No. 73 Swiss) lap to provide a resilient, soft embeddment material to accommodate coarse grit and avoid high local stresses.

The first polishing step uses 1 μm alumina on soft pitch, and removes any trace of cleavage pits that may have begun during coarse grinding. The second polishing step is on soft pitch, with 0.3 μm alumina in water. Cerium oxide of 2 μm initial size is used on soft

pitch for the third polishing step. This material breaks down in size easily; yet continues to polish CaF_2 and SrF_2 to a fine finish, leaving only a few superficial scratches and very slight surface roughness (Figure 2).

A final half-hour polish on soft pitch with 0.05 μm alumina, including a one-minute etch-polish on the lap with concentrated HCl, removes all roughness and most scratches (Figure 3). The entire procedure takes about four to six hours for each side.

SUMMARY OF GRINDING AND POLISHING PROCEDURES

Grind flat on cast iron lap with 18 μm garnet

Grind on soft pitch with 8 μm garnet

Polish on soft pitch with 1 μm alumina

Polish on soft pitch with 0.3 μm alumina

Polish on soft pitch with 2 μm cerium oxide

Pitch-polish with 0.05 μm alumina, final 1 min add concentrated HCl.

Water is used on all but the last step. Nonaqueous grinding and polishing will be tried in an attempt to obtain lowest possible HF and DF absorptions.

CALORIMETRIC TESTING

Surface preparation for calorimetric absorption testing is designed to exclude water from the window surface along with other absorbing monolayers. Procedure is listed below:

Gentle surface scrub with precipitated $CaCO_3$ slurry (aqueous), sterilized cotton

Distilled water (cotton) scrub and rinse

Pure ethanol (cotton) scrub, soak

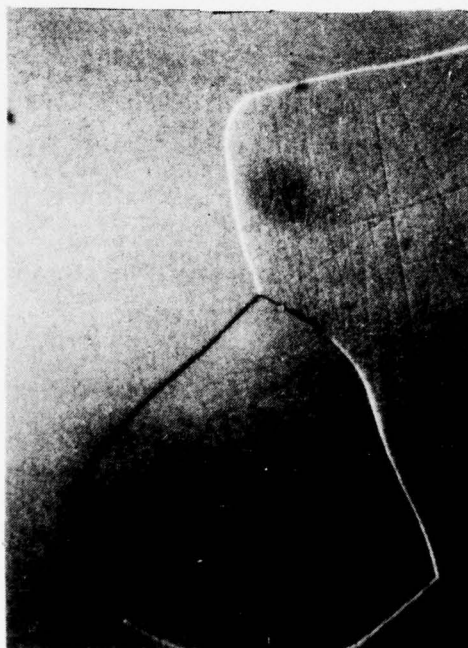With sample continuously wet with ethanol, insert into Freon vapor degreaser to dry.

9

Figure 1.   Craters in polishing CaF_2 caused by grinding.

Figure 2.   Optically finished CaF_2.

6783-6

Figure 3. CaF_2 finishing by etch polishing.

Calorimetric absorptions of one sample each of forged CaF_2 and SrF_2 at HF and DF wavelengths are shown in Table 1. These results are depicted graphically in Figures 4 and 5. Note that standing in vacuum led to increased absorption of CaF_2 at both HF and DF, almost no change in SrF_2 absorptions. Light etch-removal of surface with alcohol rinse lowered absorption of CaF_2 slightly, but probably would have been more effective if alcohol rinse had been longer and more thorough in exclusion of water. The same treatment of SrF_2 gave increased absorption at HF, decreased at DF. Thorough surface removal by abrasive etch-polishing for 7-1/2 minutes per side gave increased absorption in all cases, probably due to presence of water during cleaning.

In addition to the pitting anisotropy, CaF_2 and SrF_2 exhibit marked polishing anisotropy for different grains, if polished on cloth laps. Also, the grains show a large difference in response to etching with HCl, with some grains attacked, others passive (Figure 6). The mechanical anisotropy during polishing is not seen during optical finishing on pitch because of absence of any nap, and effects of etch anisotropy are almost absent when etching is performed simultaneously with final pitch polishing.

In the course of etching experiments, it was found that dilute HCl attacked faster than concentrated HCl, with less uniform results. HBr was also active as an etchant, but no other etchants have yet been found with the room temperature effectiveness of HCl and HBr. This work is also continuing.

We are continuing these surface preparation experiments in an attempt to develop a technique which will yield lowest absorption at both HF and DF wavelengths.
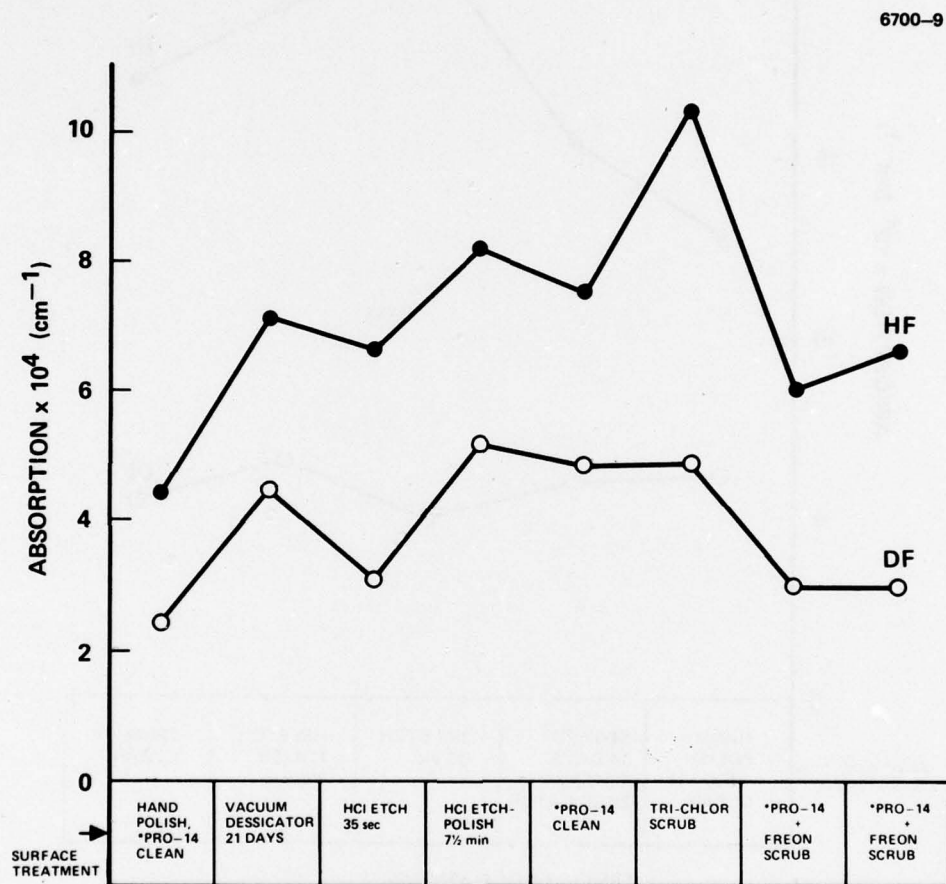
11

Table 1. Calorimetric Absorption — CaF_2 and SrF_2, at 2.8 and 3.8 μm

Material	History	B_{HF}	B_{DF}
Poly-xtal CaF_2	As-polished, cleaned, min. H_2O	4.44×10^{-4}	2.47×10^{-4}
Poly-xtal CaF_2	3 weeks - vacuum dessicator	7.13×10^{-4}	4.45×10^{-4}
Poly-xtal CaF_2	30 sec HCl etch, alcohol rinse	6.62×10^{-4}	3.15×10^{-4}
Poly-xtal CaF_2	15 min HCl etch-polish, 0.3 μm Al_2O_3, H_2O, alcohol	8.20×10^{-4}	5.19×10^{-4}
Poly-xtal CaF_2	Cleaned, minimal H_2O	7.57×10^{-4}	4.86×10^{-4}
Poly-xtal SrF_2	As-polished, cleaned minimal H_2O	12.9×10^{-4}	6.27×10^{-4}
Poly-xtal SrF_2	3 weeks - vacuum dessicator	15.4×10^{-4}	6.00×10^{-4}
Poly-xtal SrF_2	30 sec HCl etch, alcohol rinse	20.8×10^{-4}	4.90×10^{-4}
Poly-xtal SrF_2	15 min HCl etch-polish, 0.3 μm Al_2O_3, H_2O, alcohol	19.1×10^{-4}	6.58×10^{-4}
Poly-xtal SrF_2	Cleaned, minimal H_2O	17.2×10^{-4}	5.50×10^{-4}

T6030

ABSORPTION x 10^4 (cm^{-1})

10

8

HF

6

4

DF

2

0

| HAND POLISH, *PRO—14 CLEAN | VACUUM DESSICATOR 21 DAYS | HCl ETCH 35 sec | HCl ETCH- POLISH 7½ min | *PRO—14 CLEAN | TRI-CHLOR SCRUB | *PRO—14 + FREON SCRUB | *PRO—14 + FREON SCRUB |

SURFACE TREATMENT

* PRO—14 CLEANING:
   SCRUB, COTTON, PPT. $CaCO_3$, H_2O
   SCRUB, COTTON, ETHANOL
   RINSE, ETHANOL
   DRY, FREON VAPOR DEGREASER

Figure 4. Polycrystalline calcium fluoride absorption versus surface treatment.
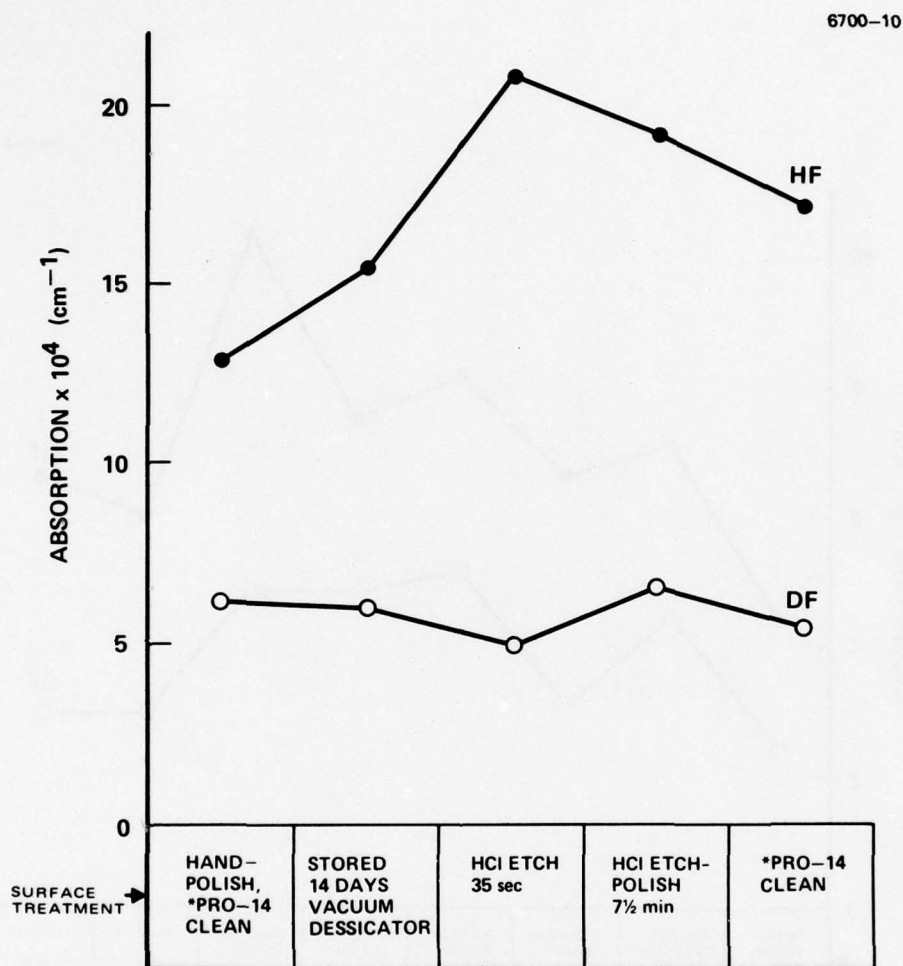
6700–10

*PRO–14 CLEANING:
SCRUB, COTTON, PPT. CaCO$_3$, H$_2$O
SCRUB, COTTON, ETHANOL
RINSE, ETHANOL
DRY, FREON VAPOR DEGREASER

Figure 5.   Polycrystalline strontium fluoride
absorption versus surface treatment.

14

6783-5

Figure 6. Etching anisotropy
in CaF$_2$.

REFERENCES

1. A. Klugman, R.F. Schneidmiller, "Investigation of Crystal
    Orientation Influence on Thin Film Coatings for CaF$_2$ Laser Windows,"
    Final Report, October 1975, for AFML, Wright-Patterson Air Force
    Base, Ohio, Contract No. F33615-75-C-5190.

2. H.W. Winston, R.R. Turk, R.C. Pastor, and R.F. Scholl, "Fluoride
    Window Materials for the 2 to 6 μm Region," pg. 437, Proc. 4th
    Conf. on Infrared Laser Window Materials, DARPA, uscon, Arizona,
    January 1975.

SCALE-UP HANDLING OF ALKALINE-EARTH FLUORIDE LASER WINDOWS UNDER A REACTIVE ATMOSPHERE

M. Robinson, K. Arita, R.C. Pastor, and M. Braunstein

Hughes Research Laboratories
Malibu, California 90265

ABSTRACT

Alkaline earth fluorides are grown in He/HF, He/HF/CF$_4$, and He/HF/BF$_3$. IR transmission curves are compared and the corrosion behavior of SF$_6$, CF$_4$ and BF$_3$ with carbon is measured.

INTRODUCTION

Since the advent of the first laser much attention and work has been directed to the preparation of highly transparent, simple fluoride crystals for solid-state laser and laser-window applications. Crystals were typically grown either in vacuum or inert gas atmosphere. The resultant crystals, although relatively transparent, exhibited extrinsic absorptions caused by lattice incorporation of oxyanion impurities. The absorptions occur in regions of the electromagnetic spectrum which especially preclude consideration for high-power laser window application; in extreme cases, a high degree of optical scattering is readily observed due to precipitation of oxide and/or hydroxide impurities throughout the material bulk.

In some instances alkaline earth fluorides, MF$_2$,[1] have been processed and grown by reactive atmosphere processing (RAP) using hydrogen fluoride gas HF$_{(g)}$. The presence of this RAP agent in the gas phase (g) suppresses

hydrolysis by $H_2O_{(g)}$ of the condensed phase (c), melt and crystal:

$$F^-_{(c)} + H_2O_{(g)} \xrightarrow{\rightarrow}_{\leftarrow} OH^-_{(c)} + HF_{(g)} \quad . \tag{1}$$
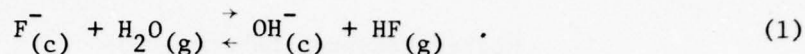
It follows from the mass-action principle that $[OH^-_{(c)}]/[F^-_{(c)}]$ is proportional to the ratio $P(H_2O)/P(HF)$, which we choose to call the RAP index, and that is the key parameter for reducing the hydroxide/fluoride ratio in the crystal. Since $HF_{(g)}$ is the only agent capable of rapid, efficientcient oxide-to-fluoride conversion at room temperature, it is used as the primary RAP agent for this study. Since the RAP index is primarily determined by the H_2O concentration in the outgas of the crystal-growing apparatus, and since $HF_{(g)}$ cannot react with H_2O, a secondary RAP is necessary to further reduce the index to a point approaching intrinsic absorption in the crystal. The secondary RAP agent lowers the index of the gas phase and reacts with impurities in the condensed phase.

Secondary RAP agents considered in this paper are SF_6, CF_4, and BF_3. The IR transmissions of SrF_2 and BaF_2 are compared for crystals grown in HF/He (RAP-1), HF/He-CF_4 (RAP-2), and HF/He-BF_3 (RAP-3). Also, the corrosion behavior at high temperatures is given for all three agents with carbon, the material comprising the growth crucible and the furnace heating elements.

EXPERIMENTAL

A graphite resistance furnace (Astro Industries) was used to grow the crystals by a vertical Bridgman mode. Graphite crucibles of 4.3 and 5.2 cm diameter were fabricated from graphite-G (Carborundum Co). Loading of the crucible with MF_2 powder charge is followed by leak checking, vacuum pumping and RAP at low temperature before melting. RAP-1 consists of HF (99.9% Matheson) diluted to 10 mole % with He flowing at 2 liters/mir RAP-2 consists of the following molar ratio: He:HF:CF_4 = 1:0.5:0.05 operating at a helium pressure of about 500 Torr, and a total pressure of one atmosphere. RAP-3 is identical in all proportions to RAP-2 except BF_3 is substituted for CF_4. All RAP agents used in crystal growth

18

are from Matheson Company, and of the following purities: HF 99.9%, CF_4 99.7%, and BF_3 99.5% C.P.

The corrosion behavior of the three RAP agents (SF_6, CF_4, and BF_3) on carbon was determined in the following manner: A vitreous SiO_2 envelope about 5 cm diameter contained the carbon workpiece under a controlled atmosphere. The workpiece, cylindrical graphite tubing, was supported on a solid graphite pedestal. Three equidistant indentations along the circumference of the SiO_2 tube held the pedestal upright. A rf coil outside the tube coupled directly to the carbon specimen. Either a flow of He or a vacuum was maintained while the workpiece temperature stabilized. The temperature was measured with an optical pyrometer. The gas flow was either switched to a premixed secondary RAP/He at a given P(secondary RAP), or the latter was obtained by balancing the flow of pure secondary RAP against a throttled pump. After a given time interval, the workpiece was cooled rapidly. The weight of the workpiece before and after the exposure was measured.

RESULTS and DISCUSSION

Figure 1 compares IR transmissions of BaF_2 grown by RAP-1 (Figure 1(a)) and RAP-2 (Figure 1(b)). For RAP-2, the melt was soaked at $200^{o}C$ above the melting point for 1 hour prior to lowering the crucible. Starting materials are 99.99% cation pure BaF_2 from E. Merck Laboratories. Figure 2 shows the improvements in infrared transparency of SrF_2 crystals grown by RAP-1, RAP-2, and RAP-3 recipes. The CF_4 eliminates the absorption at 6.9 μ (shown for RAP-1, Figure 2(a)) but a small absorption at 6.0 μ is evident. The crystal grown by RAP-3 (Figure 2(c)) shows no apparent absorptions, and was soaked at only $1700^{o}C$ for 1 hour prior to lowering the crucible, compared to $1800^{o}C/2$ hr for the other specimens. We believe the improvement is solely due to the more effective secondary RAP agent BF_3, which scavenges H_2O in the following manner:

$$2BF_{3(g)} + 3 \; H_2O_{(g)} \rightleftharpoons B_2O_{3(g)} + 6HF_{(g)} \; . \tag{2}$$
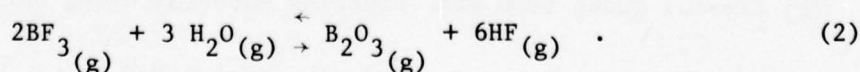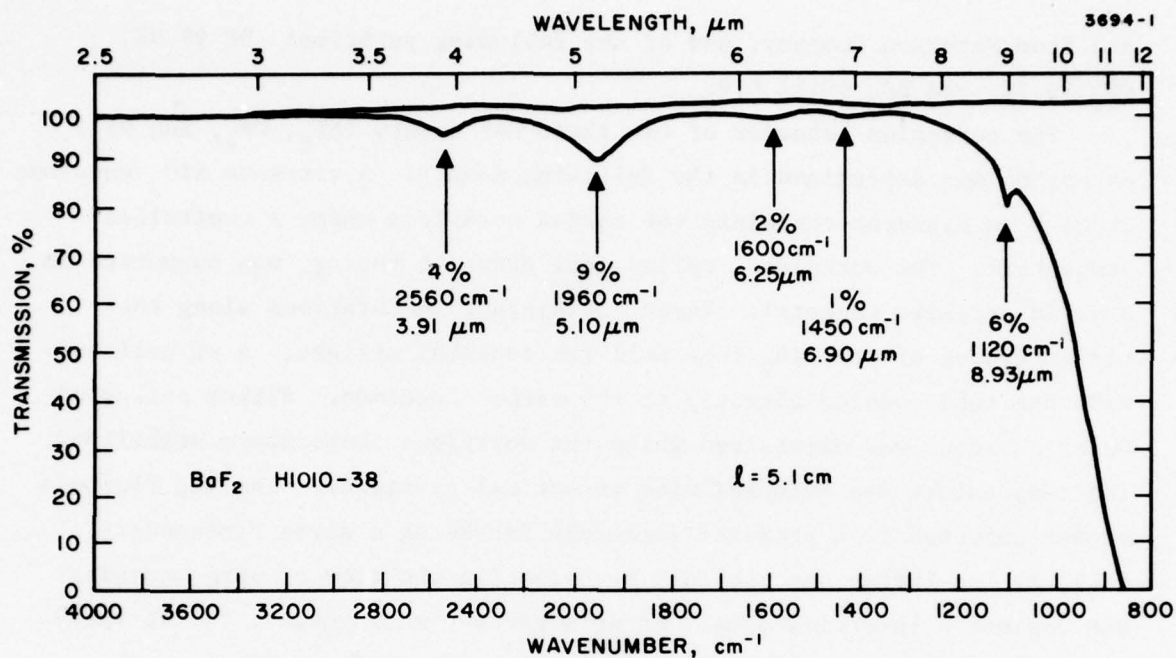
(a) BaF$_2$ crystal grown in HF/He.
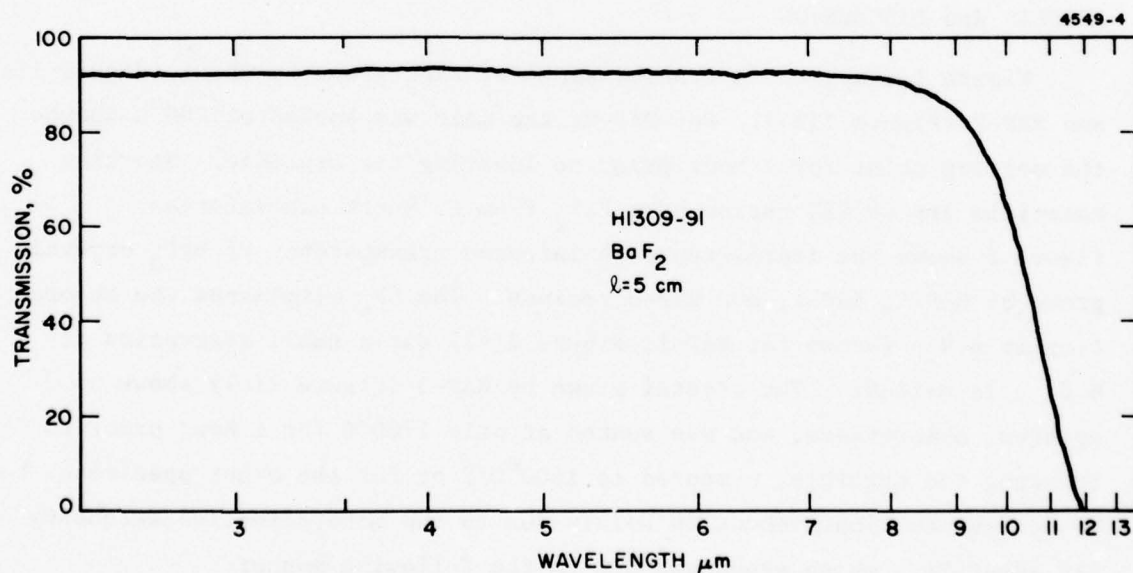
(b) Crystal grown from same starting material using (HF, CF$_4$)/He.

Figure 1.   Single crystal BaF$_2$.
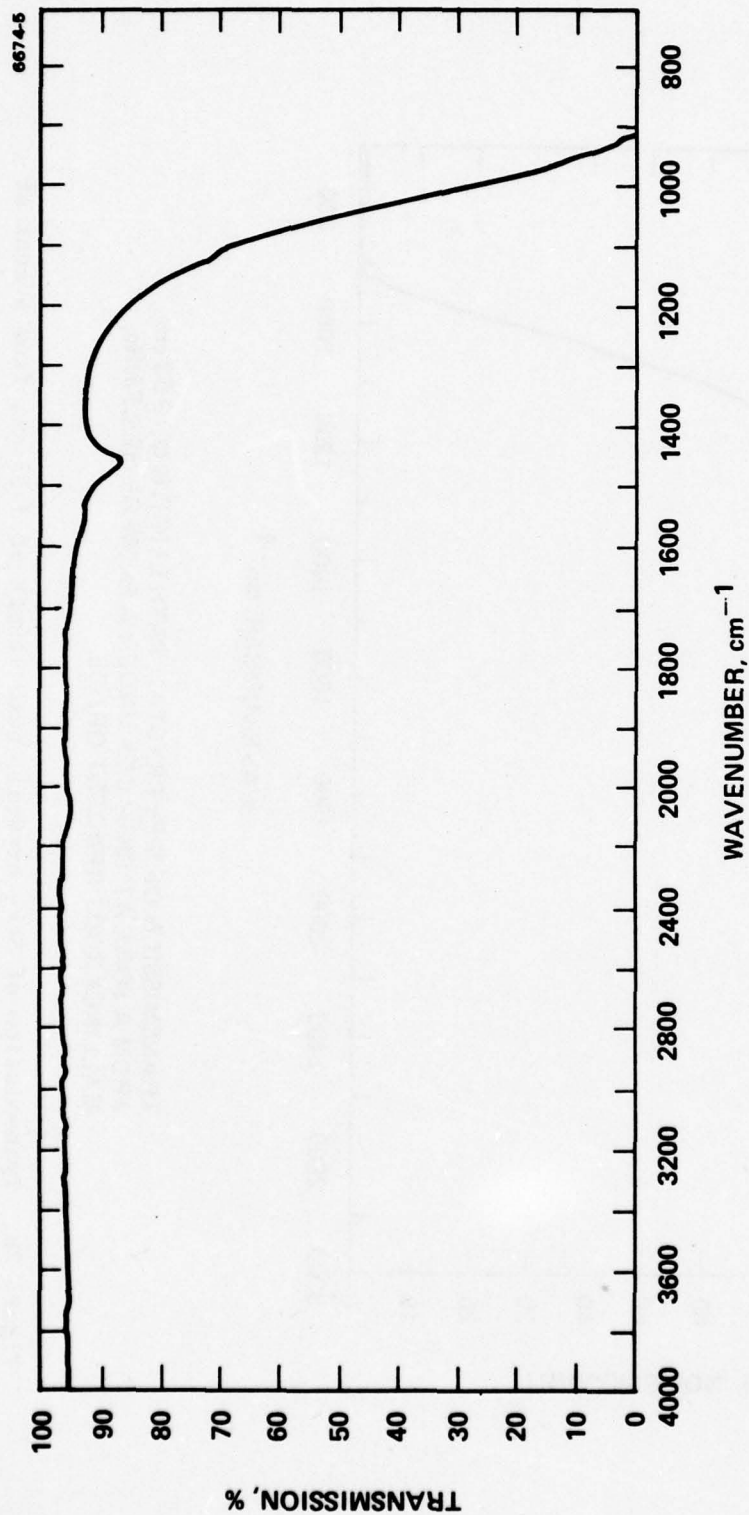
Figure 2a.   Transmission of SrF₂ crystal, path length of 3.23 cm, from a soak at 1800°C/2h, under a flow of HF/He, Mallinckrodt reagent grade.

21
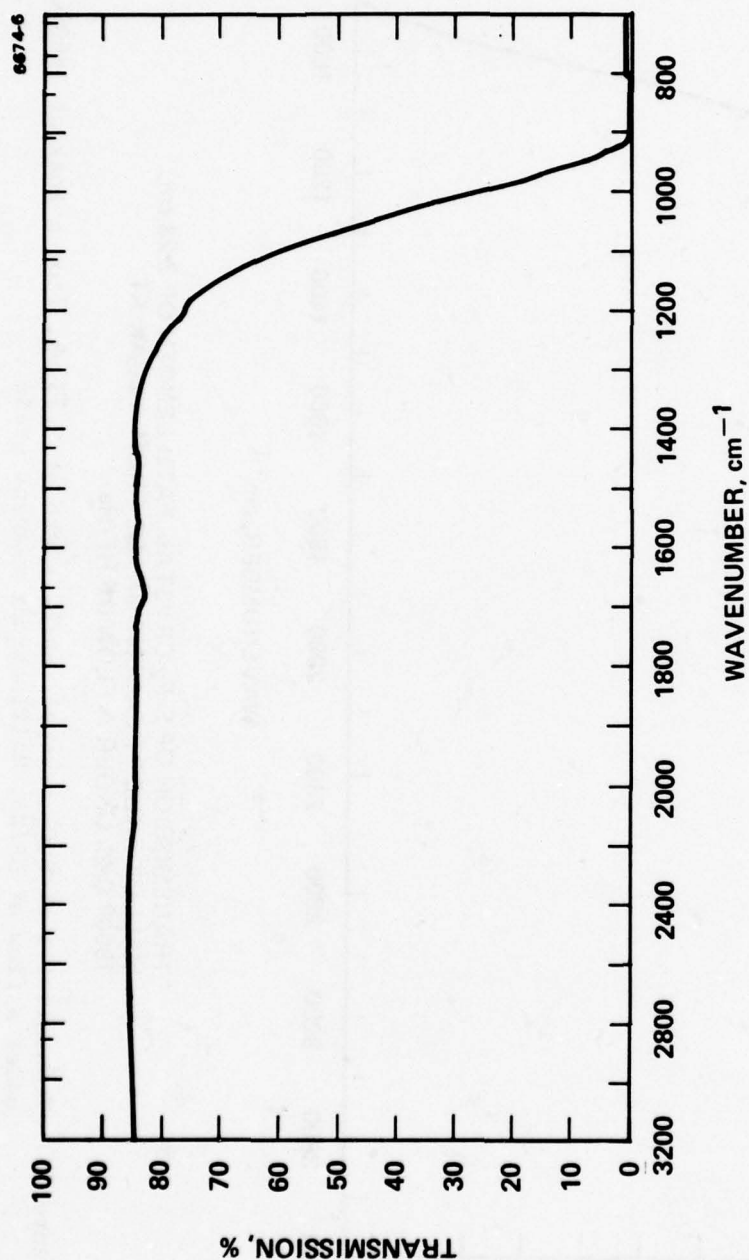
Figure 2b. Transmission of SrF$_2$ crystal, path length of 3.53 cm, from a soak at 1800°C/2h under a flow of HF/CF$_4$/He, Mallinckrodt reagent grade.

22
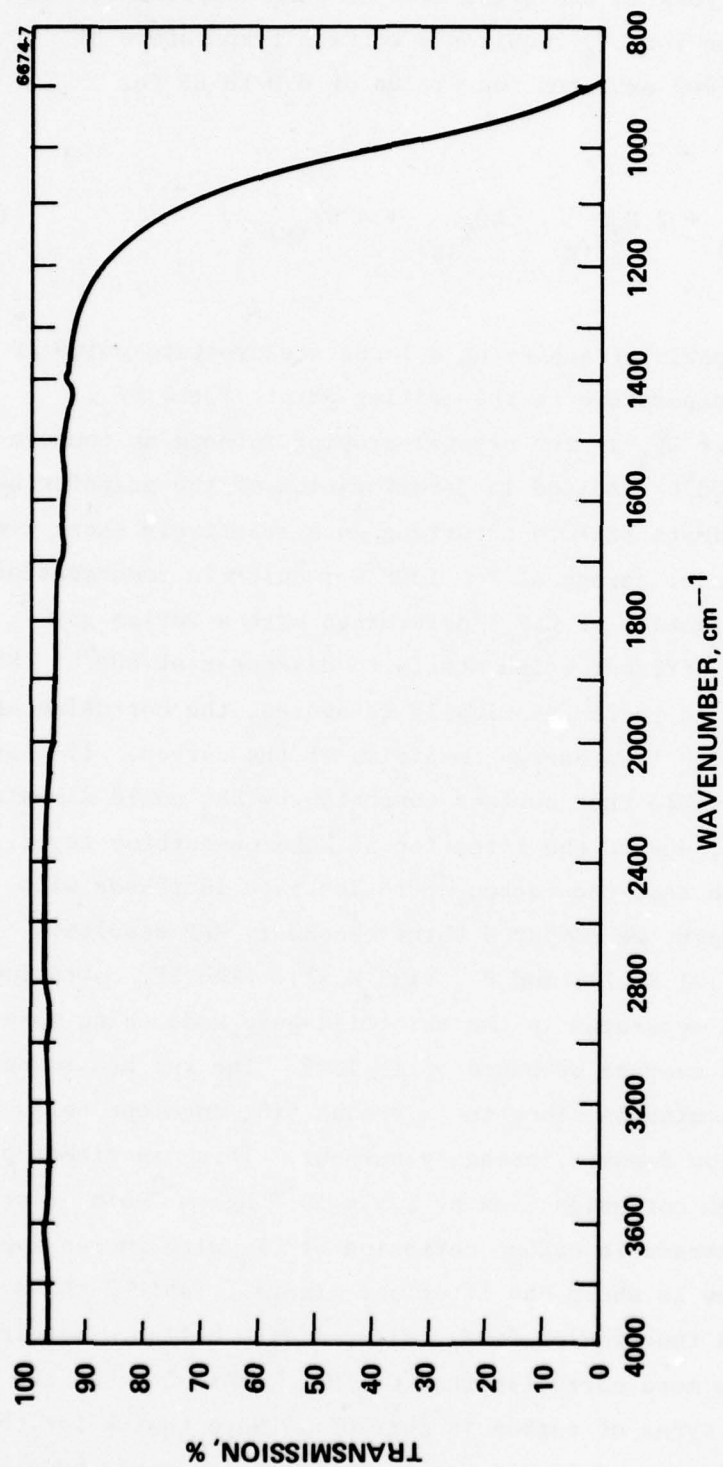
Figure 2c. Transmission of SrF$_2$ crystal, path length of 2.42 cm, from a soak at 1700°C/1h under a flow of HF/BF$_3$/He Malinckrodt reagent grade.

23

This reaction readily goes to the right even at room temperature whereas the equivalent reaction for CF_4 requires a working temperature of $900^\circ C$ (Ref. 2) for a 100% expected conversion of H_2O to HF for $[H_2O]:[CF_4] = 1:10^3$:

$$CF_{4(g)} + 2\ H_2O_{(g)} \underset{\leftarrow}{\rightarrow} CO_{2(g)} + 4\ HF_{(g)}\ . \tag{3}$$

BF_3, therefore, is capable of achieving a lower steady-state value of the RAP index from room temperature to the melting point of the MF_2.

The use of 25 Torr CF_4 in the crystal-growing furnace at temperatures greater than $1500^\circ C$ resulted in deterioration of the graphite heating element, with ultimate failure occurring in a relatively short time period. Passing CF_4 over carbo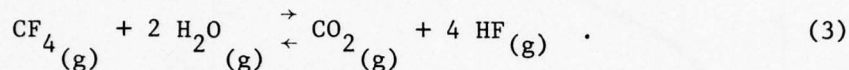n at $T > 1300^\circ C$ results in consummation of the carbon and the formation of C_2F_4 (determined with a Varian gas chromatograph) in the effluent which starts to disappear at $800^\circ C$. Since the formation of C_2F_4 is thermodynamically unfavored, the corrosion of C by CF_4 suggests a high free-energy condition of the carbon. If this is true, it is conceivable that surface corrosion by BF_3 could diminish with time, unlike CF_4, due to the formation of a boron-carbide layer.

On the assumption that the carbon corrosion rate increases with decreasing bond strength, we compared three secondary RAP results: SF_6 (∿70 Kcal), CF_4 (121 Kcal), and BF_3 (133 Kcal). The SF_6 corrosion was obtained with the apparatus in the throttled-pump mode using pure SF_6 at $1500^\circ C$, and an average pressure of 16 Torr. The run had to be terminated in only 34 minutes since the vitreous SiO_2 envelope began to fog badly with a yellow deposit, probably sulphur. This experiment produced an expected high corrosion flux of 1.5×10^{-2} Mg-cm^{-2}-min^{-1}-Torr^{-1}. Table 1 shows the increase in carbon corrosion by CF_4 with increasing temperature. CF_4 flow is about one liter per minute. Table 2 shows the carbon corrosion as a function of $P(CF_4)$ diluted with helium. Note that CF_4/Ar is three times more corrosive than CF_4/He. Table 3 shows the corrosion of various types of carbon in pure CF_4. Note that k for the non-virgin samples gives a sixfold increase in corrosion rate, possibly

24

Table 1. Corrosion of Graphite-G and Vitreous Carbon Versus
Temperature at $P(CF_4)$ = 760 Torr (Virgin Samples)

t, $^oC^{(a)}$	CF_4 - Exposure Time, Min	k, mg-cm^{-2}-min^{-1}-Torr^{-1}
1300	335	0.15×10^{-5}
1400	300	0.19×10^{-5}
1550	130	0.57×10^{-5}
1650	30	0.32×10^{-4}
1850	4	0.52×10^{-4}
[a] Temperature control at each setting is $\pm 30^oC$.		

Table 2. Corrosion of Graphite-G at 1500^oC/95 min Versus
$P(CF_4)$ in a flow of CF_4/He (Virgin Samples)

$P(CF_4)$, Torr	k, mg-cm^{-2}-min^{-1}-Torr^{-1}
61	0.47×10^{-4}
122	0.35×10^{-4} $(1.26 \times 10^{-4})^{[a]}$
182	0.55×10^{-4}
[a] Value for k for case of CF_4/Ar at $P(CF_4)$ = 122 Torr.	

Table 3. Corrosion Resistance of Carbon Wares to CF_4 at $1500^\circ C$ (No Diluent) (Virgin Samples)

P(CF$_4$), Torr	Weight Loss (mg) After 95-Minute Exposure		
	Graphite-G	GL-Carbon	Vitreous Carbon
10	6.75	44.2	20.5
20	12.95	87.9	27.3
40	23.1	—	—
80	60.7	—	—
W, [a] g	11.0	7.9	3.3
k, [b] mg-cm^{-2}-min^{-1}-Torr^{-1}	1.68×10^{-4}	12.9×10^{-4}	9.1×10^{-4}
	[c] 10.0×10^{-4}		

[a] Average weight of each sample in the series with a variation less than 3%.

[b] Least-square value of the slope of the line passing through the origin in the plot of corrosion in mg-cm^2 min^{-1} versus P(CF$_4$) in Torr.

[c] Value of k for non-virgin samples, i.e., 3 runs with two used samples.

T6030

26

indicating the free energy of C becomes positive, and/or the increase is due to the observed increase in workpiece surface area.

The corrosion resistance experiment of BF_3 on carbon was conducted as follows: Starting with a virgin sample (11.004 g) of graphite-G, baked in He at $1750^\circ C$ for min, a sequence of four 48-min exposures at $1500^\circ C$ was carried out at $P(BF_3) = 20$ Torr and a flow of 1 lpm. The resulting sequence of incremental losses in milligrams is 10.1, 6.3, 5.4, and 3.0. Thus we can expect a corrosion rate of at least a factor of seven, smaller than that of CF_4. Table 4 shows corrosion flux of the 3 RAP agents considered in this study. Note that the resulting ratio-of-corrosion rate $SF_6:CF_4:BF_3$ is 15:1:0.14.

Table 4. Corrosion Flux (k) at $1500^\circ C$ for SF_6, CF_4, BF_3

RAP Agent	k (mg-cm^{-2}-min^{-1}-Torr^{-1})
SF_6	1.5×10^{-2} (one run virgin sample)
CF_4	10.0×10^{-4} (non virgin)
BF_3	1.4×10^{-4} (non virgin)

T6030

27

CONCLUSIONS

It appears that of the three gases considered as secondary RAP, BF_3 is the most suitable for scale up of high-purity alkaline earth fluoride single crystals. BF_3 is the most reactive to H_2O, yielding HF even at room temperature. Therefore, a lower concentration is required to maintain a low RAP index. Moreover, BF_3 seems to be less reactive to carbon than the other two gases, and appears to passivate the carbon surface since incremental loss of carbon decreases with exposure time.

REFERENCES

1.   R.C. Pastor and K. Arita, Mat. Res. Bull. <u>10</u>, 493 (1975).

2.   R.C. Pastor and K. Arita, Mat. Res. Bull. <u>11</u>, 1037 (1976).

AR COATINGS FOR 2 TO 6 μm FLUORIDE WINDOWS

E. Rudisill, J.A. Harrington, and M. Braunstein

Hughes Research Laboratories
Malibu, California 90265

ABSTRACT

We report on an exploratory development program which has the goal of providing high-performance antireflection coatings on single crystal and polycrystalline alkaline earth fluoride laser window materials for DF laser wavelengths. The goal in preparation of these coatings is to achieve absorption losses of less than 0.01% for each coated surface at 3.8 μm. We discuss those material properties that are important for this application and present theoretical coating designs and experimental results of antireflection coatings on CaF_2 and SrF_2 windows. Performance of various two-layer and three-layer antireflection designs using As_2Se_3, As_2S_3, PbF_2, ThF_4, and YbF_3 are discussed.

INTRODUCTION

To prevent degradation of performance in high-power laser systems, the optical coatings must not contribute excessively to absorption. We report results on an exploratory development program with the goal of providing high-performance antireflection coatings on single crystal and polycrystalline alkaline earth fluoride laser window materials for DF laser wavelengths. The goal in preparation of these coatings is to achieve absorption losses of less than 0.01% for each coated surface at 3.8 μm. We discuss those materials properties that are important for this application and present theoretical coating designs and experimental results of antireflection coatings on CaF_2 and SrF_2 windows.

SELECTION AND OPTIMIZATION OF COATING MATERIALS

The choice of coating materials for use on this program were predominantly influenced by the need to minimize absorption in the DF laser band rather than emphasize broadband low-reflectance performance. Examination of a number of antireflection coating designs indicates that the coating materials must have an extinction coefficient, k, in the low 10^{-5} region to meet the 0.01% absorption goal. Based on intrinsic absorption considerations there should be a large number of materials for the 2 to 6 µm region which meet this requirement, even allowing for the inevitable increase of a factor of three to ten, or more, of film absorptions over bulk values. Results presented at the Fifth Laser Window Conference[1] indicate that these low absorptions can probably be achieved in a sufficient variety of materials in the CO laser band. However, there appear to be one or more extrinsic absorption mechanisms that limit bulk and film absorptions in the HF and DF laser bands at unexpectedly high levels. Our approach to this problem, which has been successful in solving similar problems at 10.6 µm, is to synthesize or purify coating materials by a reactive atmosphere process (RAP) while reproducibly controlling coating fabrication processes which maintain purity and stoichiometry of the films.

The thin-film coating materials selected for design and fabrication include As_2Se_3, As_2S_3, PbF_2, ThF_4 and YbF_3. The properties of these state-of-the-art RAP purified materials are discussed in detail elsewhere in these proceedings.[2] To compare optical performance of various coating structures, Table 1 displays several design combinations with their predicted performance at 3.8 µm. All values were calculated from the optical constants listed in the table. The index of refraction, n, is from the literature and the extinction coefficient, k, is from calorimetric evaluation of single-layer films prior to fabrication into AR structures.

Table 1. Theoretical Performance of AR-Coated
CaF_2 at 3.8 μm

Coating Design	Optical Thicknesses at λ = 3.8 μm	Reflectance Per Surface, %	Absorption Per Surface, %
PbF_2/ThF_4	0.25/0.25	0.05	0.006
As_2Se_3/ThF_4	0.454/0.141	0.00	0.004
As_2Se_3/YbF_3	0.448/0.138	0.00	0.052
As_2S_3/ThF_4	0.063/0.351	0.00	0.007
As_2S_3/YbF_3	0.063/0.352	0.00	0.099
$As_2Se_3/PbF_2/As_2Se_3$	0.132/0.186/0.079	0.003	0.001
$As_2S_3/PbF_2/As_2S_3$	0.25/0.109/0.103	0.002	0.002

	As_2S_3	As_2Se_3	PbF_2	YbF_3	ThF_4
n	2.41	2.82	1.74	1.57	1.5
k	7×10^{-6}	3×10^{-6}	6×10^{-6}	3.5×10^{-4}	2.2×10^{-5}

T6030

31

EXPERIMENTAL RESULTS

Optically polished CaF_2 and SrF_2 substrates were used to evaluate coating performance of the two-layer and three-layer designs discussed in the previous section. Deposition was accomplished by evaporation from resistance-heated sources in both turbomolecular and oil-pumped systems at 10^{-6} Torr.

The DF laser optical absorption results of these structures is compared with the predicted values in Table 2. Of the two-layer designs, the "baseline" PbF_2/ThF_4 structure satisfies the performance goal of 0.01% per surface absorption. This was accomplished by deposition at $200^{\circ}C$ of HRL's unique RAP purified starting materials. The two-layer structures with arsenic compounds are limited to substrate temperatures below $100^{\circ}C$, but to maintain ultralow absorption in the fluoride coatings, elevated substrate temperatures are required. Therefore, these coating structures do not realize their predicted absorption values. The large absorption in the YbF_3 compared with the ThF_4 design is associated with the absence of the unique RAP purification of the YbF_3 starting material.

Both three-layer structures, although also limited in substrate deposition temperature, have the advantage of placing a thin fluoride layer in the position of minimum electric field,[3] maintaining overall ultralow absorption.

The importance of the RAP purification is again illustrated with the three-layer structures. The $As_2S_3/PbF_2/As_2S_3$ design meets the performance goal, yielding 0.008% per surface absorption. The $As_2Se_3/PbF_2/As_2Se_3$ design, with a predicted lower absorption, used an earlier vintage of RAP purified PbF_2. As can be seen from Table 2, this structure, although low in absorption, has not satisfied the 0.01% absorption goal.

In conclusion, a two-layer PbF_2/ThF_4 and a three-layer $As_2S_3/PbF_2/As_2S_3$ AR coating design have been fabricated with DF laser absorption losses of 0.01% per surface.

32

Table 2. Experimental AR Coating Absorption at DF Wavelengths

Substrate		Absorption		Length, cm	Coating		
Material	Number	Uncoated $\beta(cm^{-1}) \times 10^4$	Coated $\beta(cm^{-1}) \times 10^4$		AR Design	Absorption/Surface, %	
						Experimental	Predicted
CaF_2	FC-10-0	3.24	5.02	0.894	$As_2S_3/PbF_2/As_2S_3$	0.008	0.002
CaF_2	FC-12-0	4.44	13.0	1.018	$As_2Se_3/PbF_2/As_2Se_3$	0.044	0.001
CaF_2	FC-17-H	6.46	41.8	0.890	As_2Se_3/YbF_3	0.157	0.052
CaF_2	FC-01-0	4.30	63.5	0.850	As_2S_3/YbF_3	0.252	0.099
SrF_2	1863	7.08	33.0	0.633	As_2Se_3/ThF_4	0.082	0.004
SrF_2	1839	6.61	22.7	0.627	As_2S_3/ThF_4	0.050	0.007
SrF_2	1859	4.87	8.27	0.835	PbF_2/ThF_4	0.014	0.006

T6030

REFERENCES

1. P. Kraatz et al., "Absorption of Coated Alkaline Earth Fluoride Windows at CO Laser Wavelengths," Proc. 5th Annual Conf. on IR Laser Window Materials (1976) pp. 315-328.

2. J.A. Harrington et al., "Coating Materials Evaluation for HF Laser Optical Components," these proceedings.

3. M. Braunstein et al., "Low Absorption Antireflection Coatings for KCL," Proc. 5th Annual Conf. on IR Laser Window Materials (1976) pp. 135-142.

LOW LOSS 9.27 μm AR COATINGS FOR KCl

D.E. Zuccaro
Hughes Research Laboratories
Malibu, California 90265

and

J.A. Detrio
University of Dayton Research Institute
Dayton, Ohio 45469

ABSTRACT

Low loss 9.27 μm antireflection coatings for polycrystalline KCl consisting of ZnSe/KCl/ZnSe, As_2S_2/KCl/As_2S_3, As_2Se_3/KCl/As_2Se_3 and As_2Se_3/NaF/As_2Se_3 were deposited under ultra high vacuum (UHV) conditions. Single layer films of As_2S_3 and As_2Se_3 were produced to establish the optical constants of these materials.

The films were analyzed at both 9.27 and 10.6 μm for optical absorption losses and for laser damage threshold. The 9.27 μm absorption of the substrates was about 2.5 greater than at 10.6 μm. A similar situation was observed in the 9.27 and 10.6 μm coating absorptions. The 9.27 μm absorption losses were 0.04, 0.07, 0.09, and 0.03 percent per surface for the three layer AR coatings.

A strong 9.0 μm absorption band associated with an oxide impurity in some of the As_2Se_3 caused an increase in the 9.27 μm absorption of coatings made with this material.

INTRODUCTION

Low loss 9.27 μm antireflection (AR) coatings for polycrystalline KCl were deposited under ultra-high vacuum (UHV) conditions. Three layer AR coatings of ZnSe/KCl/ZnSe, As_2S_3/KCl/As_2S_3, As_2Se_3/KCl/As_2Se_3

and As_2Se_3/NaF/As_2Se_3 were studied. The minimum values of 9.27 µm absorption were 0.043, 0.069, 0.090 and 0.033 percent per surface, respectively. Representative samples were subjected to laser damage threshold measurements at 9.27 and 10.6 µm. In addition to the three layer films, single layer films of As_2S_3 and As_2Se_3 were produced to establish the optical properties of these materials.

Most of the films were analyzed at both 9.27 and 10.6 µm for optical absorption losses. We found the 9.27 µm absorption of the polycrystalline KCl substrates to be about 2.2 times larger than the 10.6 µm absorption. A similar situation was observed in the 9.27 and 10.6 µm absorption of the coated samples. A strong 9.0 µm absorption band, which was observed in some of the films containing As_2Se_3 and As_2S_3, was associated with arsenic oxide impurity in the material.

EXPERIMENTAL

The films were deposited in an all-metal UHV system that is sputter ion and titanium sublimation pumped. After a 200°C bake out, the system has a base pressure of 3×10^{-10} Torr when empty and about 2×10^{-9} Torr when loaded with samples and materials. The 3.8 cm diameter samples of polycrystalline KCl are mounted in a stainless steel holder which can be rotated into position as well as flipped over. Thus, a set of four samples is individually coated on both surfaces during a single run. The film thickness is determined by means of a transmission optical monitor system. The residual gases and the gases evolved during the film deposition are monitored with a quadrupole mass spectrometer.

Focused laser damage measurements were performed at 10.6 µm using the same apparatus employed in previous work.[1] High power testing with spot sizes of near 1 cm^2 was done at 10.6 and 9.28 µm with an Electro Aerodynamic Laser operating in a master oscillator-power amplifier configuration. The wavelength was varied by the use of a grating mounted in the Coherent Radiation Laboratories Model 41 laser oscillator. The samples were mounted just ahead of the focus of a 2 m radius mirror. The beam profile was not Gaussian, but every effort was made to maintain a constant beam profile between the two wavelengths. The power was

measured with a total capture ballistic calorimeter and each irradiation was monitored with a fast response detector.

RESULTS

AR coatings of ZnSe/KCl/ZnSe were the first type studied because in a previous program this coating had low 10.6 μm absorption values. Similar results were obtained at 9.27 μm for these coatings. The lowest value was 0.043 percent per surface (see Table 1). These films exhibited a tendency to craze after several months. This is believed to be due to difference in the expansion coefficients of KCl and ZnSe. As a result, the studies were directed to As_2S_3 and As_2Se_3 which have expansion coefficients more nearly like KCl.

The first set of AR coatings of As_2Se_3/KCl/As_2Se_3 all had a pronounced absorption band at 9 μm. While the 10.6 μm absorption was in the range of 0.039 to 0.05 percent per surface, the 9.27 μm absorption was 0.32 to 0.35 percent per surface. The absorption band was traced to arsenic oxide. New As_2Se_3 material, which had a low oxide level, was produced. Using this material, we obtained a coating with an absorption of 0.090 percent per surface at 9.27 μm and 0.017 percent per surface at 10.6 μm (see Table 1).

The As_2S_3/KCl/As_2S_3 coating had an absorption of 0.069 percent per surface at 9.27 μm and the As_2Se_3/NaF/As_2Se_3 coating had an absorption of 0.033 percent per surface.

Early in the program, it was observed that the 9.27 μm absorption of the polycrystalline KCl substrates was larger than previous measurements of 10.6 μm absorption. In 34 samples, the absorption was measured at both points. The average ratio of 9.27 to 10.6 μm absorption was 2.2. The coatings exhibit a similar behavior in absorption.

The power density reported for the broad beam damage thresholds is an average value obtained by attempting to weigh the power distribution by the area covered. When the EAL was driven to operate nominally at 9.28 μm the laser emission occurs predominantly from the R18 transition centered at near 9.28 μm. Other lines at 9.26 and 9.27 μm are also observed. The beam profile was obtained by examining burn patterns in

Table 1. Coating Results

Sample No.	Coating Design Material/Thickness, m			9.27 μm Absorption, %			10.6 μm Absorption, %		
				Substrate	Total	Coating	Substrate	Total	Coating
1281-3-1	ZnSe 1.145	KCl 0.406	ZnSe 0.425	0.156	0.242	0.043	(a)	(a)	
9-12-5-4	As_2S_3 0.488	KCl 1.145	As_2S_3 0.279	0.040	0.177	0.069	(a)	(a)	
155-5-12-24-10-2	As_2Se_3 0.881	KCl 0.504	As_2Se_3 0.488	0.080	0.261	0.090	0.065	0.099	0.017
174-5-30-9-1	As_2Se_3 0.641	NaF 0.557	As_2Se_3 0.414	0.167	0.233	0.033	0.055	0.382	0.16
9-16-5-1	As_2S_3 5.82	(One Side Only)		0.240	0.361	0.12	(a)	0.144	<0.14
174-5-29-9-4	As_2Se_3 3.35	(One Side Only)		0.045	0.099	0.045	0.028	0.056	0.028

(a)Not measured.

T6030

38

plexiglass. The burn patterns were made as a function of power and the full width at half maximum depth was measured on an optical comparator.

The beam profile can best be described as a witch's hat... a central peak surrounded by a region of amplified edge diffraction. Every reasonable attempt was made to ensure that the beam profile was the same at 10.6 and 9.28 μm. In spite of these efforts the beam, although superficially the same, was different at the two wavelengths, especially within the central hot spot. The average power density over the entire beam (central peak and brim of the witch's hat) is nearly equal with a total area of 1.5 cm^2. The central hot spot was 0.17 and 0.06 cm^2 at 10.6 and 9.28 μm, respectively.

The focused beam tests were performed at 10.6 μm with a Gaussian beam profile of 0.1 cm diameter. Both n-on-1 and 1-on-1 tests were made on a 4 by 4 array of test points spaced 3 mm apart. Some 3.5 cm diameter samples were tested with a 9 point test array. Some UHV and non-UHV samples fabricated under a DARPA program were also tested. The results are presented in Table 2. As the damage level is variable in the focused beam tests, we present the power level at which damage first was observed and the maximum power level at which there was at least 50 percent survival.

The largest group of samples tested were AR coatings of $As_2Se_3/KCl/As_2Se_3$. The first group (9-8-6-1, 8-3-6-3, and 9-11-6-2) had a very high 9.27 μm absorption and a 9 μm absorption band which indicated the presence of oxide impurity in the As_2Se_3 films. This group had a low damage threshold. The second group (129-1-49-1, 129-2-49-2, 155-5-12-24-10-2 and 64-25-10-3), which had much lower 9.27 μm absorption, were undamaged at 10.6 μm and damaged at the maximum level at 9.27 μm. The third group (78-13, 70-3 and 78-5) were non-UHV samples which had significantly larger absorption at 9.27 and 10.6 μm. Two samples were damaged at low levels and one was undamaged at the maximum level. Two single layer films of As_2Se_3 were tested. One was undamaged at 10.6 μm and the other failed at 3.5 kW/cm^2 at 9.27 μm. Although there are fewer As_2S_3 samples, these coatings exhibited a much higher damage resistance. Of three samples of AR coatings of $As_2S_3/KCl/As_2S_3$, No. 82-8 was damaged at only

Table 2. Laser Damage Results

Coating	Sample No.	Coating Absorption % Per Surface, μm		Power Level (kW/cm²)				Remarks
		9.27	10.6	Focused Minimum Damage	10.6 μm Maximum No Damage	Broad Beam 10.6	9.27	
As_2Se_3/KCl/As_2Se_3	9-8-6-1	0.35	0.054	32[a]	108			Significant 9 μm absorption band
	8-3-6-3	0.36	0.048	49[a]	108			Significant 9 μm absorption band
	9-11-6-2	0.32	0.040				2.6	Significant 9 μm absorption band
	129-1-49-1	0.047	0.026			7.5		
	129-2-49-2	0.039	0.068				7.5	
	155-5-12-24-10-2	0.090	0.017			7.5		
	64-25-10-3	0.105	0.033			7.5		
	78-13	0.37	0.43			5.3		Non-UHV Sample-DARPA
	70-3	0.15	0.21				3.5	Non-UHV Sample-DARPA
	78-5	0.20	0.14			7.5		Non-UHV Sample-DARPA
1λ As_2Se_3	150-4-15-7-3	0.13	0.016			7.5		
	174-5-29-9-4	0.045	0.028				3.5	
As_2S_3/KCl/As_2S_3	82-8	(b)	(b)	109	109			Non-UHV Sample-DARPA-1 yr old
	63-11	0.23	0.072	109	109	7.5		Non-UHV Sample-DARPA
1/2λ As_2S_3	152-3-46-2	(b)	0.25	109	109			
	8-1-5-3	0.19	(b)	109	109		7.5	
	8-4-5-2	0.14	(b)			7.5		
As_2Se_3/NaF/As_2Se_3	174-5-30-9-1	0.033	0.16			1.8		
	174-8-33-9-2	0.079	0.27				4.5	
ZnSe/KCl/ZnSe	1274-2-3	0.15	(b)	14	109			
	1277-2-2	0.03	(b)	32	109			
	9-15-4-2	0.22	(b)	32	109			
	109-RF4	(b)	0.30	30	78			2.5 cm diameter UHV Sample - DARPA - 8 months old
	109-RF5	(b)	0.20	108	109			2.5 cm diameter UHV Sample - DARPA - 8 months old
	146-10	(b)	0.26	42	86			2.5 cm diameter UHV Sample - DARPA - 8 months old
ZnSe/ThF_4/ZnSe	67-B3	(b)	0.05	20	108			2.5 cm diameter UHV Sample - DARPA - 1 yr old
	129-8	(b)	0.04	20	108			2.5 cm diameter UHV Sample - DARPA - 1 yr old
	95-B2	(b)	0.07	32	108			2.5 cm diameter UHV Sample - DARPA - 1 yr old
	67-A3	(b)	0.20	20	39			2.5 cm diameter UHV Sample - DARPA - 1 yr old
As_2Se_3/ThF_4/As_2Se_3	82-6	(b)	(b)	49[a]	109			Non-UHV Sample - DARPA

[a] Films cleanly ablated - no substrate damage.

[b] Not measured.

T6030

40

one point at the highest power level, No. 63-11 was undamaged in both the focused and broad beam 10.6 μm tests, and sample 8-4-5-2 was damaged at 3.5 kW/cm^2 in the broad beam 9.27 μm tests. The three samples of single layer As_2S_3 films were undamaged at all tests.

The two samples of films containing NaF had high 10.6 μm absorption. These samples exhibited low damage threshold. In general, the films containing ZnSe exhibited a few sites which were damaged at low power levels and a larger number of sites which could not be damaged at the highest power levels.

While the number of samples and tests are not sufficient to establish precise values of laser damage threshold, it is possible to infer the following conclusions. The As_2S_3, which is less sensitive than As_2Se_3 to the vacuum environment during deposition, has the highest damage threshold (7.5 kW/cm^2 broad beam and 10.9 kW/cm^2 focused) of the materials tested. The As_2Se_3 films which were deposited under UHV conditions and were oxide free also had a similar damage threshold.

ACKNOWLEDGMENTS

REFERENCE

1. Detrio, J.A., Petty, R.D., Ohmer, M.C., and Swenson, O.F., Laser Induced Damage in Optical Materials: 1976 NBS Special Publication 462, p. 283.

A COMPARISON OF UHV AND CONVENTIONAL VACUUM-DEPOSITED OPTICAL COATINGS

D. Zuccaro, E. Rudisill, M. Braunstein

Hughes Research Laboratories
Malibu, California 90265

ABSTRACT

Three-layer antireflection (AR) coatings of $As_2S_3/KCl/As_2S_3$ and $As_2Se_3/KCl/As_2Se_3$ and single-layer films of As_2S_3 and As_2Se_3 were deposited under ultrahigh vacuum (UHV) and conventional vacuum conditions. The UHV samples exhibited absorption losses that were significantly lower than the films produced under conventional vacuum conditions. The absorption at 10.6 μm was 0.012 and 0.026% per surface for the $As_2S_3/KCl/As_2S_3$ and $As_2Se_3/KCl/As_2Se_3$ AR films deposited in UHV.

Impurities including oxides, water, petroleum ether, and acetic acid were identified in the As_2S_3 and As_2Se_3 by means of mass spectrometry. They were observed to have a profound affect on the optical properties of the films.

INTRODUCTION

The vacuum environment present during the deposition of optical coatings containing either As_2S_3 or As_2Se_3 has a pronounced affect on the film absorption. In this study, three-layer antireflection (AR) coatings of $As_2S_3/KCl/As_2S_3$ and $As_2Se_3/KCl/As_2Se_3$ and single-layer coatings of As_2S_3 and As_2Se_3 were deposited under either ultrahigh vacuum (UHV) or conventional vacuum conditions.

The films containing As_2Se_3 deposited under conventional vacuum conditions exhibited a significantly higher 9.28 and 10.6 μm absorption

than similar films deposited under UHV conditions. For the As_2S_3 films, the 9.28 µm absorption effect was similar, while the 10.6 µm effect was small. The increased absorption is associated with oxidation of the arsenic compounds by the residual gases.

Impurities in the As_2S_3 and As_2Se_3 were found to have a pronounced effect on the optical properties of the materials and the films made from these materials. Careful control of the purity of the starting materials and of the reaction system were necessary to produce oxide-free As_2S_3 and As_2Se_3. This is essential as the several forms of arsenic oxide have strong absorption bands in the 10 µm region.

EXPERIMENTAL

The UHV system used in this study is all metal and is sputter-ion and titanium-sublimation pumped. After a bakeout at $250^{\circ}C$, the system has a base pressure of about 1×10^{-10} Torr when empty, and about 1×10^{-9} Torr when loaded with samples and film materials. The 2.5 cm diameter KCl samples are mounted in a stainless-steel support that can be rotated and flipped so that it is possible to individually coat four samples on both surfaces during a run. A Finnigan quadrupole mass-spectrometer is used to analyze the residual gas and the gases evolved during the deposition of the films.

The conventional vacuum system is turbomolecular pumped and contains a liquid nitrogen cooled Meisner trap. The base pressure of the system is in the low 10^{-7} Torr range.

RESULTS

Of the two types of AR coatings tested, the $As_2Se_3/KCl/As_2Se_3$ films exhibited the greater sensitivity to vacuum environment. Although there were some differences in film thickness, source of As_2Se_3, and substrate deposition temperature, they were not great enough to account for the observation that the average 10.6 m absorption of the conventional system samples was five times larger than that of the UHV samples and that the average 9.28 µm absorption was eight times larger. These data are summarized in Table 1. The lowest values were obtained with sample

44

Table 1. $As_2Se_3/KCl/As_2Se_3$ AR Coatings on KCl

Sample No.	Source As_2Se_3	9.28 μm Absorption			10.6 μm Absorption		
		Substrate, %	Coated Sample, %	Coating % Surface	Substrate, %	Coated Sample, %	Coating % Surface
DEPOSITED UNDER CONVENTIONAL VACUUM CONDITIONS							
151-1	HRL-1	0.061	0.632	0.29	0.017	0.342	0.16
78-13	HRL-1	0.060	0.802	0.37	0.022	0.886	0.43
78-5	HRL-1	0.094	0.501	0.20	0.035	0.315	0.14
70-3	Vacuum Outgassed HRL-1	0.057	0.358	0.15	0.021	0.437	0.21
164-2-11	ACC	(a)	0.605	<0.30	0.094	0.508	0.21
DEPOSITED UNDER UHV CONDITIONS							
164-5A-10-48-3	ACC	0.137	0.211	0.037	(a)	0.059	<0.030
164-5A-11-48-4	ACC	0.111	0.148	0.019	(a)	0.045	<0.022
129-1-49-1	ACC	0.098	0.094	<0.047	0.026	0.079	0.026
129-2-49-2	ACC	0.071	0.148	0.039	0.021	0.156	0.068

(a) Not measured

NOTE: The predicted absorption for these coatings is 0.02% per surface.

T6030

45

164-5A-11-48-4, which had a 9.28 μm coating absorption of 0.019% per surface and a 10.6 μm coating absorption of less than 0.022% per surface.

In the case of As_2S_3/KCl/As_2S_3 AR coatings, the conventional vacuum samples had an average coating absorption at 9.28 μm about three times greater than did the UHV samples and about 1.3 times larger at 10.6 μm. These data are presented in Table 2. The lowest values were observed in sample 147-10-52-3, which had a 10.6 μm coating absorption of 0.012% per surface and a 9.28 μm value of less than 0.07% per surface.

Similar results were observed in single-layer films. In Table 3, a comparison of the non-UHV films and the UHV films that were formed from HRL-1 As_2Se_3 shows a significant vacuum dependence in the 9.27 and 10.6 μm absorption. A similar situation exists in the As_2S_3 case which is presented in Table 4.

Impurity effects were observed in the UHV study of single-layer films of As_2S_3 and As_2Se_3 made from materials obtained from different sources. In the worst case, mass spectrometric analysis of gases evolved during the deposition of samples 152-1-46-1 and 152-3-46-2 indicated the presence of water, hydrogen sulfide, arsenic oxide, acetic acid, and petroleum ether. While these impurities were removed by reaction of the As_2S_3 in CS_2, the films produced from this "cleaned" As_2S_3 had an absorption that was three times higher. Measurement of the transmission spectra of the films and of thin plates of the bulk material showed that high absorption values were related to the presence of a strong 9 μm absorption band which is caused by arsenic oxide. Evidence for the vacuum clean-up of As_2Se_3 is shown in Table 5, where we see the improvement in absorption values from the first sample (45-BF8-48-1) to the last sample (164-5A-11-48-4) in a single run.

ACKNOWLEDGMENT

Table 2. $As_2S_3/KCl/As_2S_3$ AR Coatings on KCl

Sample No.	9.28 m Absorption			10.6 m Absorption		
	Substrate, %	Coated Sample, %	Coating % Per Surface	Substrate, %	Coated Sample, %	Coating % Per Surface
DEPOSITED UNDER CONVENTIONAL VACUUM CONDITIONS						
63-11	0.043	0.507	0.23	0.019	0.163	0.072
147-3-51-1	0.030	0.892	0.43	0.038	0.142	0.052
147-1-51-2	0.027	0.900	0.44	0.037	0.192	0.078
147-5-51-3	(a)	0.674	0.34	0.068	0.158	0.045
147-4-51-4	(a)	0.833	0.42	0.046	0.184	0.069
DEPOSITED UNDER UHV CONDITIONS						
147-6-50-1	(a)	1.043	0.52	0.067	0.276	0.104
147-8-50-2	0.260	0.159	0.08	0.086	0.154	0.034
147-7-50-3	0.045	0.662	0.31	0.028	0.088	0.030
147-13-50-4	0.026	0.178	0.076	0.015	0.088	0.036
152-11-52-1	(a)	0.153	0.08	0.055	0.144	0.045
147-12-52-2	(a)	0.204	0.10	0.059	0.058	0.029
147-10-52-3	(a)	0.138	0.07	0.042	0.066	0.012
152-9-52-4	(a)	0.247	0.14	0.041	0.206	0.083
(a)Not measured.						

T6030

47

Table 3. Single Layer As_2S_3 Films on KCl

Sample No.	Source of As_2Se_3	Film Thickness, μm	9.28 μm Absorption			10.6 μm Absorption		
			Substrate, %	Sample, %	Coating % Per Surface	Substrate, %	Sample, %	Coating % Per Surface
DEPOSITED UNDER CONVENTIONAL VACUUM CONDITIONS								
70-6	HRL-1	3.31	(a)	0.46	<0.46	0.209	0.256	0.23
70-4	HRL-1	1.74	(a)	0.64	<0.64	(a)	0.70	<0.70
65-11	HRL-1	1.64	0.040	0.26	0.22	0.18	0.16	0.14
63-6	HRL-1	0.96	(a)	0.47	<0.47	(a)	0.25	<0.25
DEPOSITED UNDER UHV CONDITIONS								
45-BF8-48-1	ACC	1.69	0.14	0.62	0.48	(a)	0.16	<0.16
164-2-1-48-2	ACC	1.67	0.065	0.175	0.11	(a)	0.14	<0.14
67-A1-49-3	ACC	1.01	0.023	0.109	0.086	0.018	0.060	0.042
71-12-11-1	HRL-1	1.69	0.064	0.182	0.059	0.014	0.054	0.020
71-7-11-2	HRL-1	3.73	0.054	0.180	0.063	0.015	0.051	0.018
AFML SAMPLES DEPOSITED UNDER UHV CONDITIONS								
150-4-15-7-3	HRL-1	3.38	0.098	0.226	0.129	0.097	0.113	0.016
150-5-13-8-4	HRL-1	3.45	0.075	0.164	0.090	0.073	0.052	<0.052
174-5-29-9-4	HRL-1	3.37	0.045	0.099	0.045	0.028	0.056	0.028
174-8-31-9-3	HRL-1	3.44	0.107	0.219	0.026	0.023	0.060	0.019
Minimum value of β			1.13 cm^{-1}			0.40 cm^{-1}		
Minimum value of k			8.3 x 10^{-5}			3.4 x 10^{-5}		

(a) Not measured

T6030

48

Table 4. Single Layer As_2S_3 Films on KCl

Sample No.	Source of As_2S_3	Film Thickness, μm	9.28 μm Absorption			10.6 μm Absorption		
			Substrate, %	Coated Sample, %	Coating % Per Surface	Substrate, %	Coated Sample, %	Coating % Per Surface
DEPOSITED UNDER CONVENTIONAL VACUUM CONDITIONS								
2577	HRL-1	3.96	0.031	0.284	0.28	(a)	(a)	--
152-3-46-2	ACC	2.14	0.08	0.33	0.25	(a)	(a)	--
144-D10-47-1	ACC Reacted in Cs_2	1.98	0.12	1.00	0.88	(a)	(a)	--
152-5-47-2	ACC Reacted in Cs_2	1.98	0.09	0.97	0.88	(a)	(a)	--
71-9-11-3	HRL-2	2.33	0.048	0.301	0.13	0.015	0.150	0.067
71-8-11-4	HRL-2	4.67	0.042	0.449	0.20	0.014	0.251	0.12
AFML SAMPLES — UHV DEPOSITED								
9-16-5-1	HRL-1	5.82	0.240	0.361	0.12	(a)	0.087	<0.09
8-4-5-2	HRL-1	2.08	0.185	0.325	0.14	(a)	(a)	--
8-1-5-3	HRL-1	2.08	0.081	0.270	0.19	(a)	(a)	--
Minimum value of β			2.0 cm^{-1}			2.2 cm^{-1}		
Minimum value of k			1.5×10^{-4}			1.9×10^{-4}		

(a) not measured.

T6030

Table 5. Evidence for Vacuum Clean-Up of As_2Se_3

		Coating Absorption	
		9.28 μm	10.6 μm
45–BF8–48–1	1/2λ As_2Se_3	0.48	<0.16
164–2–1–48–2	1/2λ As_2Se_3	0.11	<0.14
164–5A–10–48–3	As_2Se_3/KC1/As_2Se_3	0.037	<0.030
164–5A–11–48–4	As_2Se_3/KC1/As_2Se_3	0.019	<0.022

COATING MATERIALS EVALUATION FOR
HF LASER OPTICAL COMPONENTS

J.A. Harrington, E. Rudisill, and J.L. Bowers

Hughes Research Laboratories
Malibu, California 90265

ABSTRACT

Materials for use as low-loss optical components on high-power HF chemical lasers have received increasing interest as system needs continue to develop. To design suitable antireflection (AR) and enhanced reflectivity coatings for windows and mirrors, a study has been made of the fundamental optical properties of candidate materials for use at 2.8 μm. The materials studied, which include PbF_2, LiF, YbF_3, NaF, ThF_4, As_2S_3, Si, MgO, and Al_2O_3, were deposited as single-layer films on calcium fluoride substrates. The film absorptions extracted from a comparison of coated and uncoated substrates indicated that the As-glasses and some fluorides exhibited absorptions near 0.01% surface ($\beta \sim 1$ cm^{-1}) while oxides remained significantly higher. A comparison will also be made with similar measurements at DF laser wavelengths.

INTRODUCTION

The development of low-loss antireflection (AR) and enhanced reflection dielectric coatings requires a detailed knowledge of the optical constants n and k for a variety of materials that are suitable for use at the infrared laser wavelength of interest. At HF laser wavelengths, there have been only limited studies[1] of the optical absorption in candidate window materials with essentially no data presented on

coatings themselves. This study is, therefore, aimed at providing a more detailed analysis of the thin film properties at 2.8 μm for a wide selection of materials which might be incorporated in the design of optical components for HF laser systems.

A fundamental consideration in any basic study of coating materials properties, is the absorption index k for the film. At 2.8 μm, where absorption by OH^- can be particularly troublesome, it is expected that certain materials may have rather high k-values. In fact, our measurements have shown that the absorption in most single-layer coatings is greater at HF than at the DF chemical laser wavelengths. Nevertheless, certain materials such as the As-glasses, ZnSe, and some fluorides have k-values in the low 10^{-5} range at 2.8 μm. This is comparable to some of the best materials at 10.6, 5.3, and 3.8 μm and thus represents a good starting point for the development of low absorbing dielectric stacks.

EXPERIMENTAL PROCEDURE

The substrates used for the HF coating study were 3.8 cm in diameter by 1 cm thick single crystal CaF_2 obtained from Harshaw and Optovac. The samples were polished on Swiss pitch and Linde A. Just prior to measurement, each sample was cleaned by lightly rubbing with a solution of precipitated $CaCO_3$, followed by a rinse in deionized water, a wipe with propanol soaked cotton, and finally, a soak in a freon degreaser. It was found that this polishing and cleaning procedure yielded the most uniform absorption results for our uncoated substrates.

The coating deposition was carried out in a turbomolecular pumped vacuum of 10^{-6} Torr. Resistance heated Ta and Mo sources were used for all depositions except Si, Al_2O_3, and MgO in which an E-gun and vitreous carbon crucibles were used. Substrate temperatures ranged from 50 to 200°C. All films studied were single layer, with optical thickness λ/2 or 1 λ at 3.8 μm. The absorptances for the films were corrected for non-half wavelength reflection losses at 2.8 μm.

Measurement of the absorption index k for the films studied was carried out using a small cw HF chemical laser and a vacuum calorimeter. Absorptance data[2] for the films was obtained by comparison of coated and

52

uncoated substrates. The absorption index k was then calculated from the absorptance in the film and the known index of refraction of the film material. Finally, the absorption coefficient for the film β_{film} was computed from $\beta_{film} = 4\pi k/\lambda$.

RESULTS AND ANALYSIS

A wide variety of single-layer, fluoride, oxide, and semiconducting films was studied at 2.8 μm. A list of the different coating materials investigated is given in Table 1 along with the corresponding coated and uncoated substrate absorptances (βL), the k-values, and the absorption coefficient of the film. From Table 1 it can be seen that most fluorides, ZnSe, and the As-glasses have very low k-values while Si and the oxides have rather high k-values. In fact, the absorption in As_2S_3 is lower than the absorption in most films at DF wavelengths and thus this material represents, at $k = 6 \times 10^{-6}$, an absorption index that is one of the lowest measured for any material. The best fluorides to date have been PbF_2 and ThF_4 with k-values in the low 10^{-5} range. Based on these values, a very low absorbing AR or enhanced reflection coating should be possible using an As-glass/PbF_2 or ThF_4 stack. Our results at 3.8 μm on such a combination are included in a companion paper in these proceedings.[3]

The absorption indices contain in Table 1 represent the best coatings to date. To achieve the low values for the fluorides and As-glasses, it has been necessary to purify the starting coating materials. Table 2 indicates for two different coating materials, ThF_4 and As_2S_3, the evolutionary improvement in coating absorption as the purity of the starting material improved. The best fluoride coatings have been produced with Reactive Atmosphere Process (RAP) treated material (PbF_2 and ThF_4) while the As_2S_3 and As_2Se_3 were also grown and purified in our laboratory. The more highly absorbing ThF_4 in Table 2 was manufactured by Cerac while the low value resulted from HRL RAP treated ThF_4. In the case of As_2S_3 shown in Table 2, all starting material was produced by HRL and the data merely indicates the trend toward lower k-values as the coating material continues to improve.

Table 1.   2.8 μm Absorption in Thin Films on
CaF$_2$ Substrates

| Coating | Absorptance x 10^4 | | k x 10^4 | β_{film} (cm^{-1}) |
	Coated	Uncoated		
PbF$_2$	8.07	5.44	0.36	1.62
YbF$_3$	23.00	4.04	3.50	15.70
ThF$_4$	6.82	3.84	0.34	1.53
NaF	19.6	7.03	2.80	12.60
LiF	24.0	4.29	4.00	18.00
LaF$_3$	--	--	--	968
As$_2$Se$_3$	5.80	2.99	0.36	1.62
As$_2$S$_3$	3.56	3.09	0.06	0.27
AnSe	9.47	5.09	1.00	4.50
Si	441	19.4	19	85.3
Al$_2$O$_3$	677	19.4	72	323
MgO	611	24.6	63	283

Table 2.   2.8 μm Absorption in ThF$_4$ and As$_2$S$_3$ Films
on CaF$_2$ Substrates

| Date | Coating | Absorptance x 10^4 | | k x 10^4 | β_{film}(cm^{-1}) |
		Coated	Uncoated		
2/4/77	ThF$_4$	98.5	16.5	9.4	42.2
7/8/77	ThF$_4$	6.82	3.84	0.34	1.53
8/22/77	ThF$_4$	13.4	3.49	1.1	4.94
9/7/77	ThF$_4$	15.84	3.10	1.6	7.18
5/11/77	As$_2$S$_3$	11.7	8.11	0.80	3.6
6/13/77	As$_2$S$_3$	7.68	3.28	0.60	2.69
7/20/77	As$_2$S$_3$	3.56	3.09	0.06	0.27

T6030

54

SURFACE AND BULK ABSORPTION OF WINDOW MATERIALS AT IR LASER WAVELENGTHS

S.D. Allen and J.A. Harrington

Hughes Research Laboratories
Malibu, California 90265

ABSTRACT

The long-bar technique has been used at the CO_2, CO, DF, and HF laser wavelengths to measure the bulk and surface absorption of materials grown in a reactive atmosphere process (RAP). In addition, an investigation of absorption differences in KCl, caused by variations in RAP growth was carried out. The bulk and surface absorption of KCl was measured at 10.6, 9.6, and 9.27 μm in an attempt to identify the source of the absorption band centered at approximately 9.6 μm with one selected sample measured at all the available wavelengths of the CO_2 laser (9.21 μm to 10.8 μm). This same sample was also measured with a CO laser (5.3 μm) and a DF/HF laser (3.8 μm and 2.8 μm) with the latter measurements designed to pinpoint the source of the OH^- absorption band observed at 2.8 μm.

INTRODUCTION

An important aspect of high-power laser window fabrication is the minimization of the losses in the bulk substrate and film coatings. As materials have improved, these losses have been predominantly associated with surface and film absorption. Laser calorimetric techniques were used to measure the often extremely small surface and bulk absorption in state-of-the-art infrared laser window materials. The current sensitivity limit to laser calorimetry appears to be $\beta \leq 10^{-6}$ cm^{-1} for a bulk

absorption coefficient in a long bar, with some crystals at 5.4, 3.8, and 2.8 μm exhibiting absorptions equal to or less than the sensitivity limit of the instrumentation. The requirements are less critical for the measurement of absorption in coatings and surfaces as they usually have absorption coefficient values an order of magnitude or more greater than the bulk crystal substrate. The problem then becomes one of separating the surface (either coated or uncoated) from the total absorption of the crystal. Several variations of the long-bar technique pioneered by M. Hass[1] have been employed in this investigation to measure the bulk and surface absorption of uncoated halide crystals.

The bulk and surface absorption of a KCl bar sample grown under standard conditions was measured as a function of wavelength over the CO_2 laser range. The results show that the higher absorption at 9.27 μm relative to 10.6 μm for KCl window samples is probably a result of the increased surface absorption exhibited at the shorter wavelengths. The bulk absorption coefficient is higher than the predicted multiphonon extrapolation[2] at 9.27 μm but significantly lower than the absorption at 10.6 μm. This sample was also measured at 5.3, 3.8, and 2.8 μm.

EXPERIMENTAL

The CO_2 laser calorimeter system is illustrated in Figure 1. The output of the grating tuned CO_2 laser is folded 180° by two mirrors and focused to a beam size of less than 1 mm with an AR-coated ZnSe lens of 46 cm focal length. A He-Ne alignment laser is folded into the CO_2 beam path by a ZnSe beamsplitter antireflection (AR) coated for 45°. The CO laser calorimeter system is similar in layout and is described elsewhere.[3] The details of the HF/DF laser calorimeter operation can also be found in the literature.[4]

The calorimeter head designed to be used at CO_2, CO, and HF/DF wavelengths is illustrated in Figure 2. The body of the calorimeter is made of aluminum with removable front and back flanges also of aluminum. The windows are mounted on bellows with tilt adjustments in two directions. This enables the operator to align AR-coated windows perpendicular to the laser beam and reduces still further the chance of stray
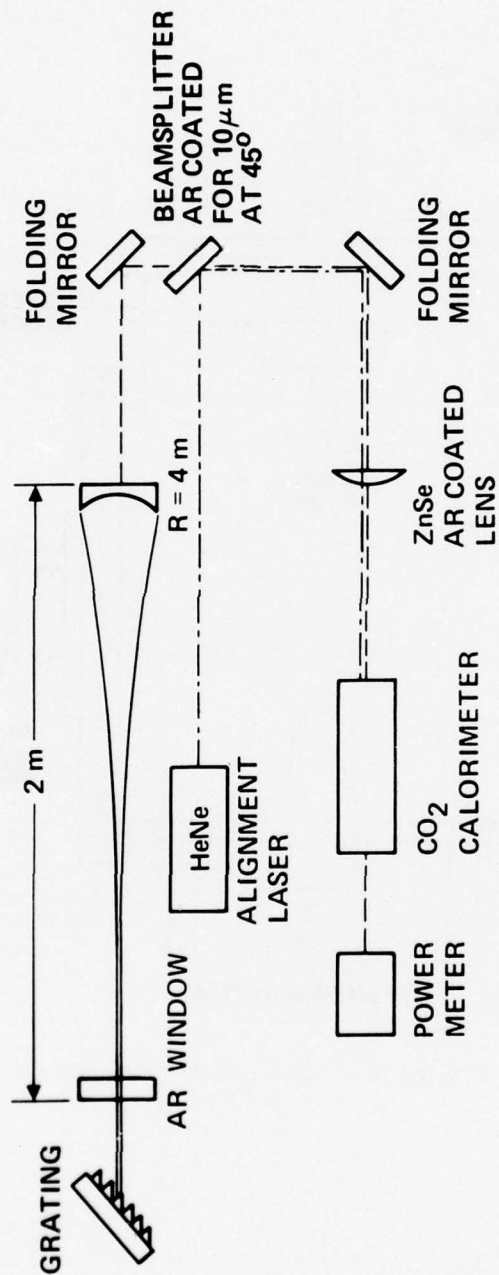
Figure 1. Optical train of the CO_2 laser calorimeter.

6201-5

GRATING

AR WINDOW

2 m

R = 4 m

HeNe
ALIGNMENT
LASER

FOLDING
MIRROR

BEAMSPLITTER
AR COATED
FOR 10μm
AT 45°

FOLDING
MIRROR

ZnSe
AR COATED
LENS

CO_2
CALORIMETER

POWER
METER

57

6201-2

ELECTRICAL
FEEDTHROUGH

REFERENCE
BLOCK

TO
SAMPLE
MOUNT

ADJUSTABLE
WINDOW
MOUNTS

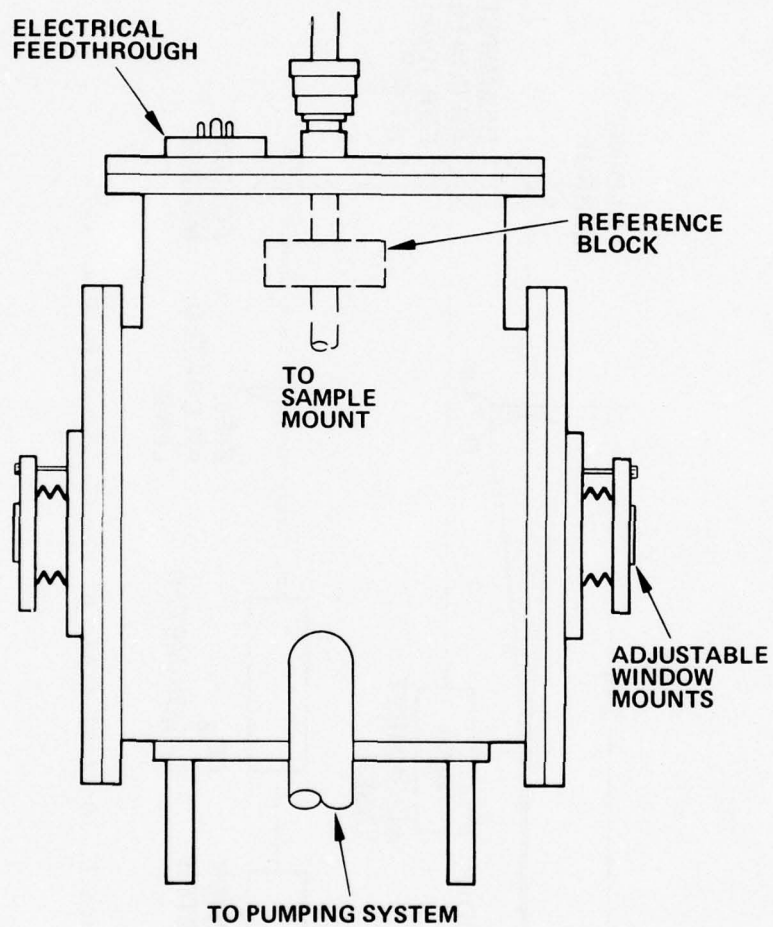TO PUMPING SYSTEM

Figure 2.   Vacuum calorimeter.

58

reflectances hitting the thermocouple. AR-coated windows were used at
5.3 μm, NaCl Brewster angle windows at 10.6 μm, and CaF_2 Brewster angle
windows at 2.8 and 3.8 μm. The sample holder is shown in Figure 3. The
thermocouples are attached to the bar with cyanoacrylic cement and the
bar is mounted on pins or nylon monofilament cradles to minimize heat
losses to the system.

The system is pumped by a high-pressure nitrogen Venturi or a carbon
vane roughing pump and liquid-nitrogen-cooled zeolite sorption pumps.
We decided to use a completely oil-free system to eliminate any possible
contamination of window and sample surfaces from oil backstreaming from
a mechanical pump. This type of pumping system also permits the atmos-
phere in the calorimeter to be carefully controlled for environmental
studies.

The thermocouples are Isonel-insulated 0.005 in. copper/constantan
wire tightly twisted together. The reference thermocouples are embedded
in the brass mounting block as shown in Figure 3. Either a Keithley
Model 150B microvoltmeter or Keithley Model 148 nanovoltmeter was used to
measure the thermocouple voltage.

RESULTS

The results of the bulk absorption measurements at 10.6 μm of three
KCl bars grown in different atmospheres are given in Table 1. These
data were taken on HCl etched bars in an air calorimeter without windows
but with long tubes at the entrance and exit to baffle air currents. The
bar grown in N_2/CCl_4 has approximately the same bulk absorption coefficient
as those grown under the other, standard conditions and the use of nitro-
gen instead of helium as a carrier gas should considerably lower the
scale-up cost of producing RAP halide boules.

RAP grown NaCl boules approximately 4 cm long were measured at 10.6,
9.27, and 5.3 μm. The results are given in the table in Figure 4. With
the exception of sample number 7 which was taken from the end of the
boule, all of the samples exhibit essentially intrinsic absorption levels
at 10.6 μm and approximately three times intrinsic absorption at 9.27 μm.
Since these samples were not long enough to use the two-slope method, the
total absorption is reported.

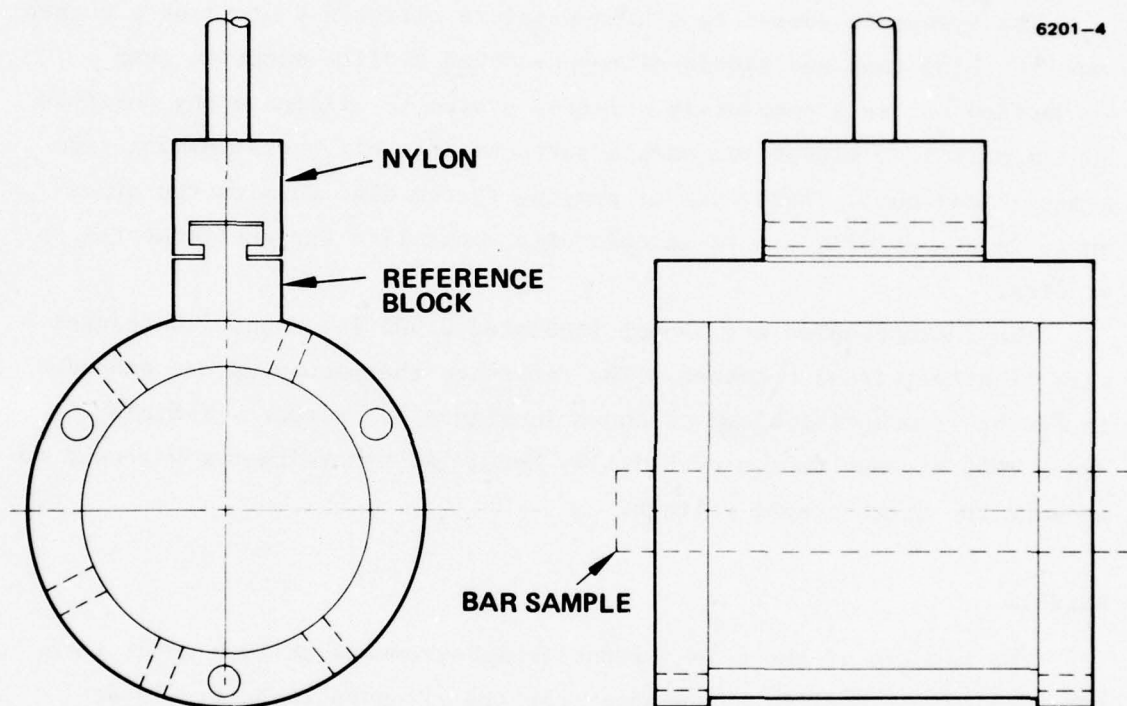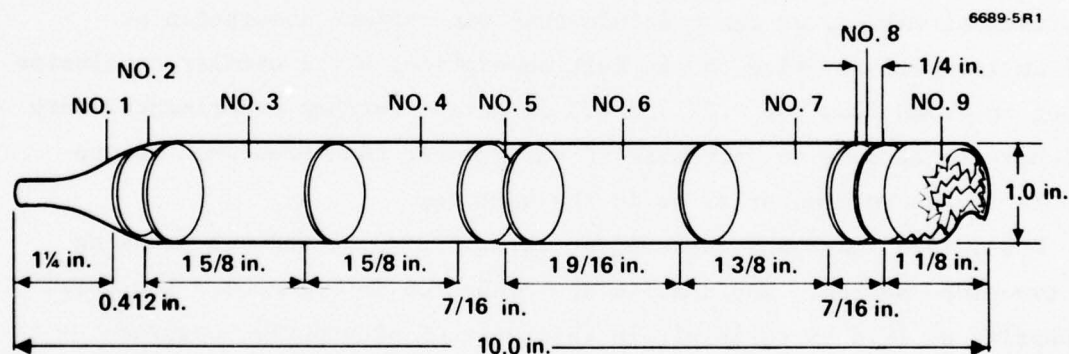Figure 3. Calorimeter mount for long bar samples.

SAMPLE	β_T (10.6 μm)	β_T (9.27 μm)	β_T (5.3 μm)
NO. 3	1.0×10^{-3}	2.6×10^{-4}	
NO. 4	$1.0 \pm 0.2 \times 10^{-3}$	$3.0 \pm 0.1 \times 10^{-4}$	$5 \pm 1 \times 10^{-5}$
NO. 6	1.0×10^{-3}	4.1×10^{-4}	
NO. 7	$1.4 \pm 0.1 \times 10^{-3}$	$8.8 \pm 0.2 \times 10^{-4}$	$3.4 \pm 0.4 \times 10^{-5}$
MULTIPHONON EXTRAPOLATION (DEUTSCH[2])	1.1×10^{-3}	1.05×10^{-4}	6×10^{-10}

$\ell \simeq 4$ cm

B - 175 NaCl (RAP = CCl$_4$/He)

Figure 4.   NaCl (B175) absorption coefficients.

61

Table 1. KCl Absorption Versus Growth Conditions 10.6 μm

Sample Number/ Growth Atmosphere	β	β_τ
B160 (N_2/CCl_4) $\ell = 16.80$ cm	$8 \pm 2 \times 10^{-5}$	$1.2 \pm 0.1 \times 10^{-4}$
B161 $(He/CO_2/CCl_4)$ $\ell = 17.50$ cm	$6 \pm 1 \times 10^{-5}$	$8 \pm 2 \times 10^{-5}$
B162 (He/CCl_4) $\ell = 17.82$ cm	$1 \pm 0.2 \times 10^{-4}$	$1 \pm 0.1 \times 10^{-4}$

T6030

From the comparison of predicted multiphonon absorption and the experimental values, we can conclude that the surface absorption at 10.6 μm is small relative to the bulk absorption, but a similar conclusion cannot be drawn from the 9.27 and 5.3 μm data. Further experimental work will have to be done to determine if the greater-than-predicted absorption is in the bulk material or in the surfaces.

KCl sample B62-B was measured at 10.6, 5.3, 3.8, and 2.8 μm using the two-slope method. The results are presented in Figure 5. The bulk absorption at 10.6 μm falls within the range of previously measured samples and the surface absorption is quite low for an etched or freshly polished sample. The results at 5.4 μm have been previously reported[3] and represent the sensitivity limit of the instrumentation. The total absorption is less than or equal to 2×10^{-6} cm^{-1}. At the HF/DF frequencies, the bulk absorption is also quite low, $\beta \leq 1 \times 10^{-6}$ cm^{-1}. At these wavelengths, however, the polished sample showed measurable surface absorption with the total absorption lower at 3.8 μm than at 2.8 μm.

Several investigators[5-7] have reported increased absorption at 9.27 μm relative to 10.6 μm in KCl samples, contrary to the predictions of the multiphonon absorption theory. An extrinsic absorption centered at 9.6 μm is responsible for the increased 9.27 μm absorption. The results
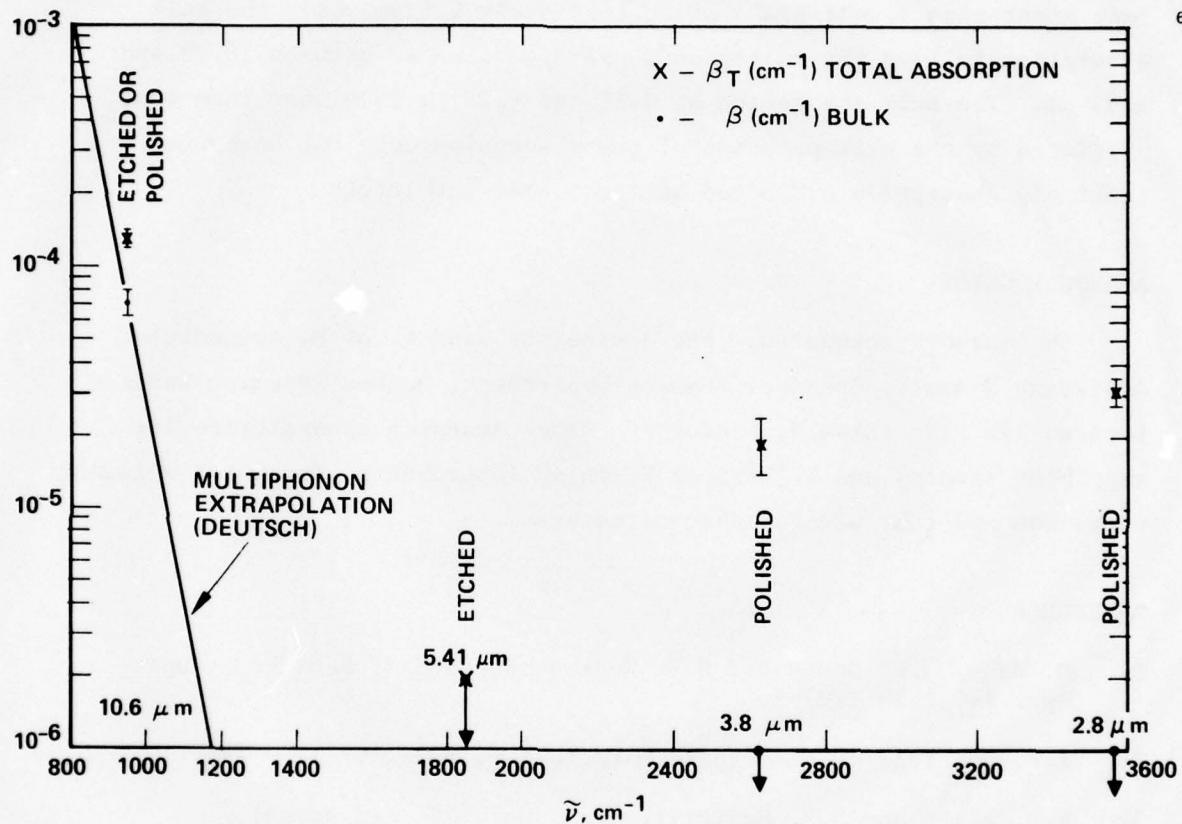
62

Figure 5. Surface and bulk absorption KCl B62-B.

63

of tunable CO_2 absorption measurements on a RAP grown bar of KCl 14 cm long with a 1 cm^2 cross section are presented in Figure 6. For crystals of this quality, at least, it is apparent that most of the absorption at 9.27 μm is caused by an impurity on the surface of the crystal. The surface absorption itself peaks at approximately 9.6 μm while the bulk absorption follows the multiphonon extrapolation to between 10.25 and 9.55 μm. The bulk absorption at 9.55 and 9.27 μm is higher than that predicted by the extrapolation of the absorption edge but below the intrinsic absorption exhibited at the longer wavelengths.

ACKNOWLEDGMENTS

REFERENCES

1. M. Hass, J.W. Davisson, H.B. Rosenstock, and J. Babiskin, Appl. Opt. 14, 1128 (1975).

2. T.F. Deutsch, J. Electronic Materials 4, 663 (1975).

3. S.D. Allen and J.E. Rudisill, Appl. Opt. 16 (in press).

4. J.A. Harrington, D.A. Gregory, and W.F. Otto, Jr., Appl. Opt. 15, 1953 (1976).

5. T.F. Deutsch, Appl. Phys. Lett. 25, 109 (1974).

6. M. Hass, J.W. Davisson, P.H. Klein, and L.L. Boyer, J. Appl. Phys. 45, 3959 (1974).

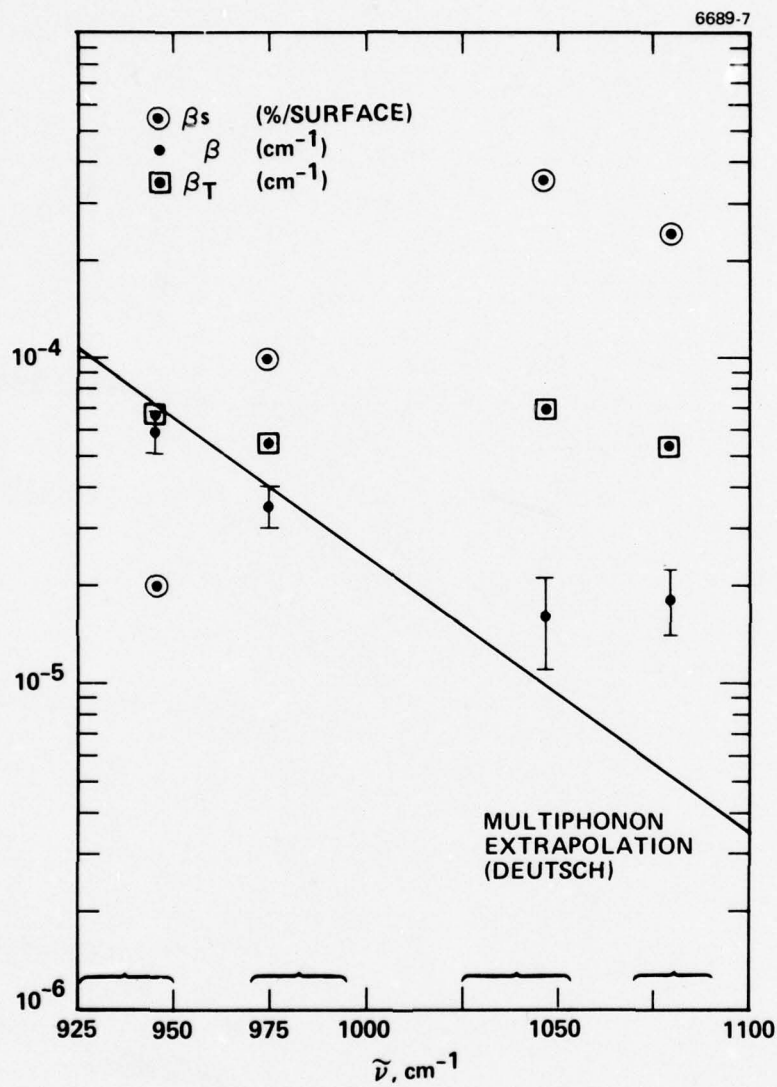7. J.M. Rowe and J.A. Harrington, J. Appl. Phys. 47, 4926 (1976).

Figure 6. Surface and bulk absorption
KCl B179-1.

65

SURFACE ABSORPTION BY LASER CALORIMETRY

M. Hass, Herbert B. Rosenstock, J.W. Davisson
Naval Research Laboratory
Washington, D.C. 20375

and

J.A. Harrington
Hughes Research Laboratories
Malibu, California 90265

ABSTRACT

A variation of long bar calorimetry is introduced which is particularly suitable for studying surface absorption. In this method, the observed signal is directly proportional to the difference in absorption between the exit and entrance surfaces of a beam passing through the sample. In the usual method, the observed signal depends on the sum of absorption of the entrance and exit surfaces. The method involves temperature sensors placed symmetrically near the ends of a long bar.

I. INTRODUCTION

The absorption of light by surfaces or thin films can be studied by a number of methods including internal reflection spectroscopy, ellipsometry, laser calorimetry, and photoacoustic spectroscopy. Each of these methods has its merits and problems. Laser calorimetry is useful when high power excitation sources are available. This technique provides a relatively simple and sensitive method for establishing both the bulk and total (bulk + surface) absorption at a particular wavelength. In this method a laser beam traverses a sample. The heat absorbed by the sample causes a temperature rise which can be measured sensitively. It is believed that the lowest bulk absorption coefficients reported to date have been measured by laser calorimetry.

In using laser calorimetry to deduce the surface absorption, the bulk contribution is subtracted from the total.[1] Another approach has involved measurement of the temperature near the end of a long rod sample coupled with a heat flow calculation,[2] but this approach has not yet been

sufficiently well developed. The present method represents an extension of these approaches. It differs from them in that the observed signal is proportional to the difference in absorption between the exit and entrance surfaces. Thus this technique may have wide application in comparing the absorption of various surfaces and thin films on substrates.

This method also should be capable of establishing a difference in absorption between exit and entrance surfaces of highly transparent crystals which are otherwise identical. Because of the interference between incident and reflected ways, the electric field at the exit surface of a crystal is higher than at the entrance surface and a corresponding difference in surface absorption is expected.[3,4]

II. EXPERIMENTAL METHOD

In the usual calorimetric method with long rod samples, one temperature sensor is placed in the middle of the rod on the periphery. The variation in temperature at the middle of the rod is monitored as a function of time relative to the surroundings which are effectively constant. The situation is illustrated in Figure 1(a). Both the bulk and total (bulk plus both entrance and exit surfaces) absorptances can be ascertained in this way.[1]

In the proposed method, shown in Figure 1, two thermocouples are placed in differentially near the ends of a rod (typically 1/4 and 3/4 along the long axis). Here bulk absorption would take place along the axis of the rod and give rise to a uniform axial heat flow. Since the temperature at symmetrical positions along the rod would rise at uniform rates, the difference would be zero. Similarly, equal absorption at both ends would also give rise to a symmetrical temperature distribution in both the transient and steady state. Consequently, such a difference temperature between corresponding positions along the rod would also be equal. Only when there is a difference in absorptance between the entrance and exit surfaces will there be an asymmetric temperature distribution

6783-4
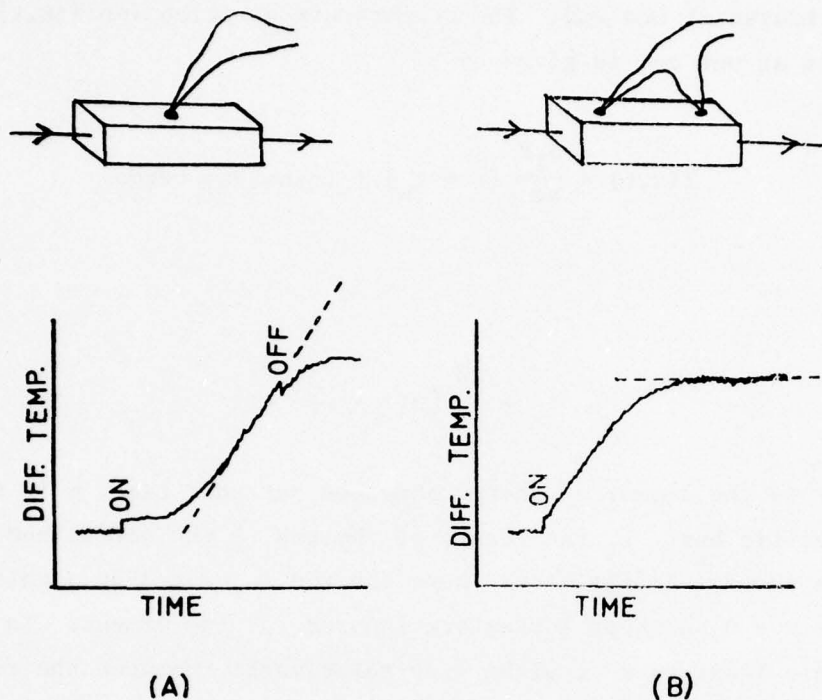
Figure 1.
(A) Thermal rise curve for long rod calorimetry in which the thermocouple is placed at the center of the rod at the periphery. The sample temperature is measured with respect to the surroundings which are assumed to be constant. Only surface absorption is assumed to be present and the magnitude of this is essentially determined by the slope of the thermal rise curve (dotted line).
(B) Thermal rise curve for new method in which the temperature difference between symmetrical positions near the ends of a rod are measured. This temperature difference becomes constant in the steady state (dotted line) and is directly proportional to the difference between the entrance and exit surface absorptances.

69

The method can be illustrated using a simple one-dimensional model of a rod heated at one end. The temperature distribution $T(\bar{x}, t)$ along a rod heated at one end is given by[5]

$$T(\bar{x}, t) = \frac{S_1 P}{mc} (t + t_x) + \text{transient terms} \tag{1}$$

where

$$t_x = \frac{L^2}{6\kappa} [3(1 - \bar{x})^2 - 1] \tag{2}$$

where $S_1 P$ is the amount of energy absorbed per unit time, m is the mass, c the specific heat, L, the length of the rod, $\bar{x}$ the normalized length, and κ the thermal diffusivity. Here the rod is heated by a uniform source at $x = 0$ and heat losses are ignored for the moment. In the steady state, this leads to a straight line relationship between the temperature and time in which the slope depends upon the heat absorbed and the intercept depends upon the position along the rod and the thermal diffusivity. In the special case where the temperature difference between points 1/4 and 3/4 along the rods are selected, the temperature difference is given by

$$T\left(\frac{1}{4}, t\right) - T\left(\frac{3}{4}, t\right) = \frac{S_1 P}{mc} \frac{\left(\frac{1}{2} L\right)^2}{\kappa} \tag{3}$$

Thus if S_1 represented the absorptance and P the power incident on the end of a rod, then the absorptance can be easily calculated from known parameters. For a highly transparent rod with absorptances S_1 and S_2 at each end, Eq. (3) can be generalized by replacing S_1 by $S_1 - S_2$, the difference in absorptances of the entrance and exit surfaces. This one dimensional model illustrates the problem qualitatively, although there are a number of important quantative differences in the real three-dimensional case with heat losses.

70

To illustrate this, a CaF_2 rod was heated at one end only by a 10.6 µm laser beam. The rod is effectively opaque at this wavelength and thus heated at one end only. The temperature $T(1/4,t)$, $T(3/4,t)$, and the difference $T(1/4,t) - T(3/4,t)$ were separately measured and calculated using the full three-dimensional heat flow formulation of Rosenstock.[6] These results are shown in Figure 2. For purposes of estimating heat losses, the cooling curves of uniformly heated rods were employed to calculate a heat loss parameter.

The essential point of Figure 2 is that fairly good agreement between experiment and calculation can be obtained and even perfect agreement could be achieved by adjusting the heat capacity somewhat from its published value. However, we have chosen to use published values of the heat capacity and thermal diffusivity.[7]

In order to carry out an experiment in an actual case, we have studied the absorption of uncoated surfaces and thin films by the differential method described here using an HF/DF laser with a long rod. The results so far are in qualitative accord with Figure 2. However, since the rod is now heated on both ends, the temperature profile is quite different. In the case studied in Figure 2, the profile is asymmetric with respect to the center of symmetry of the rod. In the real situation, the profile is more nearly symmetric. Small errors due to slightly different heat losses at different portions of the rod become more significant and this may be the source of the difficulties in reproducibility. It is hoped to improve the experimental arrangement so as to achieve the necessary temperature uniformity in the calorimeter.

ACKNOWLEDGMENT
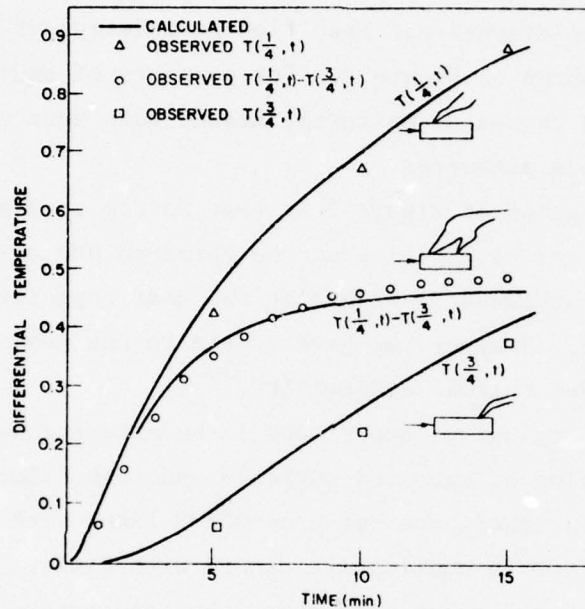
Figure 2.
Calculated and measured temperature
differences for a rod heated at one end.
The situations of T(1/4,t) and T(3/4,t)
refers to the temperature difference
between the indicated position on the
rod and surroundings at a constant tem-
perature. The situation for T(1/4,t)-
T(3/4,t) refers to a difference directly
measured between the indicated positions.

REFERENCES

1. H.B. Rosenstock, M. Hass, D.A. Gregory, and J.A. Harrington, "Analysis of laser calorimetric data," Appl. Opt. 16, 2837-2842 (1977).

2. J.A. Harrington, M. Braunstein, and J.E. Rudisill, "New Technique for Measuring Infrared Absorption on Thin Film Coatings," Appl. Opt. 16, 2843-2846 (1977).

3. P.A. Miles, "Static Profile Calorimetry of Laser Materials," Appl. Opt. 16, 2897-2901 (1977).

4. J.E. Rudisill and G. Johnson (private communication).

5. H.S. Carslaw and J.C. Jaeger, "Conduction of Heat in Solids," (Oxford Univ. Press, London), 2nd ed., 1959, p. 112.

6. H.B. Rosenstock, "Absorption Measurements by Laser Calorimetry," J. Int. Heat and Mass Transfer (submitted).

7. S.R. Dickinson, "Infrared Laser Window Materials Property Data for ZnSe, KCl, CaF_2, SrF_2, and BaF_2," AFCRL-TR-0318.

HF AND DF WINDOW ABSORPTION

Marvin Hass
Naval Research Laboratory

and

James A. Harrington
Hughes Research Laboratories
Malibu, California 90265

ABSTRACT

The infrared absorption of samples of KCl, CaF_2, and SrF_2 at the
HF/DF laser wavelengths have been studied using long rod laser calorim-
etry. These results suggest the bulk absorption coefficients are very
low in the range of 10^{-5} cm^{-1} or less and that the absorption in rods of
approximately 10 cm length is dominated by surface absorption effects.
Most previous investigations have revealed bulk absorption coefficients
in the 10^{-4} cm^{-1} range. These high values might have resulted from some
experimental difficulties.

INTRODUCTION

The bulk absorption coefficients of alkali halide and alkaline
earth fluoride laser window materials near the HF wavelength of 2.7 μm
and the DF wavelength near 3.8 μm have generally been in the range of
10^{-4} cm^{-1} in those cases where it has been possible to effect a separa-
tion between surface and bulk effects.[1-3] While it is possible to
explain such results based on selective impurity absorption at these
wavelengths, this approach is not necessarily satisfactory and may not
be correct. A common bulk impurity in these materials is OH and this
would generally give rise to resonant absorption near 2.7 μm. Thus high
values near this wavelength could arise from this source, but such OH
absorption would not be expected to contribute near 3.8 μm. Absorbed
surface water does have a broad absorption near 3 μm and CH atmospheric
contaminants are known to give sharp bands near 3.3 μm. However, it
might be stretching a point to attribute the observed results to this
origin.

In this present article, a number of new careful measurements have been taken using long rod laser calorimetry,[4-6] which indicate a bulk absorption in these samples at least which is in the low 10^{-5} cm^{-1} or lower. This is more in accord with expectations. The method is illustrated in Figure 1 which shows how inspection of the shape of thermal rise curves for long rod samples can be used to separate bulk and surface absorption. Figure 1 shows schematic results for the two limiting cases. The shape of the curves found in this investigation indicated predominant surface absorption.

Previous measurements by Davisson[7] have indicated that a number of laser window materials including CaF_2, SrF_2, KBr and KCl could have bulk absorption coefficients in the range of 10^{-5} cm^{-1} or below at 1.06 μm. In fact, one sample of KBr was essentially unmeasurable at a level of 3×10^{-6} cm^{-1} or lower. The Nd:YAG laser available at 1.06 μm provides particularly convenient, powerful, and well directed beam for laser calorimetric measurements. Since interference from scattering, if present, is less severe at longer wavelengths, measurements at 2.7 μm and 3.8 μm might also show absorption in the same range. However, in the absence of resonant impurity absorption most previous measurements indicated absorption in the 10^{-4} cm^{-1} range.

RESULTS

In an attempt to resolve this question, new measurements were started at the NRL chemical laser facility and at the Hughes chemical laser facility to answer this question. Typical data is shown in Figure 2, which indicates that at both 2.7 μm and 3.8 μm, it is difficult to measure any bulk absorption based on the initial slope of the calorimetric thermal rise curve. Some surface absorption is found and this is greater at the HF wavelength. It is also larger when the samples are run in air as compared to a vacuum. The surface absorption results for KCl, for which data is most complete, are shown in Table 1. Presumably, water is adsorbed on the surface. Water does have a broad band near 3 μm the wings of which extend to 3.8 μm. These results are in qualitative accord with corresponding investigations using internal reflection spectroscopy.[8]
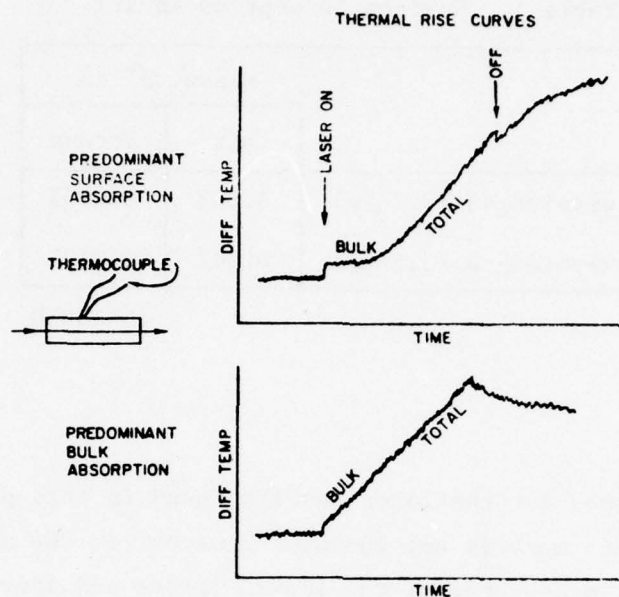
6783-2

THERMAL RISE CURVES

Figure 1. Typical thermal rise curves encountered in long rod laser calorimetry for predominant surface and predominant bulk absorption.
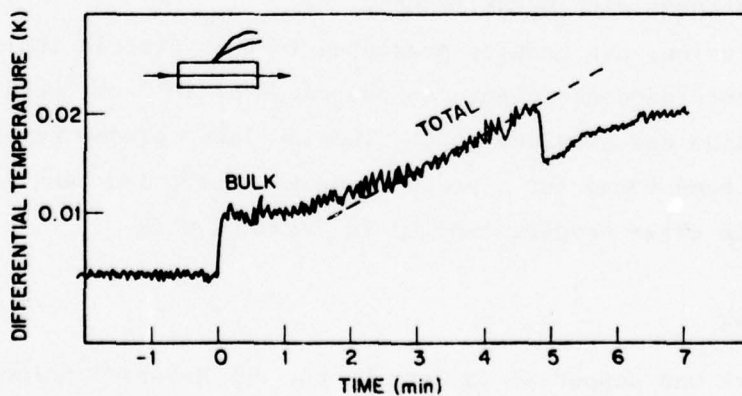

6783-3

Figure 2. Thermal rise curve for a KCl bar (Hughes-RAP grown) at an HF (2.7 μm) power of 3.7 W. The sample mass was 110 grams and its dimensions were 2.15 x 2.15 x 12.27 cm.

77

Table 1. Surface Absorption in KCl

	Measured[a] in	
	Air	Vacuum
HF wavelength (2.7 μm)	0.08%	0.025%
DF wavelength (3.8 μm)	0.04%	0.012%

T6030

DISCUSSION

The exact reason for the lower results found in this present work compared to previous work is not known. However, in the process of taking the present measurements, the laser mirrors and apertures were adjusted so as to give concentrated beam and to avoid mode structure in which the beam shape was irregular. Using this procedure low results were found. On the other hand, when the mode structure was irregular, then higher absorption was found. The HF/DF chemical lasers employed are more difficult to adjust to a circular spot than Nd:YAG or CO_2 lasers. Consequently, the above explanation might account for all or part of the high values in previous investigations. In addition, more noise interference was present with HF/DF lasers.

In conclusion, new results presented in this article indicate that very low absorption coefficients in the range of 10^{-5} cm^{-1} can be achieved in alkali halide and alkaline earth fluoride laser window crystals. No evidence has been found for a broad resonant absorption band in the 3 μm region in these samples implied in previous work.

ACKNOWLEDGMENT

REFERENCES

1. M. Hass, J.A. Harrington, D.A. Gregory, and J.W. Davisson, "Infrared Absorption Limits of HF and DF Laser Windows," Appl. Phys. Lett. 28, 610-611 (1976).

2. J.A. Harrington, D.A. Gregory, and W.F. Otto, Jr., "Infrared Absorption in Chemical Laser Window Materials," Appl. Opt. 15, 1959 (1976).

3. A. Hordvik and L. Skolnik, "Bulk and Surface Absorption in HF/DF Laser Window Materials," Appl. Opt. 16, 2919-2918 (1977).

4. H.B. Rosenstock, M. Hass, D.A. Gregory, and J.A. Harrington, "Analysis of Laser Calorimetric Data," Appl. Opt. 16, 2837-2842 (1977).

5. M. Hass, J.W. Davisson, H.B. Rosenstock, and J. Babiskin, "Measurement of Very Low Absorption Coefficients by Laser Calorimetry," Appl. Opt. 14, 1128-1130.

6. H.B. Rosenstock, D.A. Gregory, and J.A. Harrington, "Infrared Bulk and Surface Absorption by Nearly Transparent Crystals," Appl. Opt. 15, 2075-2079 (1976).

7. J.W. Davisson, "Chemical Polishing of KBr and Absorption Measurements at 1.06 m," Proc. 5th Annual Conference on Infrared Laser Window Materials, p. 113-122.

8. J.W. Gibson, R.T. Holm, and E.D. Palik, "Internal-Reflection Spectroscopy Study of Adsorption of Water on CaF_2 Surfaces," Proc. Ninth Boulder Damage Symposium, NBS Special Publication.

MODULATED LIGHT ELLIPSOMETER MEASUREMENTS OF THE REFRACTIVE INDICES OF ThF$_4$ SINGLE CRYSTALS AND As$_2$Se$_3$ and As$_2$S$_3$ FILMS ON KCl SUBSTRATES AT 10.6 μm

M.E. Pedinoff and M. Braunstein
Hughes Research Laboratories
Malibu, California 90265

and

O.M. Stafsudd
Engineering Department
University of California at Los Angeles

ABSTRACT

The measurement of infrared optical properties of thin films and/or substrates by means of an Elasto optic modulated light ellipsometer will be discussed.

Ellipsometers of this type do not yield the normal Δ and ψ variables directly but rather give this information indirectly in terms of ratios of signals Vω/Vdc (R$_1$) and V2ω/Vdc (R$_2$) where ω is the modulation frequency. These ratios are used in a suitable set of equations to calculate the equivalent sets of Δ and ψ which in turn are used in conventional programs to calculate the refractive index of substrates and the refractive index and thickness of films.

Conventional graphical aids such as Δ, ψ plots with film thickness, angle of incidence, film index, and substrate index as parameters are not useful in determining the optimum conditions of measurement with a modulated light ellipsometer because errors in R$_1$ and R$_2$ are not simply related to errors in Δ and ψ.

A new set of plots are shown in which the physically observable information, the signal ratios, R$_1$ and R$_2$ are given as functions of the parameters film thickness, angle of incidence, film index and substrate index. These plots are of significant usefulness in determining the

optimum conditions for measurement. In addition, calculations of the
sensitivity of the apparent index of refraction to errors in R_1, R_2 and
angle of incidence are also very useful for determination of the optimum
measurement conditions, i.e., film thickness, angle of incidence, etc.

Experimental results will be presented for a single crystal ThF_4
substrate and films of As_2S_3 and As_2Se_3 on KCl substrates.

INTRODUCTION

Whenever refractive index measurements are made on films or substrate
materials using a modulated light ellipsometer,[1-4] a pair of signal ratios
$R_1 = V\omega/Vdc$ and $R_2 = V_{2\omega}/Vdc$ are obtained from the signal processing
electronics which are then processed to obtain first the familiar ellip-
sometric parameters Δ and ψ and then the complex refractive index n + lk,
and the film thickness, t. Other earlier workers[5] in this field have
found it instructive to plot the parameters Δ versus ψ for the case of
an optically transparent film deposited on a transparent or an opaque
substrate. In these graphical studies usually the normalized film thick-
ness in optical wavelengths and the film index are the parameters which
are varied, and the angle of incidence of the light is held constant.
Many variations of this technique are possible and useful because changes
in Δ and ψ refer directly to changes in polarizer and analyzer angles in
some types of manual ellipsometry. However, in the case of a modulated
light ellipsometer, changes in the signal ratios R_1 and R_2 do not relate
linearly to changes in Δ and ψ, and studies of Δ and ψ plots do not pro-
vide insight into the optimum conditions for measurement of a given film
or substrate system.

It occurred to us that by plotting the variables R_1 against R_2 as a
function of the angle of incidence, the film refractive index and the
normalized film thickness, we might obtain some insight into the optimum
range for measurement of several materials of interest for laser window
coatings. In this paper, the film materials studied were As_2S_3 and
As_2Se_3 on KCl substrates. Additionally, a substrate material, single
crystal ThF_4 was studied using an ellipsometric computer simulation
technique reported earlier.[3,4]

THEORY

We shall briefly review the definitions of the complex reflection coefficients, $r_\parallel$ for a polarization vector parallel to the plane of incidence and $r_\perp$ for the polarization vector orthogonal to the plane of incidence. These are represented in terms of their real and imaginary components in equations (1) and (2).

$$r_\parallel = R_\parallel \, e^{j\Delta_\parallel} \tag{1}$$

$$r_\perp = R_\perp \, e^{j\Delta_\perp} \, . \tag{2}$$

These Fresnel coefficients can be calculated from the equations of electromagnetic wave reflection and transmission at a substrate or thin film boundary.[5] The ratio of these coefficients is generally defined by equation (3), which is the fundamental equation of ellipsometry:

$$r_\parallel / r_\perp = \tan \psi e^{j\Delta} \, . \tag{3}$$

Combining these equations, and separating the real and imaginary terms, one obtains the relative reflectivity ratio, $\tan \psi$ and the relative phase shift Δ at the surface of the film or substrate as shown in equations 4 and 5.

$$\text{Tan } \psi = \frac{R_\parallel}{R_\perp} \tag{4}$$

$$\Delta = \Delta_\parallel - \Delta_\perp \, . \tag{5}$$

The parameters Δ, ψ also correspond to the angular position settings of the polarizer and the analyzer in an ellipsometer containing a quarter wave plate phase compensator.[6]

83

The signal equations for the Hughes modulated light ellipsometer which have been derived elsewhere[1-4] are of the form:

$$R_1 = V\omega/V_{dc} = \frac{\text{Sin } (\Delta_{\|} - \Delta_{\perp})J_1 (x)}{R_{\perp}/R_{\|} + R_{\|}/R_{\perp} - 2 \cos (\Delta_{\|} - \Delta_{\perp}) \text{ Jo}(X)} \qquad (6)$$

$$R_2 = V_2\omega/V_{dc} = \frac{\text{Cos } (\Delta_{\|} - \Delta_{\perp}) J_2(x)}{R_{\perp}/R_{\|} + R_{\|}/R_{\perp} - 2 \cos (\Delta_{\|} - \Delta_{\perp})\text{Jo } (X)} \qquad (7)$$

These ratios are the actual output signals from the apparatus and they are sensitive to the various reflectivities $R_{\perp}$ and $R_{\|}$, phase shifts $\Delta_{\|}$ and $\Delta_{\perp}$, and to the modulation drive level X, which in our instrument is approximately 1.0. By substituting equations (4) and (5) into equations (6) and (7) one obtains a set of equations relating R_1 and R_2 to the variables Δ, ψ and X only. The values of Δ and ψ used in calculating R_1 and R_2 are obtained for both films and substrates from the McCracken NBS Program.[6] In the case of transparent or low loss substrates, the phase shift Δ is either 0 or 180 degrees and R_1 is equal to zero. Thus, a plot of R_1, R_2 using the angle of incidence as an independent parameter yields no information because the curve is a straight line along the R_2 axis. However, in the case of transparent films, plots of R_1, R_2 using film thickness as the independent parameter are very useful. This is illustrated for films of various film indices in Figure 1. In this case, the angle of incidence and modulator drive level X are kept constant. Each data point on the R_1R_2 plots differs by a normalized film thickness increment of $\lambda_f/20 = \lambda o/20n_f$. Where n_f is the index of the film, λ_f is the wavelength in the film and λ_o is the free space wavelength.

These plots are roughly elliptically shaped for transparent films and spiral shaped for absorbing films. It should be noted that the ellipses for different index films vary greatly in their spacing from one another as a function of film thickness and, therefore, optimum ranges of film thickness exist (places of maximum separation of curves) for obtaining accurate index values.
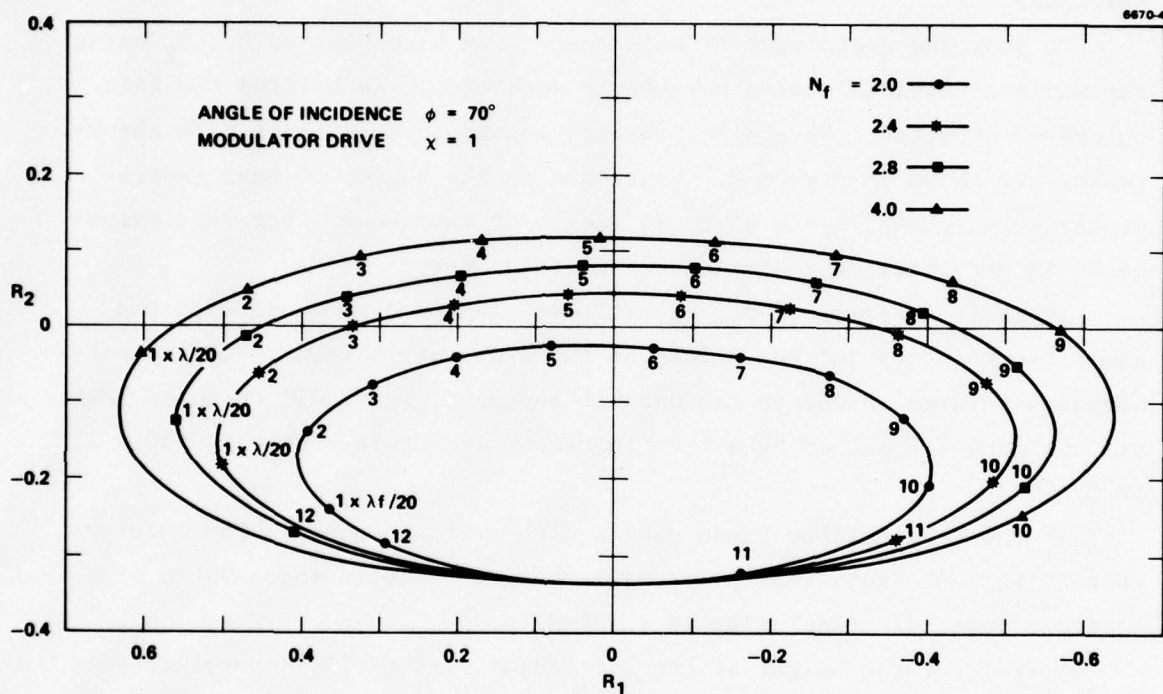
84

Figure 1. Plot of R_2 versus R_1 for films of $N = 2.0$, 2.4, 2.8, and 4 on substrate $N = 1.455$ with film thickness increments of $\lambda/20$.

In particular, one should observe the ellipses corresponding to $N_f = 2.8$ in the region of $5\lambda_f/20$. At this point, one sees that variations in film thickness only change R_1 significantly, and variations in index with constant film thickness (physical thickness) only change R_2 significantly. The opposite effect can be observed in the region of $1\lambda_f/20$ thickness.

To show the usefulness of this result, we have plotted R_1, R_2 using the angle of incidence as a parametric variable while holding the film thickness constant. Several curves corresponding to various film thicknesses are shown in Figure 2. Note that in the region of best experimental measurement, i.e., 65 to 75° angle of incidence, that this value of R_1 is extremely dependent upon film thickness.

Typical experimental R_1, R_2 data are plotted here along with the theoretical curves and the values of the angle of incidence are indicated. Although a large spread in the data is apparent, it should be noted that all the data is spanned by a film thickness uncertainly of only ±50 Å or 0.5%.

If one recalculates these curves with small changes in the index of refraction, one finds that only small changes occur in shape but a significant vertical translation in R_2 results.

Therefore, the height of the data point essentially determines the correct index of the material. This can be of significant importance to a far infrared modulated light ellipsometer. In these modulators strain induced birefringence cause errors in the R_1 channel. Pick up associated with the electrical drive of the modulators also occurs at the drive frequency ω and affects the R_1 channel only. Therefore, the R_1 data channel is more susceptible to errors than the R_2 channel.

By studying graphs similar to Figures 1 and 2, one can find a film thickness and angle regime which yields the optimum precision in determining N in the presence of an expected R_1 error. Such a condition is shown in Figure 1 at the position $R_1 = 0$, $(-0.5 \leq R_2 \leq 1.5)$ for the KCl substrates. Similar curves can be generated for other angles of incidence and arbitrary substrates. An alternate form of this plot is shown in Figure 3 with various angles of incidence and film thicknesses. For
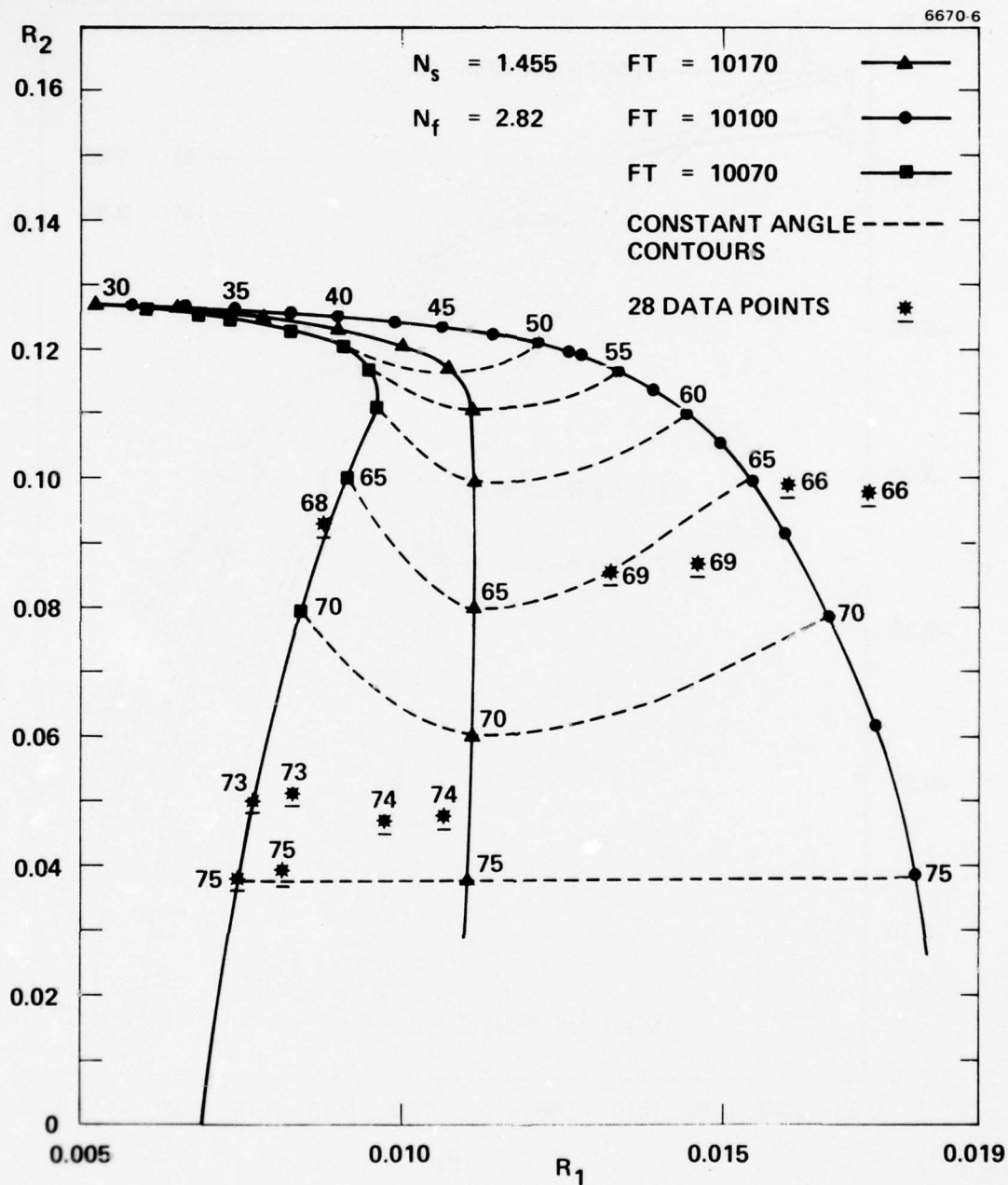
Figure 2. Plot of R_2 versus R_1 for films of $N = 2.82$ on substrate of $N = 1.455$ with film thicknesses 10,170 Å, 10,100 Å, and 10,070 Å. The corresponding angle of incidence for each coordinate is indicated.
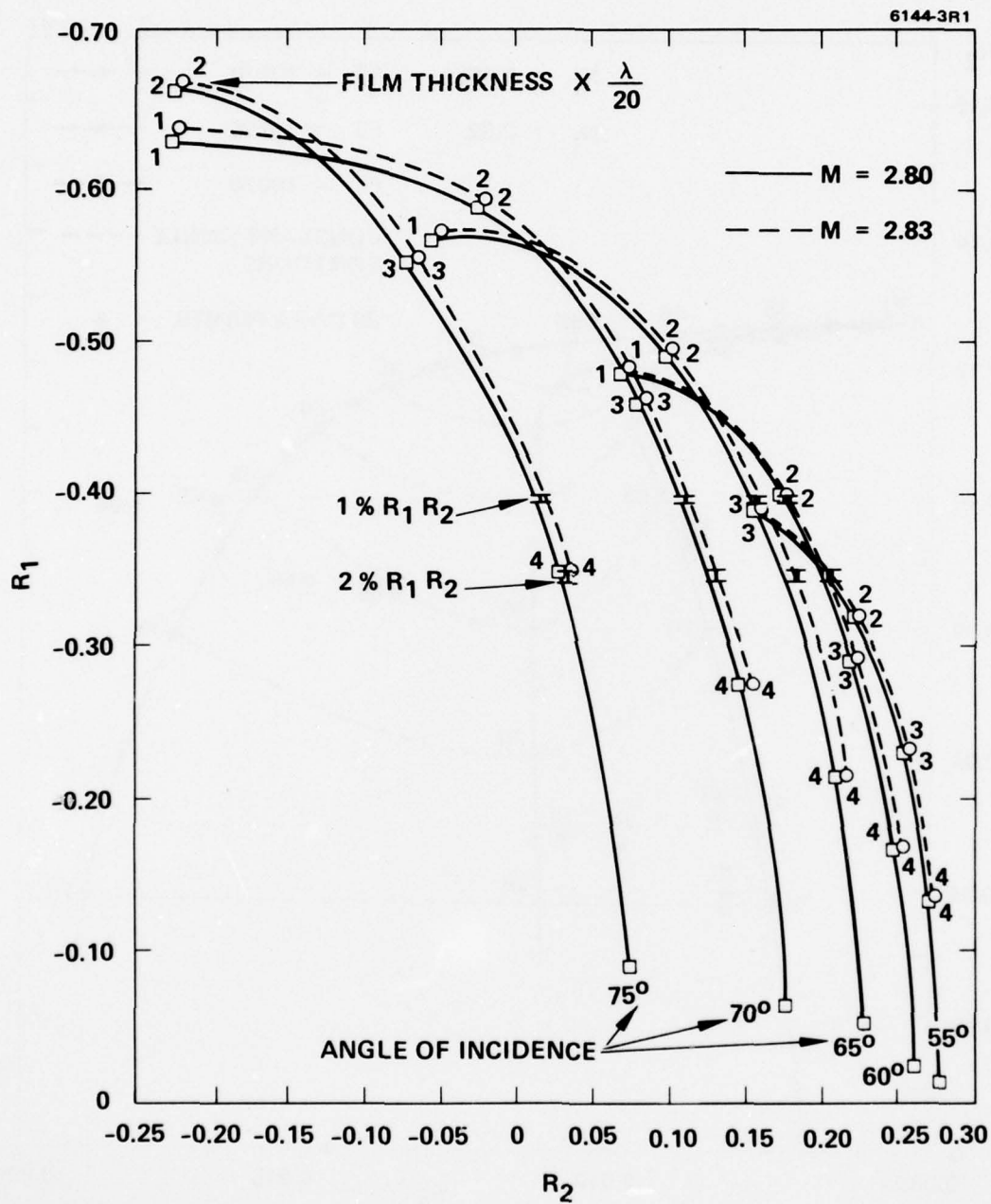
Figure 3. Dependence of R_1 on the film thickness As_2Se_3 on KCl.

comparison purposes, the calculations were performed for refractive indices differing by 1%. Again, one sees that for a specific value of film thickness, there is an optimum angular range for performing the measurements. For completeness, a theoretical curve of R_1, R_2 data for a lossy film with film thickness as an independent parameter is shown in Figure 3. The curve is observed to spiral in toward a central position with increasing film thickness. The R_1 R_2 coordinate for the infinitely thick film corresponds to those values that would be obtained for a substrate with the same index as the film.

EXPERIMENTAL RESULTS

Measurements have been made on a ThF_4 single crystal and on samples of As_2Se_3 and As_2S_3 films on KCl substrates at 10.6 μm. These results are listed in Table 1 and are in good agreement (2%) with accepted index value for these materials. The film thickness measurement results are given in Table 2. The film thickness measured ellipsometrically compares very well with Tolansky interference measurements, the agreement being better than 2% for the thick films and 5% for the thin film. This discrepancy is easily accounted for because of the lack of metallization of the samples measured by the Tolansky method.

REFERENCES

1.   S.N. Jasperson, D.K. Burge, and R.C. O'Handley, "A Modulated Ellipsometer for Studying Thin-Film Optical Properties and Surface Dynamics," 37, 548 (1973).

2.   S.D. Allen, A.I. Braunstein, M. Braunstein, J.C. Cheng, and L.A. Nefie, "A 10.6 Micron Modulated Light Ellipsometer," Optical Properties of Highly Transparent Solids, S.S. Mitra and B. Bendow, eds. (Plenum Publishing Company, New York, 1975), pp. 503-513.

3.   M.E. Pedinoff, M. Braunstein, and O.M. Stafsudd, "10.6 μm Ellipsometer Measurements of Refractive Indices of IR Materials," presented at Topical Meeting on Optical Phenomena in Infrared Materials, Optical Society of America, Dec. 1-3, 1976, Annapolis, Md.

0.2

6670-5

$\Delta FT = \dfrac{\lambda}{20} \dfrac{1}{NF}$

$N_s = 1.455$

$NF = 2.4, i\,0.24$

$x = 1$

4 15 5 6 7
3 14 26 16 27 17 18
0
25 28
13 24 38 100 39 29 30 19 8
35 37 36 40
23 34 33 32 31 20 9
12 22 21 10
$1 \times \lambda f/20$ 11

R_2

R_1

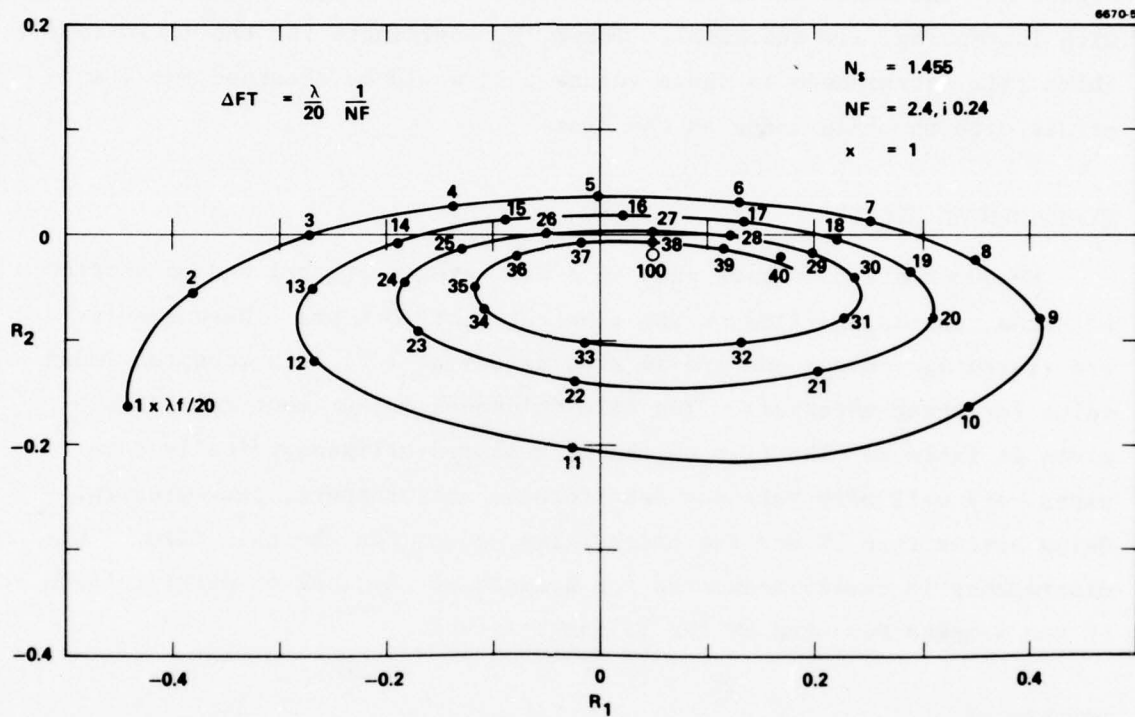-0.4   -0.2   0   0.2   0.4

-0.2

-0.4

Figure 4. Plot of R_2 versus R_1 for lossy film $N = 2.4 + 10.24$ on substrate $N = 1.455$ with film thickness increments of $\lambda/20$.

90

Table 1. Ellipsometric Measurements
of Refractive Index of Various
Film Thickness

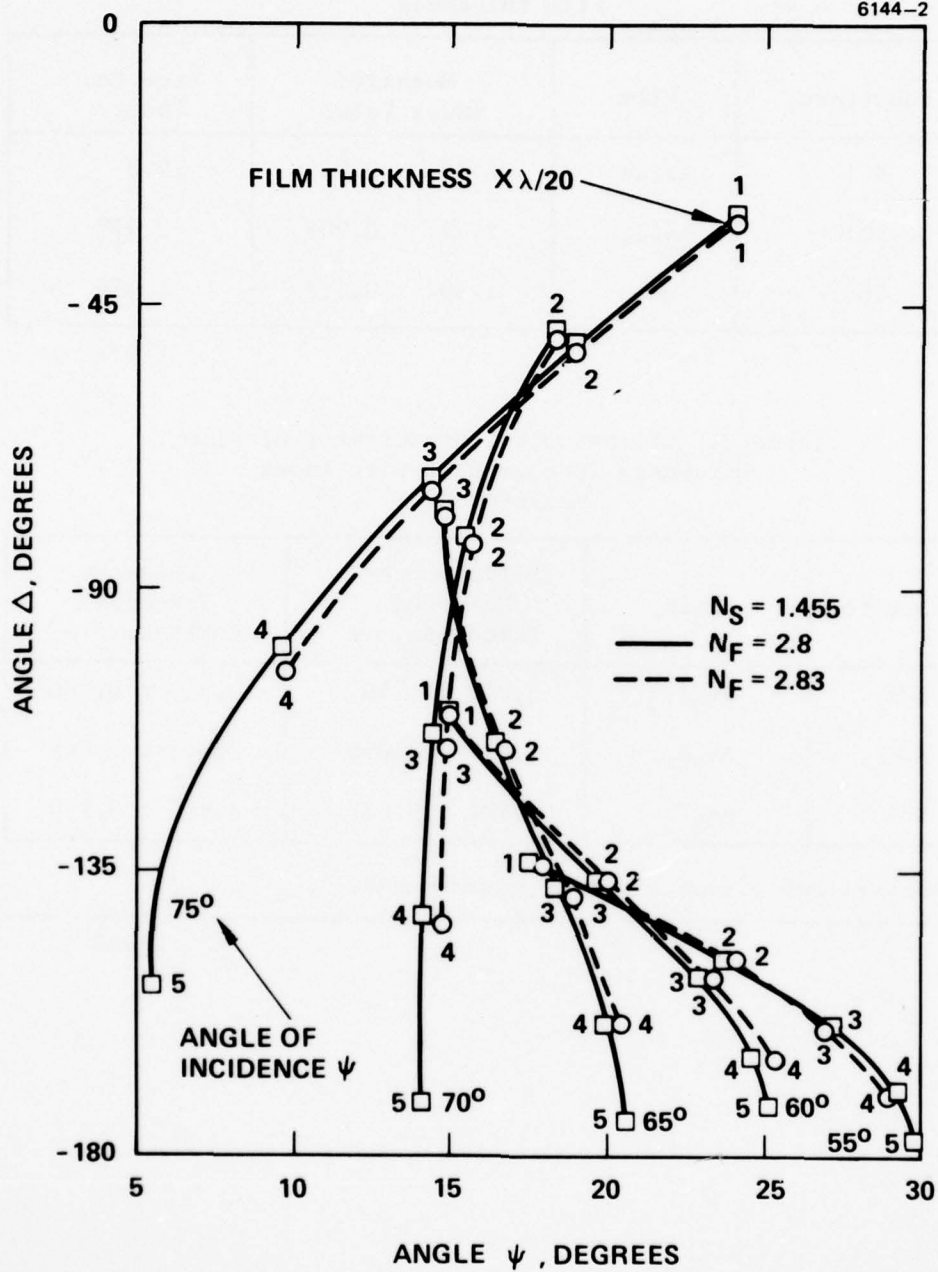| Substrate	Film	Measured Index Value	Accepted Index
KCl	As_2Se_3	2.831 ± 0.050	≈ 2.8
KCl	As_2S_3	2.35 ± 0.003	2.377
ThF_4	---	1.302 ± 0.013	1.350

T6030

Table 2. Ellipsometric Measurement of Film
Thickness Concommitant with Index
Measurement

Substrate	Film	Ellipsometer Measured Thickness, µm	Tolansky Thickness Estimate, µm[a]
KCl	As_2Se_3	3.370 ± 0.59	3.313 ± 0.166
KCl	As_2Se_3	1.017 ± 0.059	0.968 ± 0.048
KCl	As_2S_3	3.921 ± 0.037	3.970 ± 0.199
[a]Unmetallized dielectric film measurement.			

T6030

91

6144–2

FILM THICKNESS X λ/20

$N_S = 1.455$

$N_F = 2.8$

$N_F = 2.83$

ANGLE Δ, DEGREES

ANGLE ψ, DEGREES

ANGLE OF INCIDENCE ψ

75°

70°

65°

60°

55°

92

$$r_{\parallel} = R_{\parallel}\, e^{j\Delta_{\parallel}}$$

$$r_{\perp} = R_{\perp}\, e^{j\Delta_{\perp}}$$

$$r_{\parallel}/r_{\perp} = \tan\psi\, e^{j\Delta}$$

$$\tan\psi = \frac{R_{\parallel}}{R_{\perp}}$$

$$\Delta = \Delta_{\parallel} - \Delta_{\perp}$$

$$R_1 = V_{\omega}/V_{dc} = \frac{\sin(\Delta_{\parallel} - \Delta_{\perp})\, J_1(X)}{R_{\perp}/R_{\parallel} + R_{\parallel}/R_{\perp} - 2\cos(\Delta_{\parallel} - \Delta_{\perp})\, J_o(X)}$$

$$R_2 = V_{2\omega}/V_{dc} = \frac{\cos(\Delta_{\parallel} - \Delta_{\perp})\, J_2(X)}{R_{\perp}/R_{\parallel} + R_{\parallel}/R_{\perp} - 2\cos(\Delta_{\parallel} - \Delta_{\perp})\, J_o(X)}$$

4. M.E. Pedinoff, M. Braunstein, and O.M. Stafsudd, "Refractive Indices of IR Materials: 10.6 μm Ellipsometer Measurements," to be published in Appl. Opt., November 1977.

5. F.L. McCrackin, E. Pasaglia, R.R. Stromberg, and H. Steinberg, "Measurement of the Thickness and Refractive Index of Very Thin Films and the Optical Properties of Surfaces by Ellipsometry," J. Res. Natl. Bur. Stand. 67A, 363-377 (1963).

6. F.L. McCracken, "A Fortran Program for Analysis of Ellipsometer Measurements," Natl. Bur. Std. Technical Note No. 479 (1969), (U.S. Govt. Printing Office, Washington, DC, 1969).

MODULATED LIGHT ELLIPSOMETER MEASUREMENTS OF STRAIN-INDUCED ANISOTROPY IN THE REFRACTIVE INDEX OF As_2Se_3 AND As_2S_3 FILMS ON KCl SUBSTRATES AT 10.6 μm

M.E. Pedinoff and M. Braunstein
Hughes Research Laboratories
Malibu, California 90265

and

O.M. Stafsudd
Engineering Department
University of California at Los Angeles

The measurement of strain-induced anisotropy in the refract. e index of thin films by means of an Elasto-optic modulated light ellipsometer is discussed.

Ellipsometers of this type yield refractive index information indirectly in terms of ratios of signals $V\omega/Vdc$ (R_1) and $V2\omega/Vdc$ (R_2) where ω is the modulation frequency.

Computational routines have been developed that (differentially) relate changes in film and substrate refractive index to changes in the signal ratios R_1 and R_2. These calculations enable us to estimate the anisotropic change in the refractive index, Δn, of an optical film due to a unidirectional stress applied to the substrate. Assumed anisotropies of 1%, give signal ratio changes of 1% to 120%, depending on the experimental conditions. Preliminary ellipsometric measurements show anisotropies of 0.6% generated in films of As_2S_3 and As_2Se_3 on KCl by strains of 4×10^{-5} induced in the substrate.

An exact calculation of the change in signal ratios R_1 and R_2 was obtained using D. Den Engleston's model of reflection from a uniaxial

---

1. Figures in brackets indicate the literature references at the end of this paper.

anisotropic film with the strain axis in the film orthogonal to the plane of incidence.

The presence of large refractive index anisotropy cannot be discerned from measurements made on a single film thickness sample by ellipsometric techniques. Experimental data is presented for various thickness samples.

INTRODUCTION

The measurement of strain induced anisotropy in the refractive index of thin films by means of an Elasto-optic modulated light ellipsometer will be discussed.

Ellipsometers of this type [1,2,3,4] yield refractive index information indirectly in terms of ratios of signals $V\omega/Vdc$ (R_1) and $V2\omega/Vdc$ (R_2) where ω is the modulation frequency. These ratios are used in a suitable set of equations [1,2] to calculate the equivalent sets of Δ and ψ which in turn are used in conventional computer programs [5] to calculate the refractive index of substrates and the refractive index and thickness of films.

Computational routines [6] have been developed that (differentially) relate changes in film and substrate refractive index to changes in the signal ratios R_1 and R_2. These calculations enable us to estimate the anisotropic change in the refractive index, Δn, of an optical film due to a unidirectional stress applied to the substrate, from a measurement of the signal ratio changes ΔR_1 and ΔR_2.

An exact calculation of the change in signal ratios R_1 and R_2 has also been obtained using a variation of D. Den Engleston's [7] model of electromagnetic reflection from a uniaxial anisotropic film. In this case, the optic axis lies in the plane of the film and is orthogonal to the plane of incidence. Assumed anisotropies of 1%, give rise to signal ratio changes of 10% to 300%, depending on the film thickness, film index, and the angle of incidence. Preliminary ellipsometric measurements on this effect show that anisotropies of the order of 1/2% have been generated in films of As_2S_3 on KCl by strains of the order of 2.5×10^{-5} piezoelectrically induced in the substrate.

96

In those cases where the film is deposited on the substrate at high temperatures and then allowed to cool to room temperature, thermal expansion coefficient differences between the film and the substrate can give rise to a uniaxial anisotropy in which the optic axis is orthogonal to the plane of the film. In this "perpendicular" anisotropy, the signal ratios R_1 and R_2 will show a different dependence on film thickness than the signal ratios of the isotropic case. We have found that the plots of R_1 versus R_2 as a function of angle of incidence as a parameter, were not useful in separating isotropic and anisotropic effects. However, when the signal ratios R_1 and R_2 are plotted at the constant angle of incidence using the film thickness as a parameter, the cases of an isotropic film and a film with 10% anisotropy can easily be resolved. This method of measurement of perpendicular optical anisotropy requires that the measured signal ratio data be plotted on a theoretically calculated chart of the signal ratios for several values of anisotropy and film thickness. The curve which best fits the data is then the best estimate of the anisotropy. It is feasible but non-trivial to program the computer to find that set of film thickness and refractive indices which best fit the data.

ANALYSIS

Analysis of an anisotropic film has been approached by several workers [7,8] and in general is very difficult due to the admixture of r and s polarized fields by the anisotropy of the film. However, a more tractible problem occurs if the film exhibits uniaxial properties and if the unique axis is either perpendicular to the surface of the film (perpendicular case) or parallel to the plane of the film and orthogonal to the plane of incidence (planar case). Using the coordinate system of Figure 1 for these two cases, the index tensor can be expressed as:
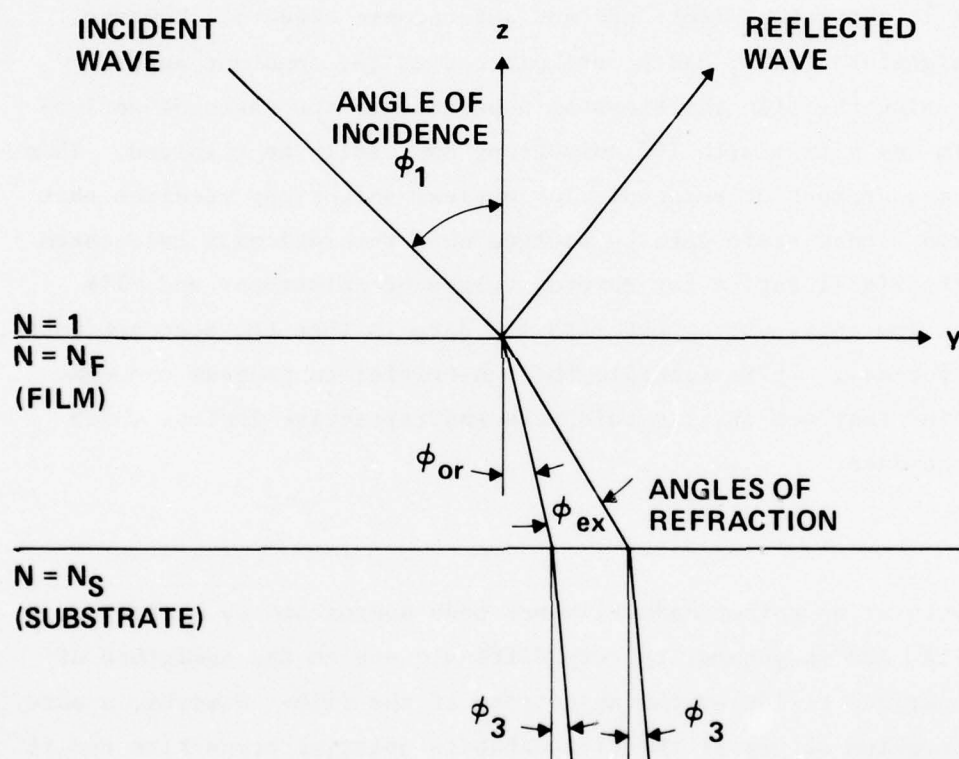
Figure 1. Theoretical model of anisotropic film.

$$\bar{\bar{N}} = \begin{pmatrix} N_{or} & 0 & 0 \\ 0 & N_{or} & 0 \\ 0 & 0 & N_{ex} \end{pmatrix} \text{ for the perpendicular case}$$

$$\bar{\bar{N}} = \begin{pmatrix} N_{ex} & 0 & 0 \\ 0 & N_{or} & 0 \\ 0 & 0 & N_{ex} \end{pmatrix} \text{ for the planar case.}$$

We will assume that the films and substrates are transparent in all cases.

PLANAR ANISOTROPY

Let us first examine the planar case (Figure 1). To calculate the reflection coefficients for the r and s polarizations of the film sub-strate system requires *calculating the fresnel* coefficients of the inter-faces and the phase factor associated with traversal of the film for each polarization. At the first interface (air - film), the reflection coef-ficients are of the form:

$$r_{\perp}^{(1)} = \frac{\cos \phi_1 - N_{ex} \cos \phi_{ex}}{\cos \phi_1 + N_{ex} \cos \phi_{ex}} \tag{1}$$

$$r_{\parallel}^{(1)} = \frac{\cos \phi_{or} - N_{or} \cos \phi_1}{\cos \phi_{or} + N_{or} \cos \phi_1} \tag{2}$$

at the film-substrate interface.

$$r_{\perp}^{(2)} = \frac{N_{ex} \cos \phi_{ex} - N_s \cos \phi_3}{N_{ex} \cos \phi_{ex} + N_s \cos \phi_3} \tag{3}$$

$$r_{\parallel}^{(2)} = \frac{N_{or} \cos \phi_3 - N_s \cos \phi_{or}}{N_{or} \cos \phi_3 + N_s \cos \phi_{or}} \tag{4}$$

The phase factors associated with the two polarizations are

$$\beta_\perp = \frac{2\pi \ F_t}{\lambda} \left(N_{ex}^2 - \sin^2\phi_1 \right)^{1/2} \tag{5}$$

$$\beta_\| = \frac{2\pi \ F_t}{\lambda} \ N_{or} \cos \phi_{or} \quad . \tag{6}$$

The total reflection coefficients can then be calculated from:

$$R_\perp = \frac{r_\perp^{(1)} + r_\perp^{(2)} \ e^{-2i\beta}}{1 + r_\perp^1 \ r_\perp^2 \ e^{-2i\beta}} \tag{7}$$

and

$$R_\| = \frac{r_\|^{(1)} + r_\|^{(2)} \ e^{-2i\beta_\|}}{1 + r_\|^{(1)} \ r_\|^{(2)} \ e^{-2i\beta_\|}} \quad . \tag{8}$$

All angles other than ϕ_1 can be eliminated from $R_\perp$ and $R_\|$ by using Snell's law:

$$\sin \phi_1 = N_{or} \sin \phi_{or} = N_{ex} \sin \phi_{ex} = N_s \sin \phi_3 \quad . \tag{9}$$

The ratio of $R_\|$ to $R_\perp$ can be used to find the usual ellipsometric variables Δ and ψ from:

$$\frac{R_\|}{R_\perp} = \tan \psi \ e^{i\Delta} \quad . \tag{10}$$

The observable signal ratios R_1, R_2 can then be calculated directly from $R_\|$ and $R_\perp$ from Δ and ψ as defined above 1,2 .

The results shown in Figure 2 were obtained by calculating the R_1, R_2 parameters of a typical isotropic film (such as ZnSe on KCl) as a
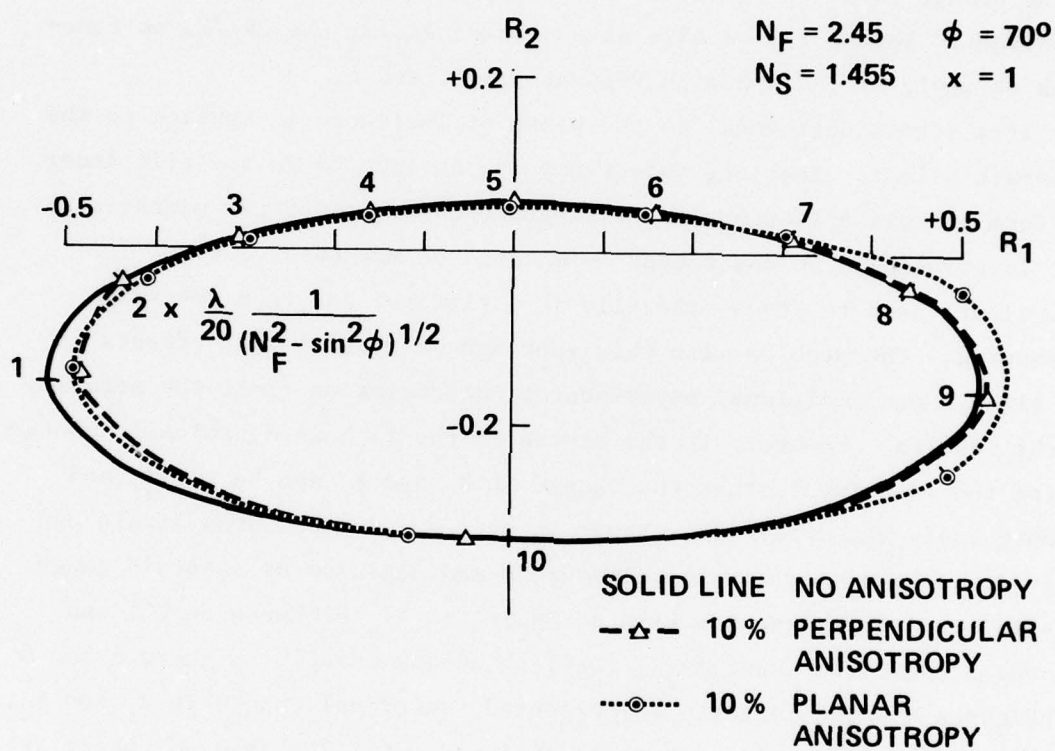
100

Figure 2. Plot of R_1 versus R_2 for NF = 2.45, NS = 1.455, x = 1.

function of thickness or angle of incidence and then comparing it to a film of moderately strong anisotropy (e.g., $N_{ex} = 1.1 N_{or}$). It is somewhat more enlightening, particularly for smaller anisotropies (e.g., 1%), to plot R_1 and R_2 separately as functions of angle of incidence, as shown in Figures 3,4,5, and 6. The parameter most easily observed experimentally is the change in R_1 or R_2 (i.e., ΔR_1 or ΔR_2) caused by stress-induced anisotropy. Therefore, we have also plotted $\Delta R_1/R_1$ and $\Delta R_2/R_2$ as functions of angle of incidence in Figures 3,4,5, and 6.

If a stress orthogonal to the plane of incidence is applied to the substrate film combination, anisotropy can be induced in the film index. The form of this anisotropy corresponds to our model of the planar case.

In principle, an unstressed film could be measured, a clamp (or equivalent) used to stress the film in a fixture, and then the film remeasured. The problem with this approach is that thermal effects in the fixture and additional experimental uncertainties limit the accuracy of the results. However, if the stress on the film is dynamically changed during the experiment, then the change in R_1 and R_2 can be easily and unambiguously measured. The change in stress and associated strain can be produced by piezoelectric transducers and measured by a strain gauge. Figures 3 and 4 represent a film of As_2Se_3 ($\lambda/4$) thickness on KCl and Figures 5 and 6 represent As_2S_3 ($\lambda/4$) thickness on KCl. Figures 3 and 5 and Figures 4 and 6 indicate the expected fractional change in R_1 and R_2, respectively, as functions of angle of incidence. The assumed change in the index of refraction in each case is 1%. The curves show that there exists an optimum range in the angle of incidence for the measurement of this effect.

The results of our first series of measurements on planar anisotropy generated by an externally applied strain are shown in Table 1. In this experiment, the strain was generated in the sample by a piezoelectric transducer and monitored by a piezoresistive strain gauge. One sample consisted of a film of As_2S_3 on a KCl substrate. The mechanically induced strain in the substrate and the film was 2.45×10^{-5} and the attendent fractional change in refractive index was 0.006 ± 0.0003. Using these values, the experimental strain optic constant [11] defined
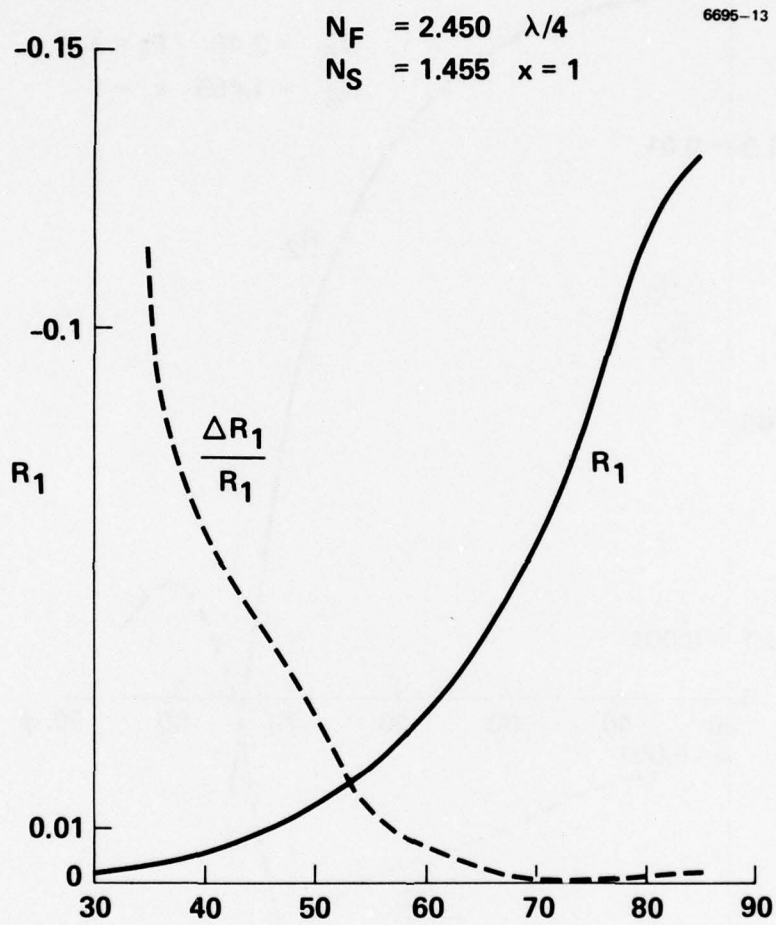
102

Figure 3. Signal ratio R_1 and $\Delta R_1/R_1$ versus ϕ with 1% planar anisotropy.
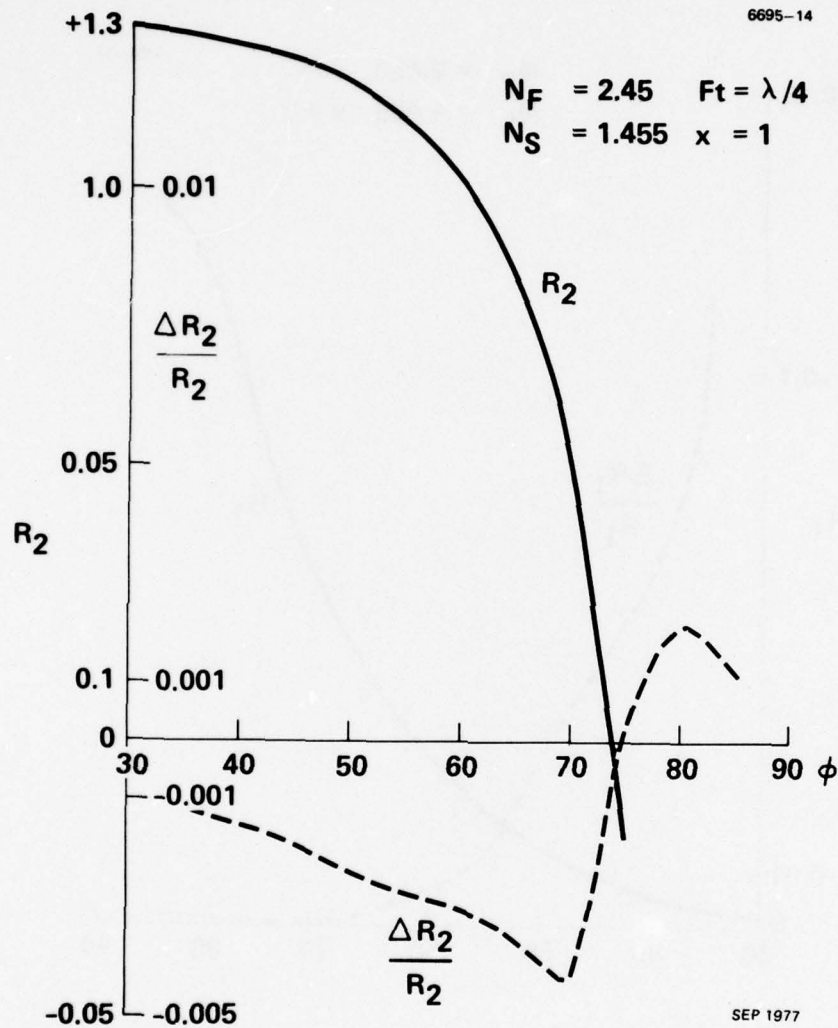
Figure 4. R_2 and $\Delta R_2/R_2$ versus ϕ with 1%
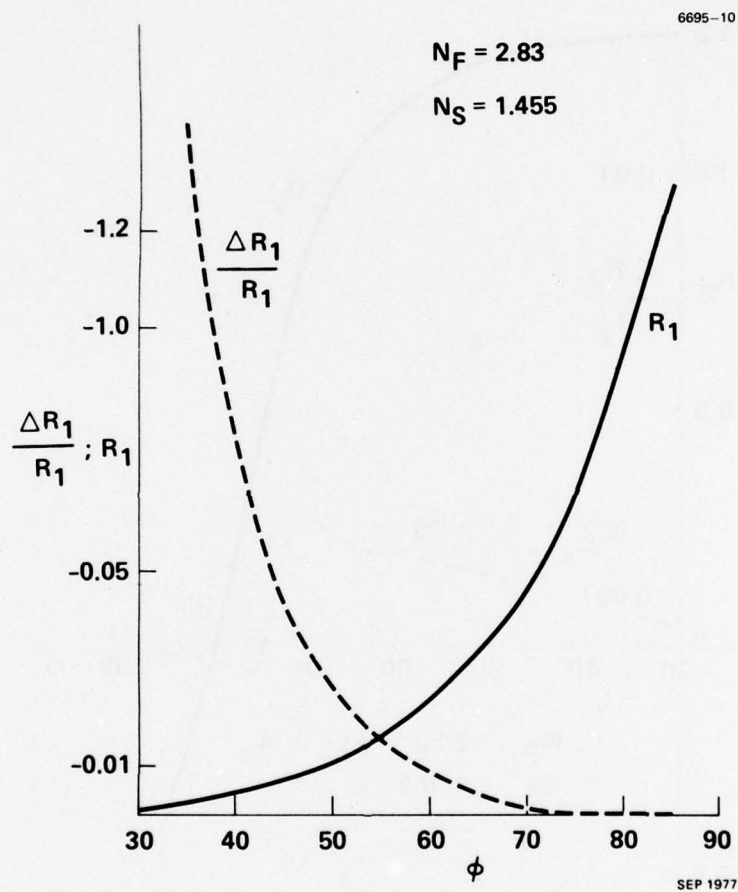planar anisotropy.

104

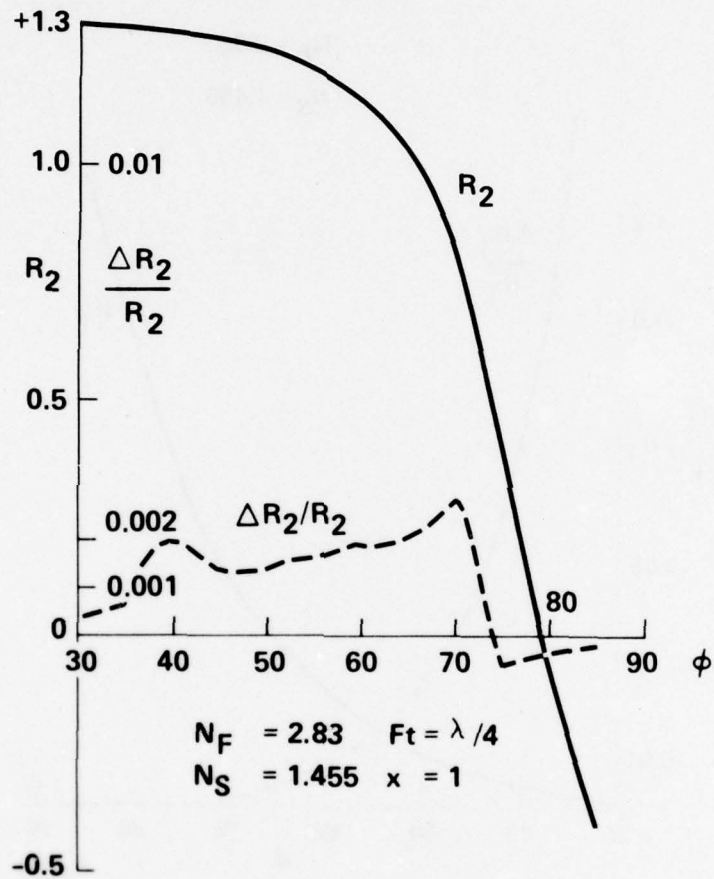Figure 5. R_1 and $\Delta R_1/R_1$ versus ϕ with 1% planar anisotropy.

105

Figure 6. Signal Ratio R_2 and $\Delta R_2/R_2$ versus ϕ with 1% planar anisotropy.

Table 1. Squeeze Experiment Results

Film Material	As_2S_3	As_2Se_3
Substrate	KCl	KCl
Nf (film index)	2.35	2.8
N_s (substrate index)	1.455	1.455
Ft (film thickness A	11610	9914
$\Delta \ell / \ell$ (strain)	$2.45 \times 10^{-5} \pm 1.2 \times 10^{-5}$	$4 \times 10^{-5} \pm 2 \times 6^{-5}$
$\Delta N/N$ (index change)	0.006 ± 0.0003	0.01 ± 0.0005
Strain optic coefficient		
$P_{11} = -2 \dfrac{\Delta N}{N_3} \quad \dfrac{\Delta \ell}{\ell}$	89 ± 40	64 ± 32

as $-2(\Delta N/N^3)$ $(\Delta\ell/\ell)$ was found to be 89 ± 10. This thin-film strain optic value is more than two orders of magnitude larger than the bulk strain optic values measured at 1.15 μm (0.31); similar results were obtained for the As_2Se_3 samples.

The typical maximum values for stress in optical films [9], observed by other methods, can be of the order of 10^9 dyne/cm^2. By assuming a stress value of 10^7 dyne/cm^2 and 1.6 x 10^{10} dyne/cm^2 for Young's modulus in As_2S_3 the strain in a typical film can be estimated to be as large as 6×10^{-4}. Using this value for the strain and the strain optic constant empirically determined above, the expected change in refractive index $\Delta N/N$ due to the thermal expansion coefficient mismatch effect is equal to 0.14. This externally induced change in refractive index is much larger than the sample-to-sample variation observed in our conventional modulated light ellipsometer measurements of the refractive indices of As_2S_3 films. However, significant sample-to-sample variations were observed in the measured refractive index of As_2Se_3 films on KCl substrates. We have attributed these effects to strain-induced anisotropic, and we shall show that the existence of moderate to large perpendicular anisotropies are essentially undetectable ellipsometrically in a single-thickness film.

PERPENDICULAR ANISOTROPY

A summary of the results of our conventional modulated light ellip-someter measurements* on As_2S_3 and As_2Se_3 films is given in Table 2. The variation of the measured refractive index from sample-to-sample is less than 2% for the As_2S_3 film and more than 14% for the As_2Se_3 film. The existence of these variations in refractive index for different film samples from the same startup materials tends to indicate that the condi-tions prevailing during the evaporation play a significant role in the properties of the film.

The fact that these films showed no significant variation in their refractive index when measured at various angles has led to a theoretical investigation of the effects of perpendicular anisotropy which arises when isotropic films deposited on isotropic substrates are internally

---

*These are not a result of squeezing the substrate.

strained. The tension or compression forces that produce this strain
are expected to be isotropic and planar. In this case, the s-polarized
wave always "sees" a constant index as a function of angle of incidence
(mainly N_{or}). The polarization component, however, sees a varying index
as a function of angle of incidence due to the anisotropy of the film.
Again, just as in the planar case, to calculate the reflection coefficient
of the film-substrate system only requires calculating the fresnel coef-
ficients at the interfaces and the phase factors for traversal of the
film.

The fresnel coefficients of the film air interface are

$$r_\perp^{(1)} = \frac{\cos \phi_1 - N_{or} \cos \phi_{or}}{\cos \phi_1 N_{or} \cos \phi_{or}} \tag{11}$$

$$r_\parallel^{(1)} = \frac{\cos \phi_1 N_{or} N_{ex} - (N_{ex}^2 - \sin \phi_1)^{1/2}}{\cos \phi_1 N_{or} N_{ex} + (N_{ex}^2 - \sin^2 \phi_1)^{1/2}} \tag{12}$$

The fresnel coefficients of the film substrate interface are

$$r_\perp^{(2)} = \frac{N_o \cos \phi_o - N_s \cos \phi_3}{N_o \cos \phi_o + N_s \cos \phi_3} \tag{13}$$

$$r_\parallel^{(2)} = \frac{N_s (N_{ex}^2 - \sin^2 \phi_1)^{1/2} - N_{or} N_{ex} \cos \phi_3}{N_s (N_{ex}^2 - \sin^2 \phi_1)^{1/2} + N_{or} N_{ex} \cos \phi_3} \tag{14}$$

and the phase factors for traversal of the film are

$$\beta_\perp = \frac{2\pi F_t}{\lambda} (N_{or}^2 - \sin^2 \phi_1)^{1/2} \tag{15}$$

$$\beta_\parallel = \frac{2\pi F_t}{\lambda} \frac{N_{or}}{N_{ex}} (N_{ex}^2 - \sin^2 \phi_1)^{1/2} . \tag{16}$$

$R_\perp$ and $R_\parallel$ can be calculated as before:

$$R_\perp = \frac{r_\perp^{(1)} + r_\perp^{(2)} e^{i2\beta_\perp}}{1 + r_\perp^{(1)} r_\perp^{(2)} e^{i2\beta_\perp}} \tag{17}$$

$$R_\parallel = \frac{r_\parallel^{(1)} + r_\parallel^{(2)} e^{i2\beta_\parallel}}{1 + r_\parallel^{(1)} r_\parallel^{(2)} e^{i2\beta_\parallel}} \tag{18}$$

Inserting the expressions for the phase factors and the single surface fresnel coefficients into Eqs. (17,18) yields R and R as functions of F_t, N_s, N_f, ϕ, etc. As before, all angular variables (ϕ_{or}, ϕ_{ex}, and ϕ_3) can be eliminated by using a modified Snell's law. $R_\perp$ and $R_\parallel$ can then be used to calculate the ratios R_1 and R_2.

Figure 2 shows a plot of R_1 versus R_2 at a fixed angle of incidence (70°). In this plot, the parametric variable is the film thickness. The tick marks are spaced by film thickness increments of $\lambda/20$ ($N^2 - \sin^{-2} \phi_1)^{1/2}$. The solid curve indicates the increment of calculated values of R_1 and R_2 for a film of ZnSe on KCl with no anisotropy. The Δ and 0 marks indicate the calculated values of R_1 and R_2 for anisotropic films of the same thickness on a KCl substrate. In the case of Δ, the film has planar anisotropy with $N_{or} = 2.45$ and $N_{ex} = 1.1 N_{or}$. For the 0 marks, the film is perpendicularly anisotropic with $N_{or} = 2.45$ and $N_{ex} = 1.1 N_{or}$. The figure shows that even anisotropies of 10% give relatively small shifts in the R_1 R_2 plots. In fact, there are film thickness values for an isotropic film that give R_1 and R_2 values identical to those of an anisotropic film of slightly different thickness values at a fixed angle of incidence.

We have calculated the variation of R_1 and R_2 with angle for a series of anisotropic films with optical axes perpendicular to the surface of the film. This corresponds to the usual case of an optical film deposited at high temperature on a substrate with thermal expansion properties than the film. These calculations indicate generally that the presence of this type of anisotropy cannot be detected by measuring

110

a single film sample. For example, Figures 7 and 8 show the theoretically expected values of R_1 and R_2 as functions of angle of incidence for isotropic films of index values 2.4 and 2.448. Also plotted are the data points for an anisotropic film of N_{or} equal to 2.4 and N_{ex} equal to 2.448. These curves show that an anisotropic film exhibits R_1 and R_2 values as a function of the angle of incidence, ϕ_1, that are essentially identical to the behavior of an isotropic film of slightly different index and/or thickness. This indicates that there will be very little variation in the experimentally determined refractive index as a function of the angle of incidence even though the film being measured is highly anisotropic. This conclusion only applies to the perpendicular anisotropic case.

In principle, following the work of De Smet [8] and Den Engleston [7], the anisotropy can be evaluated using a series of optically identical films of vastly different thickness. With reference to Figure 2 for the anisotropic case, the R_1, R_2 curves will spiral rather than form a closed figure. This is analogous to the Δ, ψ plots for anisotropic film as shown by De Smet and Den Engleston. In practice, however, this is not feasible with a 10.6 μm ellipsometer because the method requires films that range in thickness over many wavelengths. This film thickness variation method for determining anisotropy is viable for short wavelength ellipsometers provided the film is transparent at the measurement wavelength.

CONCLUSIONS

We have demonstrated the feasibility of measuring the anisotropy induced in a thin optical film by piezoelectric or other external means. Measurements of these effects have been used to estimate the strain optic constants of thin optical films at 10.6 μm. These constants, when used in conjunction with typical strains associated with optical films, predict strong anisotropies of the perpendicular type defined here. The existence of thermal expansion coefficient mismatch effects between the film and the substrate can cause the films to have perpendicular anisotropy characteristics. These effects, combined with the planar anisotropy effects that occur whenever an external stress is applied, can lead to biaxial optical anisotropy, which has not been analyzed here.
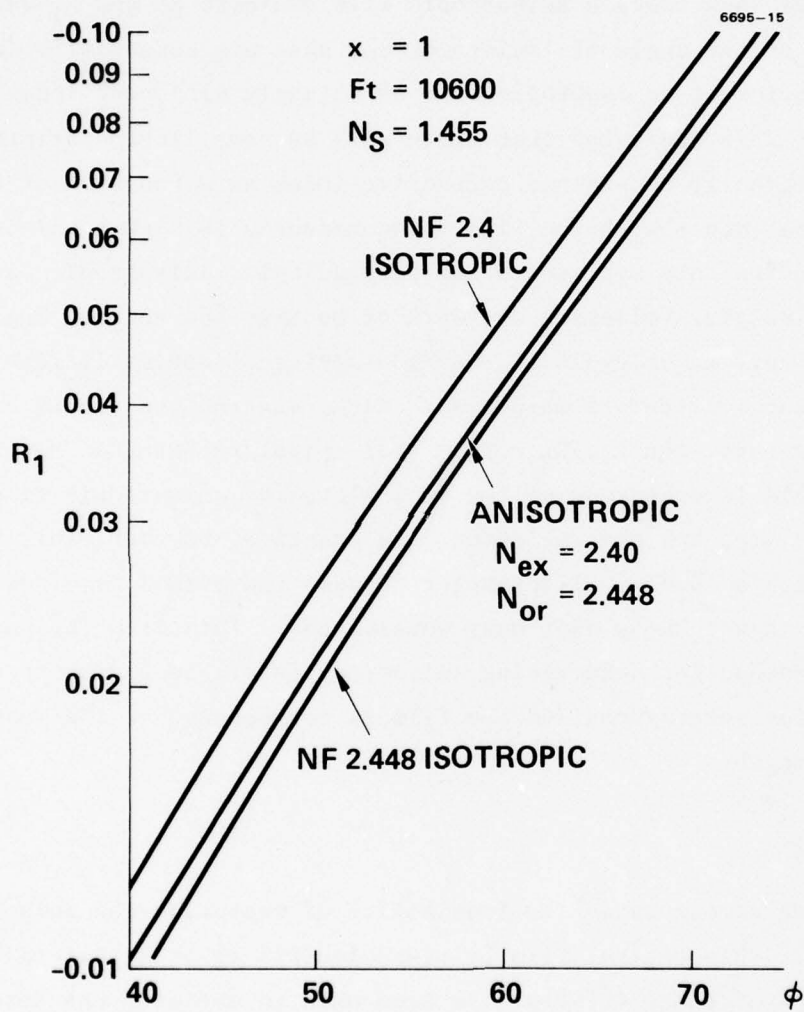
111

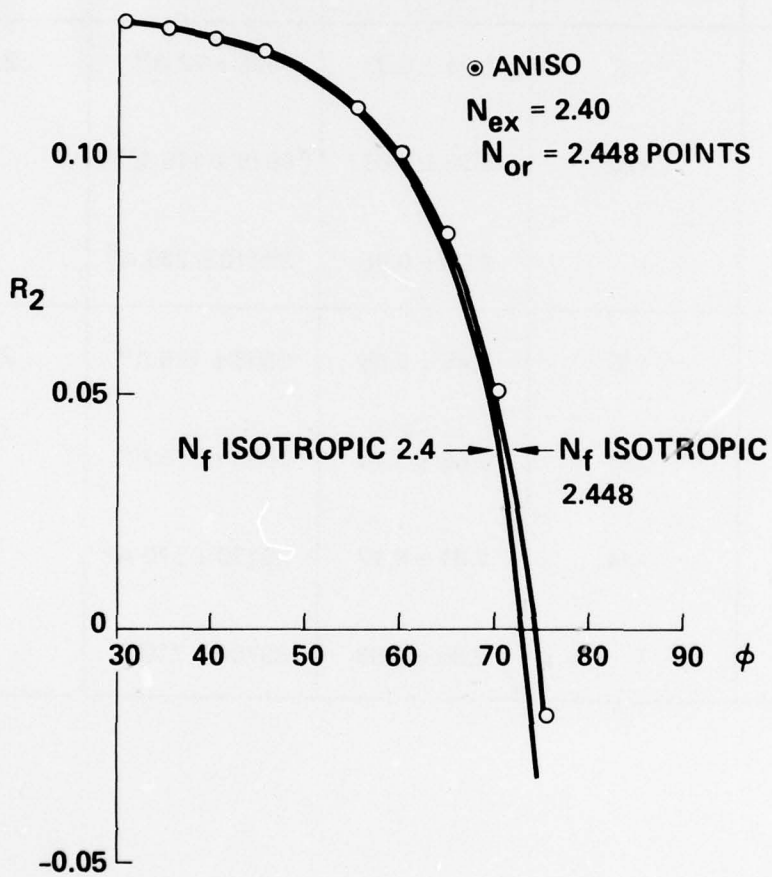Figure 7. Perpendicular anisotropy R_1 versus ϕ.

Figure 8. Perpendicular anisotropy R_2 versus ϕ.

Table 2. Discrepancies in Refractive Indices
Measured Film

6695–18R1

MATERIAL	OPTICAL THICKNESS	MEASURED INDEX	MEASURED THICKNESS	ACCEPTED INDEX
$\dfrac{AS_2S_3}{KC\ell}$	$\sim \lambda/8$	2.34 ± 0.03	6826 ± 72 A^o	2.38
$\dfrac{AS_2S_3}{KC\ell}$	$\sim \lambda/4$	2.35 ± 0.03	9916 ± 116 A^o	
$\dfrac{AS_2S_3}{KC\ell}$	$\sim \lambda$	2.36 ± 0.06	39210 ± 205 A^o	
$\dfrac{AS_2Se_3}{KC\ell}$	$\sim \lambda/8$	2.45 ± 0.05	6808 ± 120 A^o	2.80
$\dfrac{AS_2Se_3}{KC\ell}$	$\sim \lambda/4$	2.66 ± 0.14	9683 ± 376 A^o	
$\dfrac{AS_2Se_3}{KC\ell}$	$\sim \lambda/4$	2.81 ± 0.17	10170 ± 570 A^o	
$\dfrac{AS_2Se_3}{KC\ell}$	$\sim \lambda$	2.85 ± 0.03	33700 ± 710A	

114

Theoretical calculations of the effects of perpendicular anisotropy on the measurement of the refractive index of films show that these measurements cannot be used to determine whether or not the film is anisotropic from a single sample. However, a series of measurements with films of various thicknesses can be used to determine the perpendicular anisotropy, provided that the strain in the films is independent of thickness. Experimental data taken on various films agrees with the theoretical result that the perpendicular anisotropy alters the index but does not yield different index values for different measurement angles.

TABLE OF SYMBOLS

F_t film thickness

λ wavelength in free air

N_s index of substrate

N_{or} ordinary index of refraction of the film

N_{ex} extraordinary index of refraction of the film

ϕ_1 angle of incidence

ϕ_{or} angle of refraction in the film of the ordinary polarization

ϕ_{ex} angle of refraction in the film of the extraordinary polarization

ϕ_3 angle of refraction in the substrate

R_1 the reflection coefficient of film substrate for s polarization

R_{11} the reflection coefficient of the film substrate for p polarization

β_{or} phase factor for the ordinary wave

β_{ex} phase factor for the extraordinary wave

115

REFERENCES

[1] Pedinoff, M.E., Braunstein, M., and Stafsudd, O.M., "Modulated Light Ellipsometry at 10.6 m," Proceedings of SPIE, San Diego, CA, August 1977.

[2] Pedinoff, M.E., Braunstein, M., and Stafsudd, O.M., "Measurements of Refractive Indices of IR Materials: 10.6 m Ellipsometry," Appl. Opt., to be published November 1977.

[3] Allen, S.D., Braunstein, A.I., Braunstein, M., Cheng, J.C., and Nefie, L.A., "A 10.6 Micron Modulated Light Ellipsometer," Optical Properties of Highly Transparent Solids, S.S. Mitra and B. Bendow (Plenum Publishing Co., New York), pp. 503-513, 1975.

[4] Jasperson, S.N., Burge, D.K., and O'Handley, R.C., "A Modulated Ellipsometer for Studying Thin-Film Optical Properties and Surface Dynamics," 37, pp. 548, 1973.

[5] McCrackin, F.L., "A Fortran Program for Analysis of Ellipsometer Measurements," Matl. Bur. Std. Technical Note No. 479 (1969), (U.S. Govt. Printing Office, Washington, D.C. 1969).

[6] Pedinoff, M.E., Braunstein, M., and Stafsudd, O.M., "Modulated Light Ellipsometer Measurements of the Refractive Indices of ThF_4 Single Crystals and As_2Se_3 and As_2S_3 Films on ICCl Substrates at 10.6 m." Topical Conf. on High Power Laser Optical Components and Component Materials, Boulder, Colorado, October 3, 1977.

[7] Den Engleston, D., "Ellipsometry of Anisotropic Films," J. Opt. Soc. Am. 61, pp. 1460-1466, 1971.

[8] DeSmet, D.J., "Ellipsometry of Anisotropic Thin Films," J. Opt. Soc. Am. 64, pp. 631-638, 1974.

[9] Ennos, A.E., "Stress Developed in Optical Film Coatings," Appl. Opt. Vol. 5, pp. 51, 1966.

OPTICAL ABSORPTION IN UV LASER WINDOW MATERIALS

James A. Harrington, Bradley L. Bobbs, and Morris Braunstein
Hughes Research Laboratories
Malibu, California 90265

and

R.Y. Kim, R. Stearns, and Rubin Braunstein
Department of Physics
University of California
Los Angeles, California 90024

The requirements for low-loss optical components for high-power excimer lasers has stimulated the investigation of optical absorption in a variety of highly transparent materials at visible and uv wavelengths. The absorption coefficient β has been measured, using laser calorimetric techniques, for CaF_2, SrF_2, BaF_2, LaF_3, CeF_3, MgF_2, SiO_2, MgO, Al_2O_3, NaF, LiF, $NaCl$, and KCl at 3511, 3638, 4579, 4880, and 5145 Å. The absorption was found to decrease with increasing wavelength to a low value of 4×10^{-5} cm^{-1} for SrF_2 at 5145 Å. In addition, wavelength modulation spectroscopy was used to obtain absorption coefficients for some of the samples. In this technique, the energy derivatives of β are integrated, using the calorimetrically determined values of β as constants of integration to fix β at the laser wavelengths, to obtain absorption coefficients continuously from 2500 to 5000 Å.

Key words: Laser windows; uv laser components; Urbach tail; extrinsic uv absorption; laser calorimetry; wavelength modulation spectroscopy.

1. INTRODUCTION

There has recently been considerable interest in low-loss optical components for uv excimer lasers. To provide reliable coating and window materials that have high damage thresholds at uv laser wavelengths requires making a systematic study of the optical absorption in a wide variety of transparent materials. The materials with large band gaps that have been investigated include alkali halides, alkaline earth fluorides, oxides, and some rare earth fluorides. The small, residual

117

absorption coefficients (β's) were measured at five visible and uv wavelengths using Ar ion laser calorimetry; they were also measured continuously from approximately 400 to 250 nm using wavelength modulation spectroscopy. A comparison of our data with published data (Urbach tail region) indicates that, although the spectral regions of the Urbach tail data and our data do not overlap, our absorption data is significantly lower than a simple extrapolation of the "extrinsic" Urbach tail. These results suggest that the materials studied are considerably more transparent around 350 nm than originally expected from published data.

2. EXPERIMENTAL PROCEDURE AND TECHNIQUES

The small optical absorption coefficients were measured in a variety of single- and polycrystalline samples using laser calorimetric techniques [1]. A Coherent Radiation Laboratories model CR-12 Ar ion laser equipped with visible or uv optics was used in conjunction with a simple air calorimeter to obtain absorption results at 514.5, 488.0, 457.9, 363.8, and 351.1 nm. The schematic of the uv calorimeter shown in Figure 1 also contains the quartz half-wave plate utilized to maximize the power in each uv line. The procedure yielded about 1 W at each uv wavelength and between 5 and 6 W for the strong blue-green lines. Wavelength modulation spectroscopy was performed on some of the samples that had been measured calorimetrically. The basic principles of this technique are discussed elsewhere [2]. Certain refinements in the original apparatus have been made to provide the greater sensitivity required to measure these extremely small absorption coefficients [3].

3. EXPERIMENTAL RESULTS

3.1 Calorimetric Measurements

Eleven different materials were measured at visible and uv wavelengths. In some cases, more than one source or different forms of the

---

1. Figures in brackets indicate the literature references at the end of this paper.

118

6696-2

VERTICALLY
POLARIZED

HORIZONTALLY
POLARIZED

CRL Ar ION LASER
WITH UV OPTICS

FUSED
SILICA
PRISM

QUARTZ HALF-WAVE PLATE
FOR 351.1 nm OR 363.8 nm
WITH OPTIC AXIS AT 45°

~1 m

BARRIER TO BLOCK
ONE OF TWO BEAMS

AIR
CALORI-
METER
HEAD

THERMOCOUPLE LEADS

KEITHLEY
MICROVOLTMETER

SAMPLE

HP
CHART
RECORDER

MASSIVE Al
BLOCK FOR
TEMPERATURE
REFERENCE

POWER
METER
HEAD
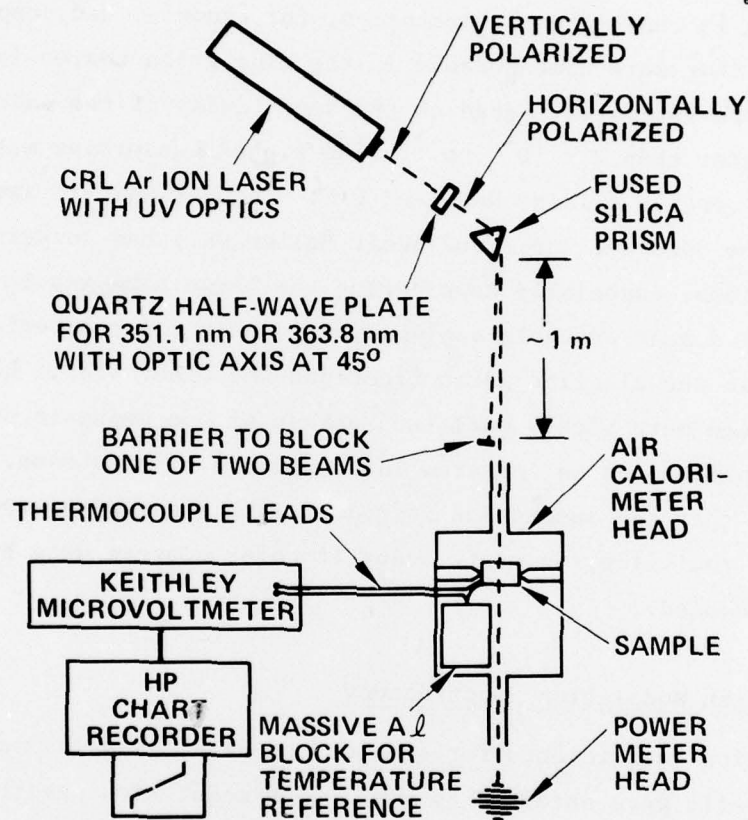
Figure 1. UV Calorimeter.

119

same material were studied. Figures 2 and 3 display all the calorimetric data for the various samples studied. In each case, absorption increases with increasing energy. The lowest absorbing crystals are the alkaline earth fluorides, KCl, NaCl, and SiO_2 (one sample), where β's in the low 10^{-4} cm^{-1} region were measured at visible wavelengths. The single crystal KCl grown in the Hughes Laboratories, for example, had absorption coefficients that were unmeasurable in the blue-green region (cf. Figure 3) but were estimated, based on the sensitivity of the calorimeter, to be no greater than 2 x 10^{-5} cm^{-1}. The highest absorbing materials tended to be certain oxides, NaF, and LiF. The NaF and LiF samples (obtained from Optovac, Inc., and Adolf Meller Co.) had surprisingly high absorptions, especially considering the large band gap in these materials. The most probable explanation is that these materials are not as pure as the alkaline earth fluorides and other alkali halides, which have been more highly purified because of the emphasis on these hosts for applications as infrared laser windows. In no case, however, was it found that the absorption increased with increasing exposure to the uv laser radiation, as might occur if color centers were being continuously produced.

3.2 Wavelength Modulation Spectroscopy

Absorption coefficients for some of the sample samples measured calorimetrically were obtained by wavelength modulation spectroscopy from approximately 450 to 280 nm. The results of this work for several materials are shown in Figures 4 and 5. The raw data is returned as a derivative of the absorptance with respect to wavelength. These spectra are then integrated to yield the relative absorption coefficients, shown as the upper curves in Figures 4 and 5. An absolute calibration of these curves is then obtained by comparing these to the calorimetric data of Figures 2 and 3 (reproduced as the dashed-bottom curves in Figures 4 and 5). In general, there is excellent agreement between the calorimetric and λ-modulation data for each host material studied.
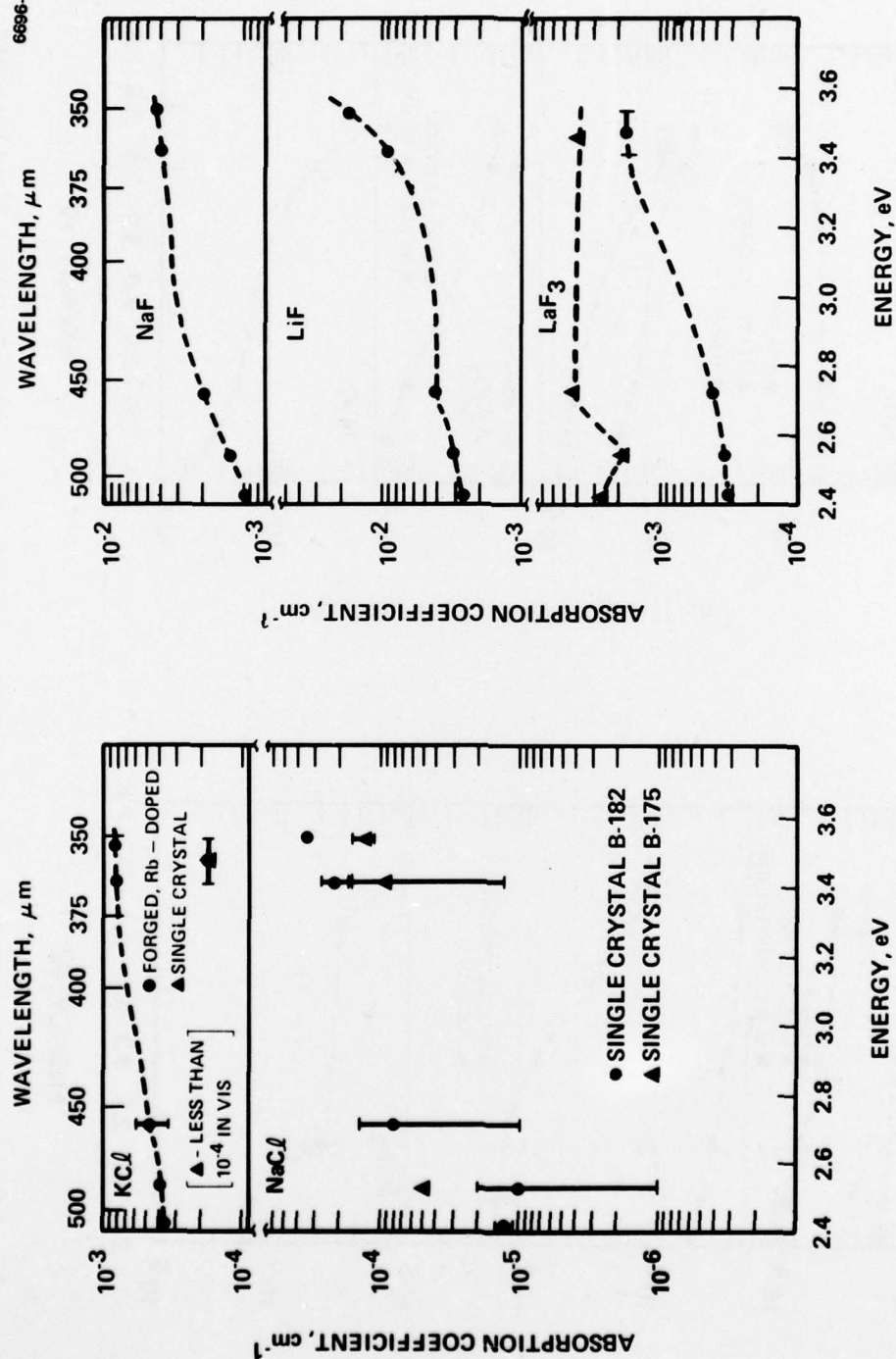
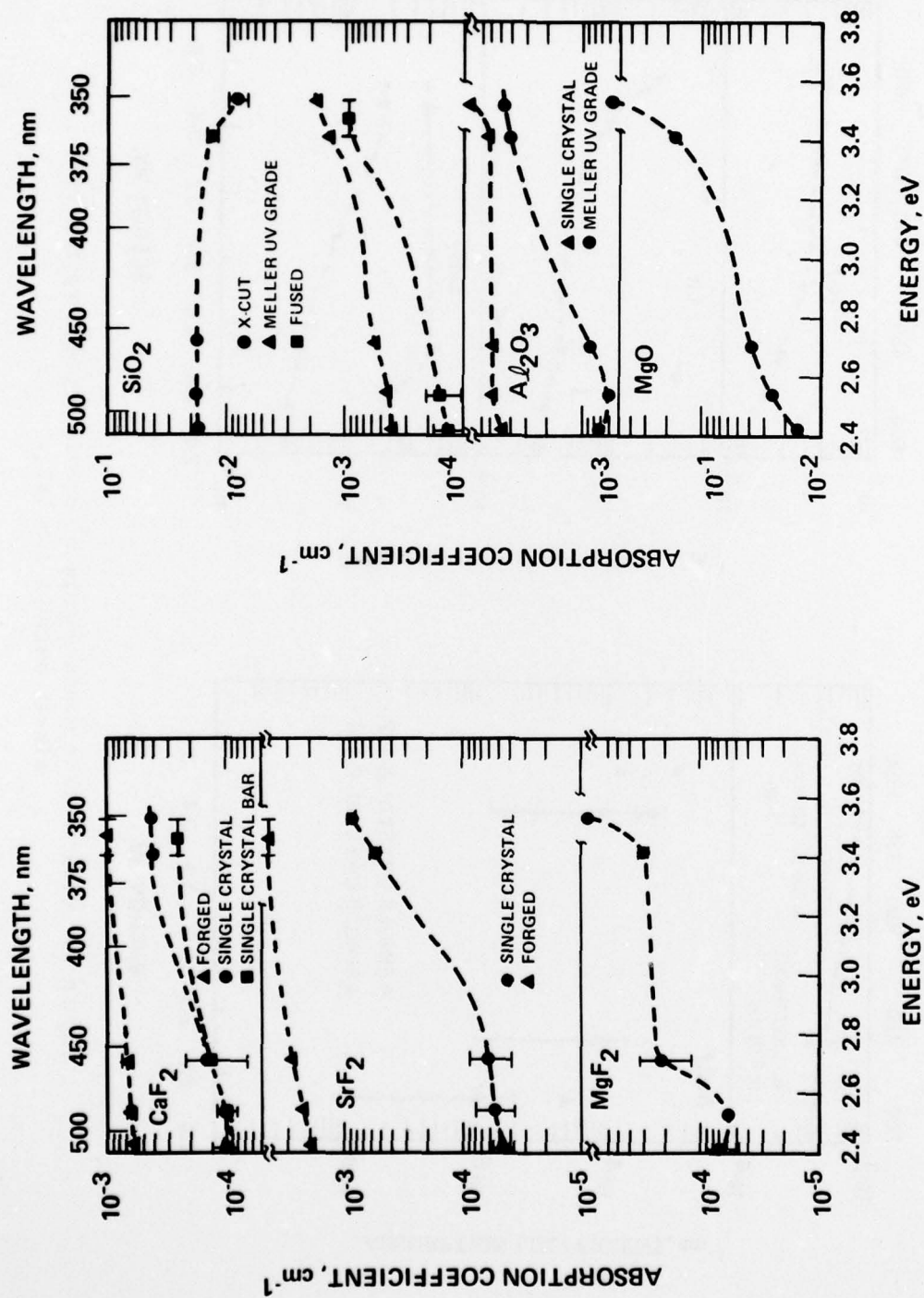Figure 2. Calorimetric measurements of uv-visible absorption in alkali halides and LaF$_3$.

121

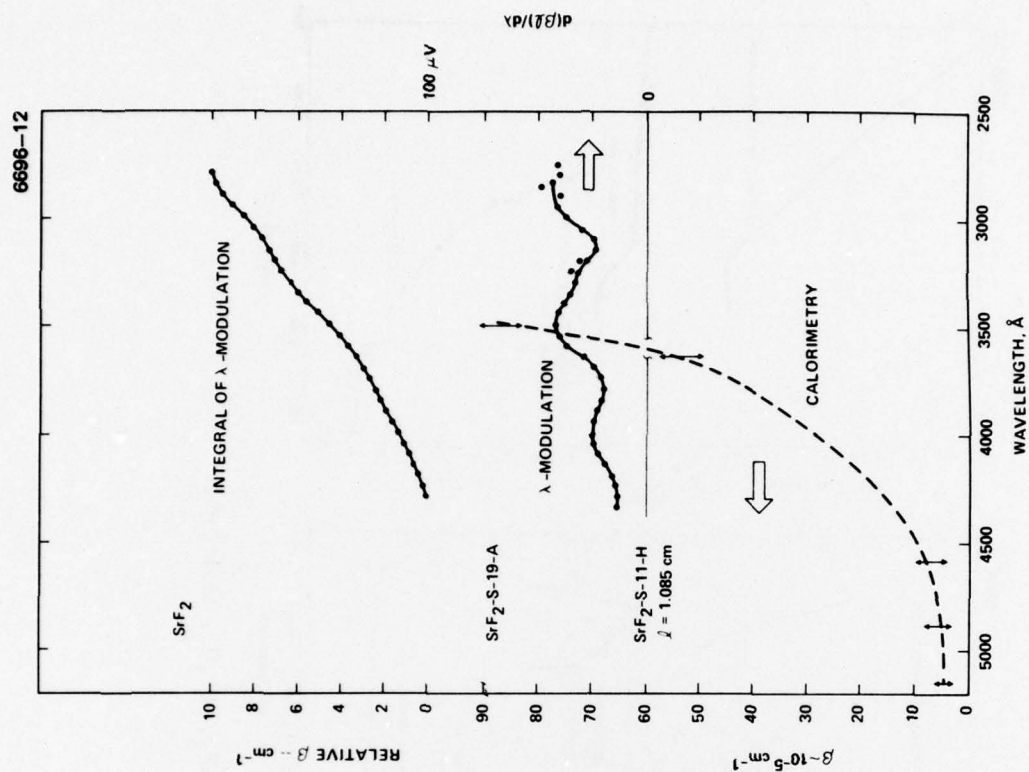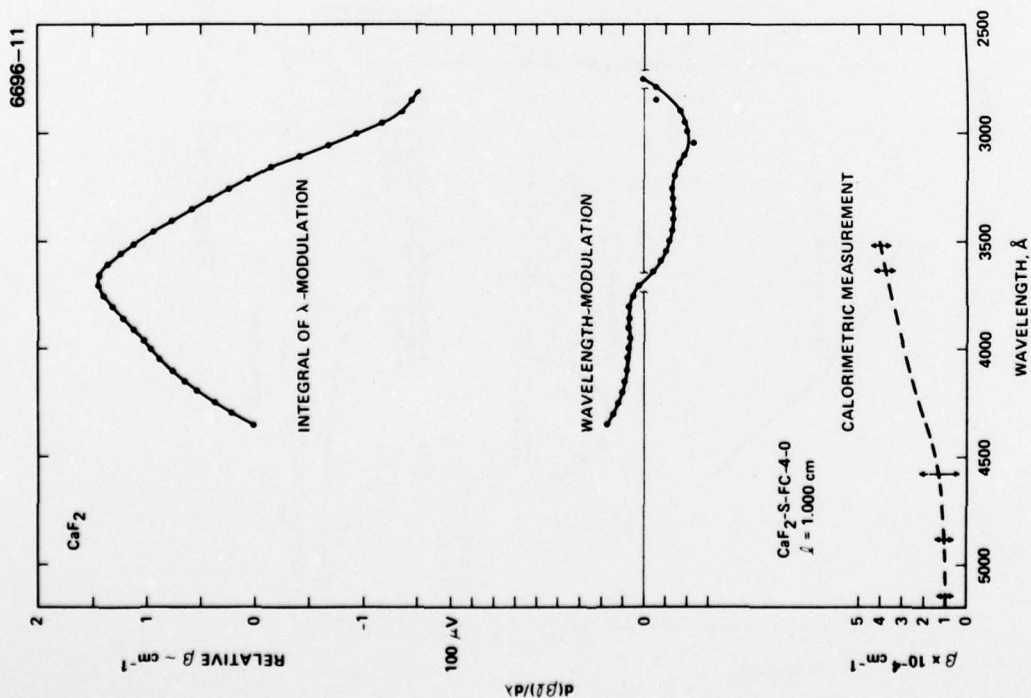Figure 3. Calorimetric measurements of uv-visible absorption in alkaline earth fluorides and various oxides.

6696—13

122

Figure 4. Absorption in LaF$_3$, Al$_2$O$_3$, and SiO$_2$.

123

Figure 5. Absorption in CaF$_2$ and SrF$_2$.

The increasing absorption at uv wavelengths is clearly evident in Figure 4 for LaF_3, Al_2O_3, and SiO_2. The high sensitivity of λ-modulation methods in comparison to other forms of spectroscopy may also be seen by noting the spectra of some older LaF_3 material measured on a conventional (Cary 14) spectrometer. Contrasting the conventional spectroscopic data and the calorimetric/λ-modulation data, one can see that some structure is visible in the integrated λ-modulation spectrum that is impossible to observe in the Cary 14 data because the Cary 14 is less sensitive than derivative spectroscopy. For Al_2O_3, one observes another complementary feature of λ-modulation spectroscopy. The peak in the absorption near 380 nm is missed by calorimetry because of the lack of laser lines at this energy. By comparison, SiO_2 data in Figure 4 merely indicates a monotomic increase in absorption with increasing energy. This is in agreement with the calorimetric results (i.e., no sharp absorption bands appear in the spectra).

CaF_2 data (cf. Figure 5) exhibits a peak in the absorption near 370 nm. This is not entirely evident from calorimetry alone, but derivative spectroscopy clearly delineates this band. A likely explanation for this absorption is that it is due to F-centers. The absorption in SrF_2, even though it is at an extremely low level, indicates some structure on an otherwise monotomically increasing absorption with increasing energy.

3.3 Comparison with Band Edge Data

The alkaline earth fluorides were singled out for comparison with data in the Urbach tail region taken from existing literature. Figure 6 includes the band edge data of Tomiki and Miyata [4] and our λ-modulation/ calorimetric data. Unfortunately, the two spectral regions do not overlap; however, the data from this study is significantly lower than any extrapolation of the "extrinsic" Urbach tail data would imply. Presumably, the purity of the samples has increased and, with more sensitive techniques being used, this has led to the "extrinsic" absorption observed by us being less than that previously observed. Experiments are underway to extend our measurements to 11 eV so that an accurate comparison can be made. The attenuation due to scattering, calculated theoretically [5], is negligible when compared to the other absorption losses.
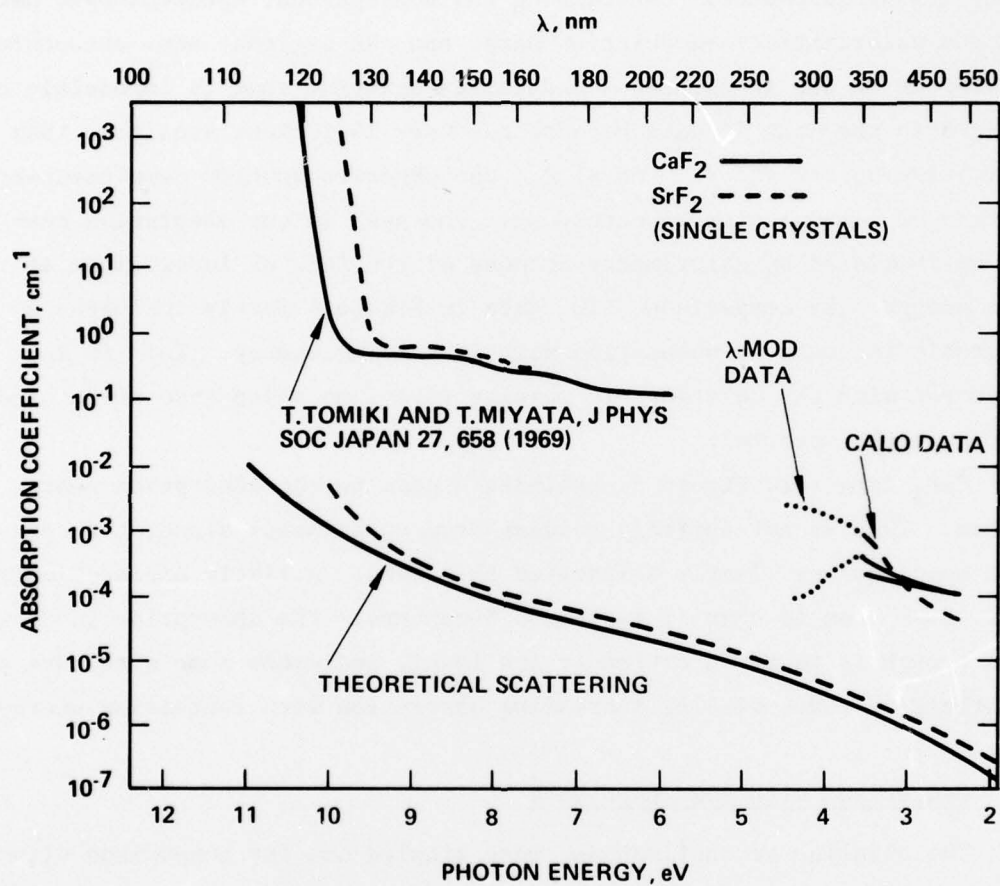
125

λ, nm

Figure 6. UV and visible absorption in SrF$_2$ and CaF$_2$.

4. CONCLUSIONS

Our absorption studies of highly transparent solids for use as low-loss components on uv excimer lasers has led us to conclude that the lowest absorbing materials near 350 nm are the alkaline earth fluorides, NaCl, KCl, and SiO_2. More highly absorbing materials are Al_2O_3, MgO, alkali fluorides, and rare earth fluorides. One reason for this is that the low absorbing uv materials are also those that have been extensively studied and purified for low-loss at infrared laser wavelengths. A comparison of our experimental data with "extrinsic" ch tail region data indicates less extrinsic absorption than previou ly expected.

REFERENCES

[1] Hass, M., Davisson, J.W., Klein, P.H., and Boyer, L.L., J. Appl. Phys. 45, 3959 (1974).

[2] Welkowsky, M. and Braunstein, R., Rev. Sci. Inst. 43, 399 (1972).

[3] To be published.

[4] Tomiki, T. and Miyata, T., J. Phys. Soc. Japan 27, 658 (1969).

[5] Rich, T.C. and Pinnow, D.A., Appl. Phys. Lett. 20, 264 (1972).

ACKNOWLEDGMENTS